

WestminsterResearch

<http://www.westminster.ac.uk/research/westminsterresearch>

Miniaturised waveguide filters for wireless and satellite transceiver front ends

Nandun Mohottige

Faculty of Science and Technology

This is an electronic version of a PhD thesis awarded by the University of Westminster. © The Author, 2015.

This is an exact reproduction of the paper copy held by the University of Westminster library.

The WestminsterResearch online digital archive at the University of Westminster aims to make the research output of the University available to a wider audience. Copyright and Moral Rights remain with the authors and/or copyright owners.

Users are permitted to download and/or print one copy for non-commercial private study or research. Further distribution and any use of material from within this archive for profit-making enterprises or for commercial gain is strictly forbidden.

Whilst further distribution of specific materials from within this archive is forbidden, you may freely distribute the URL of WestminsterResearch: (<http://westminsterresearch.wmin.ac.uk/>).

In case of abuse or copyright appearing without permission e-mail repository@westminster.ac.uk

MINIATURISED WAVEGUIDE FILTERS FOR WIRELESS AND SATELLITE TRANSCEIVER FRONT ENDS

Nandun Darshana Mohottige

A thesis submitted in partial fulfilment of the
requirements of the University of Westminster
for the degree of Doctor of Philosophy

May 2015

ABSTRACT

Conventional waveguide filters, implemented using planar mounted E-plane circuits, can provide two major advantages in terms of low cost and ease of fabrication. However, they suffer from large sizes as well as poor upper stopband performance. The core aim of this thesis is to address these problems and present the design and realisation of highly compact E-plane waveguide filtering structures, with improved stopband performance in comparison to the conventional E-plane filters. The thesis provides two different solutions for achieving compactness. The first uses a direct-coupled approach and the second, a cross-coupled one. The work presented, can be categorised in to the following sections.

The first section introduces a novel ultra-compact E-plane extracted pole filter. The proposed structure has been derived through a modification of the standard E-plane extracted pole section. Filters formed from cascaded E-plane extracted pole sections is considered to be highly compact, in comparison to conventional E-plane filters. However, it is found that the proposed ultra-compact E-plane filter is capable of achieving further size reductions. In addition, it is shown to be capable of providing significantly better stopband attenuation due to the formation of transmission zeros in both the upper and lower stopbands.

In the second section, compact modular E-plane cross-coupled waveguide filters, exhibiting pseudo-elliptic frequency responses is introduced. The basic filtering modules known as the singlet and the doublet have each been realised within a rectangular waveguide using two metal E-plane inserts. The arrangement of the E-plane inserts within a waveguide to form stripline like resonators has allowed the filters to achieve a considerable size reduction. A technique for obtaining the initial dimension has been demonstrated, which can facilitate the development of the proposed filters.

Thirdly, the thesis also investigates the possibility of using an optically activated switch to realise compact reconfigurable E-plane waveguide resonators and filters. A dice of silicon is used as the switching element, due to the numerous benefits it can offer in contrast to other available substitutes. Experimental verification of an optically reconfigurable E-plane waveguide resonator is provided.

ACKNOWLEDGEMENTS

I would like to convey my sincere gratitude and gratefulness to my director of studies, Dr. Djuradj Budimir, for offering me a research opportunity at the University of Westminster and providing me with continuous guidance as well as motivation throughout my doctoral programme. I would also like to thank my secondary supervisor, Dr Andrzej Tarczynski for the valuable advice and support he has given me.

I am extremely grateful for the University, for understanding the financial burdens of my family and providing me with financial support by covering my living expenses as well as granting me a full fee waiver for the entire duration of the research work.

I would also like to express my sincere gratitude to the external examiner, for going through my thesis in detail and providing constructive feedback.

Special thanks to my friend and former colleague, Dr. Oleksandr Glubokov, who has always been there to provide me with encouragements and guidance on my research.

Support from all my friends and colleagues from the Wireless Communication Research Group, is thankfully acknowledged.

Finally, I would like to dedicate this work to my mother and father, Aunt Cynthia and Uncle Tony, for their patience, investment and continuous support for the duration of my higher education.

Nandun Darshana Mohottige

24/08/2015

AUTHOR'S DECLARATION

I declare that all the material contained in this thesis is my own work.

TABLE OF CONTENTS

CHAPTER 1 Introduction

1.1 Filters For Wireless Communication Systems	1
1.2 Overview of Past Research Work in Compact Rectangular E-plane Waveguide Filters	4
1.3 Overview of Past Research Work in Reconfigurable Rectangular Waveguide Filters	8
1.4 Aims and Objectives of the Thesis	10
1.5 Outline of the Thesis	12
1.6 References	14

CHAPTER 2 Background

2.1 Rectangular Waveguides	17
2.2 Bandpass Filter Theory	21
2.2.1 Butterworth Approximation	24
2.2.2 Chebyshev Approximation	25
2.2.3 The Generalised Chebyshev Approximation	26
2.3 Filter Prototypes	28
2.4 Lowpass to Bandpass Frequency Transformation	31
2.5 Multiple Coupled Resonators	32
2.6 The General $N \times N$ and $N+2$ Coupling Matrix	33
2.7 Extracted Pole Filters	36
2.8 Non-Resonating Nodes in Filters	38
2.9 References	40

CHAPTER 3 E-plane Extracted Pole Waveguide Filters

3.1 Introduction	42
3.2 Conventional E-plane Waveguide Filters	43
3.3 E-plane Extracted Pole Waveguide Filters	46

3.4 Two-pole E-plane Extracted Pole Sections and Filters.....	53
3.4.1 Filters Implemented using the Two-pole E-plane Extracted Pole Sections....	60
3.5 Ultra-compact E-plane Extracted Pole Waveguide Filters	63
3.5.1 Development of the Ultra-compact E-plane Extracted Pole Filters.....	63
3.5.2 Investigating the Effects of Parametric Variations	68
3.5.3 Simulation and Experimental Verification	70
3.6 Summary	73
3.7 References	74

CHAPTER 4 E-plane Cross-coupled Waveguide Filters

4.1 Introduction.....	77
4.2 Cross-coupled Filtering Modules Using E-plane Waveguide Inserts.....	79
4.2.1 Singlets.....	79
4.2.2 Physical Realisation of Singlets Using E-plane Inserts	80
4.2.3 Doublets Implemented Using E-plane Inserts	83
4.3 Coupling Coefficients for Filter Design.....	87
4.4 Compact Higher Order E-plane Cross-coupled Filters	91
4.5 Compact Modular Cross-coupled Filters with Cascaded Extracted Pole Sections	96
4.5.1 Extraction of GCCs for Singlets	97
4.5.2 Extraction of GCCs for Symmetric Doublets	99
4.5.3 Compact 3 rd Order Cross-coupled Waveguide Filter Using Singlets and Extracted Pole Sections	102
4.5.4 Compact 4 th Order Cross-coupled Waveguide Filter Using Doublets and Extracted Pole Sections	108
4.6 Summary	114
4.6 References	115

CHAPTER 5 Optically Reconfigurable E-plane Waveguide Resonators and Filters

5.1 Introduction.....	118
5.2 The Silicon Photoconductive Switch	121

5.3 Optically Reconfigurable E-plane Waveguide Resonator	124
5.4 Optically Reconfigurable E-plane Waveguide Filter	130
5.5 Summary	132
5.6 References	133

CHAPTER 6 Conclusion and Future Work

6.1 Contributions of the Thesis	139
6.2 Suggestions for Future Work	140
List of Publications	141

LIST OF FIGURES AND TABLES

CHAPTER 1

- Figure 1.1-1 Block diagram of a full-duplex super heterodyne transceiver.
- Figure 1.2-1 Inside view of a 3rd order E-plane rectangular waveguide filter.
- Figure 1.2-2 Frequency response of a 3rd order E-plane rectangular waveguide filter.

CHAPTER 2

- Figure 2.1-1 Conventional rectangular waveguide configuration.
- Figure 2.1-2 Cut off Frequencies of TE and TM Modes of a conventional rectangular waveguide.
- Figure 2.2-1 Typical frequency response of a rectangular waveguide.
- Figure 2.2-2 A doubly terminated lossless linear network.
- Figure 2.2-3 Frequency response of the maximally flat filter for various filter orders N .
- Figure 2.2-4 Chebyshev Lowpass filter prototype frequency response.
- Figure 2.2-5 Generalized Chebyshev (psudeo-elliptic) response of a third order filter with two prescribed transmission zeros in the upper stopband.
- Figure 2.3-1 Lumped element lowpass prototypes: (a) Odd order filter network; (b) Even order filter network.
- Figure 2.3-2 Immitance inverters: (a) Impedance (K) inverter; (b) Admittance (J) inverter.
- Figure 2.3-3 Impedance inverter lowpass lumped element prototype.
- Figure 2.5-1 Model of the general coupled-resonator filter.
- Figure 2.5-2 Cameron's modified model of the general coupled-resonator filter.

- Figure 2.5-3 The lowpass prototype of the multiple coupled resonator filter.
- Figure 2.6-1 The multiple coupled resonator filter including source E with impedance R_S and load impedance R_L .
- Figure 2.6-2 The $N+2$ multiple coupled resonator network.
- Figure 2.7-1 Schematic representation of a bandstop section.
- Figure 2.7-2 Deduction of a transmission line section from the filter network.
- Figure 2.7-3 Extraction of a bandstop section from the remaining network.
- Figure 2.8-1 Modules that are widely used for cascaded filter design: (a) The singlet; (b) The square doublet; (c) The diamond shaped doublet; (d) The extended doublet.

CHAPTER 3

- Figure 3.2-1 Conventional rectangular E-plane waveguide configuration: (a) E-plane filter; (b) Metal insert for a 4th order E-plane filter.
- Figure 3.3-1 Transformation of a transmission line section in extracted pole prototypes.
- Figure 3.3-2 EPS: (a) Schematic representation; (b) Coupling scheme representation.
- Figure 3.3-3 Schematic representation of a doubly loaded EPS.
- Figure 3.3-4 Configuration of an E-plane EPS within a rectangular waveguide.
- Figure 3.3-5 Simulated S-parameter response of an E-plane EPS with dimensions: $L_{NRN}=5\text{mm}$; $L_{fin}=6.4\text{mm}$; $W_{fin}=1.5\text{mm}$; $W_{sep}=3.5\text{mm}$, inserted in a WG16 (WR90) waveguide housing.
- Figure 3.3-6 Coupling schematic of the 4th order EPS filter.
- Figure 3.3-7 Layout of the E-plane insert for the 4th order EPS filter.
- Figure 3.3-8 Photograph of the fabricated insert for the 4th order EPS filter, placed within a channel of a split block waveguide housing.

- Figure 3.3-9 Comparison between simulated and measured results of the fabricated 4th order EPS filter.
- Figure 3.4-1 Configuration of a conventional E-plane resonator.
- Figure 3.4-2 Configuration of the E-plane EPS.
- Figure 3.4-3 Circuit schematic representation of an E-plane EPS.
- Figure 3.4-4 Graphical illustration of the poles and zeros of an E-plane EPS.
- Figure 3.4-5 Comparison of the s-parameter responses between a standard EPS and a two-pole EPS.
- Figure 3.4-6 Figure 3.4-6: Effect of varying width of metallic fin (W_{RES}): (a) On S_{11} ; (b) On S_{21} .
- Figure 3.4-7 Effect of varying length of metallic fin (H_{RES}): (a) Effect on S_{11} ; (b) Effect on S_{21} .
- Figure 3.4-8 Effect of varying length of non-resonating node (L_{NRN}): (a) Effect on S_{11} ; (b) Effect on S_{21} .
- Figure 3.4-9 Coupling scheme of the 4th order filter.
- Figure 3.4-10 Configuration of the E-plane insert for the 4th order filter implemented using two cascaded two-pole EPS.
- Figure 3.4-11 Comparison between simulated and measured results of the fabricated filter.
- Figure 3.4-12 Photograph of the fabricated insert for the 4th order filter.
- Figure 3.5-1 Configuration of a E-plane insert for realisation of ultra-compact EPS filters.
- Figure 3.5-2 Equivalent circuit model for the ultra-compact EPS filter.
- Figure 3.5-3 Graphical illustration of pole and zero locations for the ultra-compact filter.
- Figure 3.5-4 Arrangement of the E-plane insert for the ultra-compact EPS filters.

- Figure 3.5-5 Comparison of the S-parameter responses of the standard E-plane two pole EPS, the proposed ultra-compact EPS filter and a conventional 2nd order E-plane filter.
- Figure 3.5-6 Comparison of the S-parameter responses of the ultra-compact EPS filter and frequency response of its equivalent schematic.
- Figure 3.5-7 Effect of varying length of centre metallic fin (H_{RES2}): (a) Effect on S_{11} ; (b) Effect on S_{21} .
- Figure 3.5-8 Effect of simultaneously varying the length of first metallic fin (H_{RES1}) and last metallic fin (H_{RES3}): (a) Effect on S_{11} ; (b) Effect on S_{21} .
- Figure 3.5-9 Effect of varying length of non-resonating node (L_{NRN}): (a) Effect on S_{11} ; (b) Effect on S_{21} .
- Figure 3.5-10 Configuration of the E-plane insert for the proposed ultra-compact EPS filters.
- Figure 3.5-11 Simulated and measured S-parameter response of the designed ultra-compact EPS filter.
- Figure 3.5-12 Photograph of the fabricated ultra-compact EPS filter insert placed within a channel of a split block waveguide housing.

CHAPTER 4

- Figure 4.2-1 Coupling schematic representation of singlet.
- Figure 4.2-2 Configuration of E-plane metallic inserts for the formation of a singlet.
- Figure 4.2-3 S-parameter response of the proposed structure with inductive source-load coupling.
- Figure 4.2-4 S-parameter response of the proposed structure with capacitive source-load coupling.

- Figure 4.2-5 Configuration of E-plane metallic inserts for the formation of a doublet.
- Figure 4.2-6 Coupling schematic representation of the doublet representing filter configuration in Figure 4.2-5.
- Figure 4.2-7 Coupling schematic representation of the doublet with corresponding phase shifts.
- Figure 4.2-8 Layout of the two E-plane inserts for the proposed compact E-plane doublet.
- Figure 4.2-9 Simulated S-parameter response of the proposed E-plane doublet structure and the frequency response of the coupling schematic.
- Figure 4.3-1 Circuit representation of two synchronously tuned coupled resonators with mixed couplings.
- Figure 4.3-2 Circuit representation of a doubly loaded resonator.
- Figure 4.3-3 Extracting k_{12} and Q_{ext} : (a) Simulated frequency responses of the doublet with different septa widths for extraction of coupling coefficient k_{12} ; (b) Extracted coupling coefficient k_{12} for different septa widths; (c) Extracted external quality factor Q_{ext} .
- Figure 4.4-1 Coupling Schematic of a 3rd order filter with source-load coupling.
- Figure 4.4-2 Configuration of the E-plane inserts for the 3rd order filter with source-load coupling.
- Figure 4.4-3 Coupling Schematic of a 3rd order cross-coupled filter taking into consideration of parasitic couplings and the spurious resonance.
- Figure 4.4-4 Comparison between the proposed 3rd order filter with source-load coupling, a 3rd order conventional E-plane filter and a 3rd order EPS filter.
- Figure 4.4-5 Layout of the two E-plane inserts for the proposed compact 3rd order source-load coupled filter.

- Figure 4.4-6 Comparison between coupling schematic, EM simulation and measurement S-parameter responses of the proposed compact 3rd order filter with source-load coupling.
- Figure 4.4-7 Fabricated prototype of the compact 3rd order E-plane waveguide filter with source-load coupling.
- Figure 4.5-1 Cascaded singlet blocks in series to form modular higher order cross coupled filters.
- Figure 4.5-2 Singlet block cascaded in series with extracted pole sections.
- Figure 4.5-3 Doublet block cascaded in series with extracted pole sections.
- Figure 4.5-4 Coupling schematic of the singlet module with the GCCs denoted by k_N and k_{N1} .
- Figure 4.5-5 Analysis of the singlet using even and odd mode technique.
- Figure 4.5-6 Coupling schematic of the symmetric doublet module with the GCCs denoted by k_N , k_{N1} and k_I .
- Figure 4.5-7 Analysis of the symmetric doublet using even and odd-mode technique.
- Figure 4.5-8 An inside view of the configuration of proposed compact 3rd order cross-coupled waveguide filter.
- Figure 4.5-9 Coupling schematic of the proposed 3rd order cross-coupled filter.
- Figure 4.5-10 Layout of the two metallic inserts for realisation of compact 3rd order cross coupled filter.
- Figure 4.5-11 Extracted generalized coupling coefficients against insert dimensions: (a) k_{N1}^2 from extracted pole section; (b) external quality factor (Q_{ext}); (c) k_{N2}^2 from singlet section; (d) k_{12}^2 from singlet section; (e) susceptance B_I from EPS.
- Figure 4.5-12 Simulated and measured S-parameter response of the compact 3rd order cross-coupled filter.

- Figure 4.5-13 Photograph of the fabricated inserts for the compact 3rd order cross-coupled filter, placed within the custom made split block waveguide housing.
- Figure 4.5-14 An inside view of the configuration of proposed compact 4th order cross-coupled waveguide filter.
- Figure 4.5-15 Coupling schematic of the proposed 4th order cross-coupled filter.
- Figure 4.5-16 Extracted generalized coupling coefficients against insert dimensions (refer to Figure 4.5-18 for insert notations):
 (a) Susceptance B_1 against length of fins from extracted pole sections; (b) k_{N1}^2 against L_{SEG1} from extracted pole section; (c) external quality factor (Q_{ext}); (d) Susceptance B_2 against length of fins from doublet; (e) Susceptance B_2 against L_{SEG2} from doublet; (f) k_2 against W_{SEPT3} from doublet section.
- Figure 4.5-17 Extracted generalized coupling coefficients against insert dimensions Cont.: (a) k_{12} against GAP from doublet; (b) k_{N2}^2 against W_{SEP2} from doublet.
- Figure 4.5-18 Layout of the two metallic inserts for realisation of compact 4th order cross-coupled filter.
- Figure 4.5-19 Simulated S-parameter response and the measure results of the compact 4th order cross-coupled filter.
- Figure 4.5-20 Photograph of the fabricated inserts within the custom made split block waveguide housing for the 4th order E-plane Cross-coupled filter.

CHAPTER 5

- Figure 5.2-1 A simplified energy band diagram of a semiconductor.
- Figure 5.2-2 The basic layout of a photoconductive switch.
- Figure 5.3-1 Effect of varying length of embedded metallic fin (L_{FIN}) on the S-parameter response of the E-plane extracted pole section: (a) S_{21} ; (b) S_{11} .

- Figure 5.3-2 Inside view of an optically reconfigurable E-plane extracted pole section.
- Figure 5.3-3 Layout of the proposed optically reconfigurable resonator: (a) Complete E-plane insert; (b) Side view of the metallic fin with silicon switch
- Figure 5.3-4 Photograph of the fabricated prototype of the proposed optically reconfigurable resonator.
- Figure 5.3-5 Simulated and measured S-parameters of the optically reconfigurable E-plane waveguide resonator: (a) Switch OFF; (b) Switch ON.
- Figure 5.4-1 Layout of the proposed optically reconfigurable Filter: (a) Complete E-plane insert; (b) Side view of the metallic fins with silicon switches.
- Figure 5.4-2 Simulated S-parameter responses of the optically reconfigurable E-plane waveguide filter in OFF and ON states.

CHAPTER 1

- Table 1.5-1 Table of achievements.

CHAPTER 3

- Table 3.3-1 Dimension of the E-plane insert for the designed 4th order EPS filter.
- Table 3.4-1 Dimension of the E-plane insert for the designed 4th order filter using cascaded two-pole EPS.
- Table 3.5-1 Dimension of the E-plane insert for the designed ultra-compact EPS filter.
- Table 3.5-2 Comparison of the ultra-compact EPS filter with that of Conventional E-plane filters, and E-plane EPS filters. All filters are designed for a centre frequency of 9.5 GHz and 0.3 GHz bandwidth.

CHAPTER 4

Table 4.2-1	Dimensions of the E-plane insert for the compact E-plane doublet.
Table 4.4-1	Comparison of overall length of the compact 3 rd order source-load coupled filter with E-plane EPS filter and conventional E-plane filters.
Table 4.4-2	Dimensions of the E-plane insert for the compact 3 rd order source-load coupled filter.
Table 4.5-1	Dimensions of the E-plane insert for the compact 3 rd order cross-coupled filter.
Table 4.5-2	Dimensions (mm) of the E-plane insert for the compact 4 th order cross-coupled waveguide filter (refer to Figure 4.5-18).
Table 4.5-3	Comparison of overall length of the compact cross-coupled filter with E-plane EPS filter and conventional E-plane filter.

CHAPTER 5

Table 5.3-1	Dimensions of the E-plane insert for the reconfigurable resonator.
Table 5.4-1	Dimensions of the E-plane insert (mm) for the proposed optically reconfigurable filter.

LIST OF ACRONYMS

ABCD	Transfer matrix
dB	Decibel
DC	Direct current
EPS	Extracted pole section
FBW	Fractional bandwidth
GCC	Generalised coupling coefficient
GHz	Gigahertz
K-band	Portion of the electromagnetic spectrum covering the microwave range of frequencies from 18 GHz to 27 GHz. Specified by IEEE.
LED	Light emitting diode
LNA	Low noise amplifier
MEMS	Micro-electro-mechanical systems
mm	Millimetre
NRN	Non resonating node
RF	Radio frequency
SRR	Split ring resonator
TE	Transverse electric propagation mode
TEM	Transverse electromagnetic propagation mode
TM	Transverse magnetic propagation mode
X-band	Portion of the electromagnetic spectrum covering the microwave range of frequencies from 8 GHz to 12 GHz. Specified by IEEE.

CHAPTER 1

INTRODUCTION

The telecommunication industry has seen a rapid growth in its commercial success which in turn has enthused the research and development of new technologies for modern wireless communication systems. Advancements in mobile and broadband communication systems and satellite navigation systems have paved the way for high demands in high performance and compact microwave and millimetre wave modules capable of meeting strict requirements. Current and future wireless systems require devices capable of providing efficient means of communication over several bands. Such systems will require the use of passive microwave components; such as filters, diplexers and multiplexers which are responsible for frequency selectivity. Since the electromagnetic spectrum is continually being populated, it is necessary that these components provide an efficient utilisation of the spectrum. This requirement, in turn, has placed challenges on the design of compact microwave and millimetre wave filters [1-1] and called for low loss, low cost, improved selectivity and stopband performance of filters and multiplexers.

1.1 Filters for Wireless Communication Systems

Electronic filters play a vital role and are requisite components of any RF and microwave wireless systems. These components are used to differentiate between wanted and unwanted signals in a communication system. In other words, they permit wanted signals of certain frequencies and block unwanted signals of certain frequencies, as specified by a given application [1-1]-[1-2]. This allows multitude of different wireless services to share the electromagnetic spectrum.

In order to further highlight the important roles of filters in a trans-receiver front end of a communication system, an example of a super heterodyne transceiver architecture with a single conversion stage is shown in Figure 1.1-1 [1-3]-[1-4].

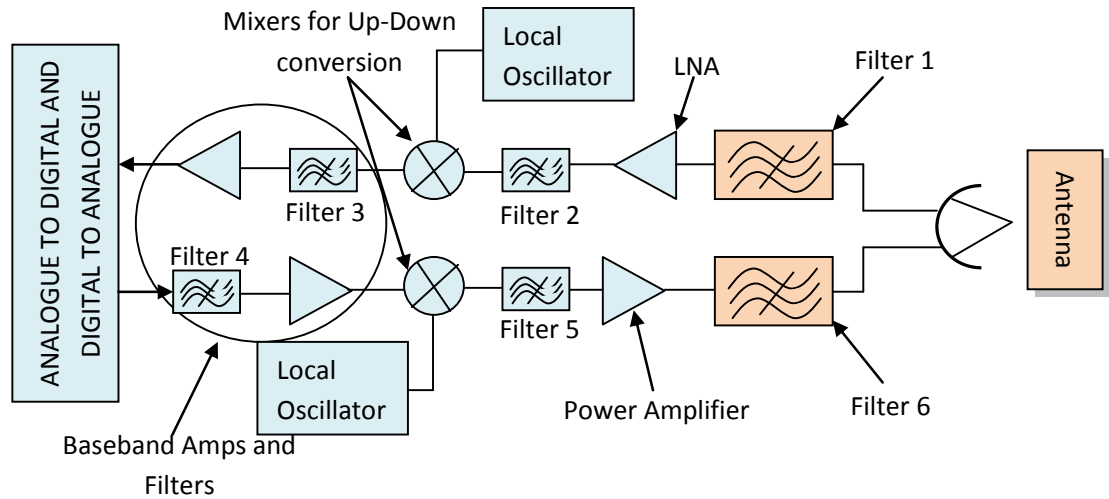


Figure 1.1-1: Block diagram of a full-duplex super heterodyne transceiver

The RF front-end as shown in Figure 1.1-1 consists of two parallel branches for receiving and transmitting information. Both branches are combined at the antenna through a diplexer, which constitutes of two RF filters (Filter 1 and Filter 6), thus allowing the transmitter and the receiver to share a common antenna. The two filters forming the diplexer must adhere to strict specifications, such that Filter 1 must provide a low insertion loss in the receiving band and a high attenuation in the transmitter band, in order to prevent interference caused by the leakage of transmitted signal power into the receiver. Filter 6 must have a low insertion loss and a wide stopband in order to reduce the spurious radiated power and prevent noise from the receiver. Filter 2 and Filter 5 are image rejection filters. Their respective purposes are to suppress the unwanted image frequency signal before the down converter and to prevent unwanted mixing products created after the up-conversion. Filter 3 plays the role of channel selection and has a centre frequency equal to the intermediate frequency (IF). Filter 4, which is located in the transmitter section, rejects unwanted components from the baseband signal before up-conversion.

There is a wide range of technologies that is available for filter implementation, where the type of technology to employ is dictated by the application. At very low frequencies, resonators and filters can be realised using lumped elements [1-2] due to their small size. However when it comes to applications at RF and microwave frequencies, this approach for realising filters becomes less effective. A reason for this is due to the parasitic effects inherent in lumped elements, which prevents realisation of such elements with adequate accuracy. Furthermore, a lumped element resonator suffer from

a poor quality factor and can lead to a filter having severe loss and in turn hinder performance of the system. Therefore resonators and filters operating at RF and microwave frequencies are generally implemented using distributed circuit elements. On the other hand, the size of a distributed filtering circuit is directly proportional to the operating frequency, and sometimes it may prove difficult to integrate it into an IC at low frequencies.

Planar transmission line technologies such as microstrip and stripline are popular in the design of distributed filters due to their low cost, compactness of the structures they can realise and ease of integration with other subsystems [1-4]. Typically constructed as sections of transmission lines and printed on a dielectric substrate, these structures can create various shapes; such as meander, hairpin, ring, or patch configurations. However, these types of structures again suffer from relatively poor quality factors, which range roughly from 50-300 at 1 GHz [1-1], and also have low power handling capabilities. Thus these technologies are not a viable solution for realising filters for high power applications.

Waveguides and coaxial transmission line technologies offer advantages over the previously mentioned planar and lumped elements in terms of high quality factor and high power handling capabilities [1-1]. Cavity resonators formed out of coaxial, waveguide or dielectric technologies have quality factors up to 30000. Thus they provide an attractive alternative for realising filters for high frequency and high power applications. Generally coaxial and waveguide cavity resonators [1-5]-[1-7] are formed by having shorted half wave length ($\lambda/2$) transmission line sections, whereas dielectric resonators [1-8] are formed by having specially cut pieces of dielectrics mounted inside a waveguide housing using supporting structures. Due to the nature of their construction, waveguide resonators and filters suffer from disadvantages; such as increased time consumption due to design complexities, large sizes and high costs. A solution to the problem of high cost came with the invention of E-plane planar circuit mounted technology (E-plane technology), though large sizes and relatively poor stopband performance are areas still considered for improvement and achieving it will be the aim of this thesis.

Nowadays many communication systems are required to provide multiple services. Such multiservice systems will need to operate on different frequency bands and therefore require fixed filters operating at different frequencies. However, this can lead

to an increase in size as well as in cost. Tuneable and reconfigurable filters have a distinct advantage for such modules, as they are capable of providing compactness for these multifunctional systems [1-1]. Reconfigurable and tuneable elements, such as the PIN diode and varactor diodes [1-9]-[1-11] have been proposed and investigated for coplanar and microstrip based filters. Tuneable and reconfigurable waveguide filters have previously been proposed using magnetic tuning, such as YIG [1-12]-[1-13], and microelectromechanical system (MEMS) switches [1-14]-[1-15]. Magnetically tuned filters suffer from increased size and high cost of production, whereas MEMS shows good isolation and insertion loss characteristics, they are incapable of handling high power, involve a high level of design complexity and suffer from poor reliability [1-16].

This thesis addresses the fundamental issues pertaining to rectangular conventional E-plane waveguide filters. The aforementioned concerns, such as filter size, loss and selectivity, will be the core of the thesis and intend to propose E-plane waveguide filters that can achieve a size reduction of over 50% in comparison to conventional filters, while maintaining an acceptable passband insertion loss values which may be dictated by application. The structures proposed in this thesis may also lead to cost saving potential due to the interchangeable E-plane metallic inserts, which can be realised using copper sheets. Investigation into a compact reconfigurable E-plane waveguide filter using optically activated switches will also be presented. The rest of this chapter will provide a brief overview of the past research work carried out in the area of compact E-plane waveguide filters in order to provide a survey and a basis for comparison, followed by the aims and objectives of this investigation. Next, an outline of the thesis with a summary of each chapter is provided.

1.2 Overview of Past Research work in Compact Rectangular E-plane Waveguide Filters

Waveguides are one of the earliest devices used as a guiding medium for propagating electromagnetic waves. They usually take the form of hollow circular or rectangular shapes and are constructed out of conductive metal (mostly brass or aluminium). In perspective of wireless communication systems, these structures are widely used for high frequency filtering applications due to the numerous advantages they offer over other mediums, such as microstrip and coplanar transmission lines. These advantages include low loss at high frequencies, high quality factors of resonators and high power handling capabilities, which are of paramount importance for satellite, mobile base

stations and radar applications [1-17]. Conventional waveguide filters are formed using split-block housing and employ resonant cavities separated by inductive or capacitive irises.

The process for creating such resonant structures involves the use of micro-machining techniques. Due to this, despite the numerous advantages that waveguides offer, the fabrication process can be quite time consuming as well as costly. Furthermore, realisation of a structure with a new filtering function would require the fabrication of a completely new waveguide housing. Another disadvantage is the size of the resonant cavities at microwave frequencies, which are quite large and bulky. For applications where space is at a premium, such as in satellite systems, this may pose a considerable inconvenience. Hence, this method of realising waveguide filters can be quite inappropriate when taking into consideration of the ever growing developments towards cheap, compact and mass producible devices.

There are several methods of achieving size reduction of waveguide resonators and filters. The classical means of achieving compactness was to use dielectric filling within the cavities, which reduces the guided wavelength of the structure by the square root of the material permittivity. However, miniaturisation using this method is limited by the permittivity of the material. Furthermore, the practicality of this approach is constrained by the lack of dielectric material with a high permittivity and a low loss.

In 1974, Konishi and Uenakada introduced the planar circuit mounted E-plane strip [1-18] in order to address the cost related problems with waveguide filters. These types of waveguide filters soon came to be more commonly known as E-plane filters. E-plane filters utilise all metal inserts or metallo-dielectric inserts placed within the E-plane of a split block waveguide housing. These inserts consist of a sequence of periodically placed metallic obstacles known as septa. The distance between two metallic septa is roughly a half of the guided wavelength. Realisation of half wavelength resonators using E-plane inserts is very cost efficient and less time consuming, since the metal septa can be realised by using either copper foil or etched on to a dielectric substrate. Furthermore, the housing can be reused to form different filtering functions as only the insert is required to be interchanged. An example of a 3rd order conventional E-plane waveguide filter designed for a centre frequency of 9.5 GHz and 300 MHz bandwidth is shown in Figure 1.2-1 together with its S-parameter response given in Figure 1.2-2.

Having considered the cost saving potential of the E-plane filters, conventional E-plane filters still suffer from considerable large size as well as poor stopband performance. The 3rd order E-plane insert for the filter in Figure 1.2-1 has a length of 75.25mm. The large size is primarily due to the length of the half wavelength resonators and partly due to the large septum widths required for realising low couplings between adjacent resonators. In addition such filters also have poor upper stopband selectivity and the spurious resonance occur at 1.5 times the central frequency of the resonators, which may be insufficient to be used in diplexer or multiplexer configurations. Selectivity and stopband attenuation can be improved by increasing the filter order; however this will in turn increase the size of the filters.

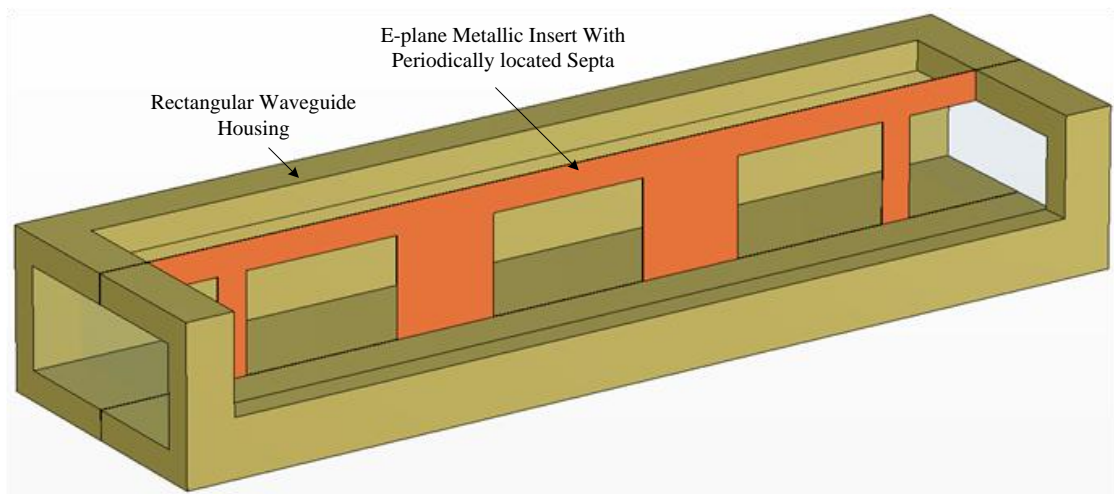


Figure 1.2-1: Inside view of a 3rd order E-plane rectangular waveguide filter.

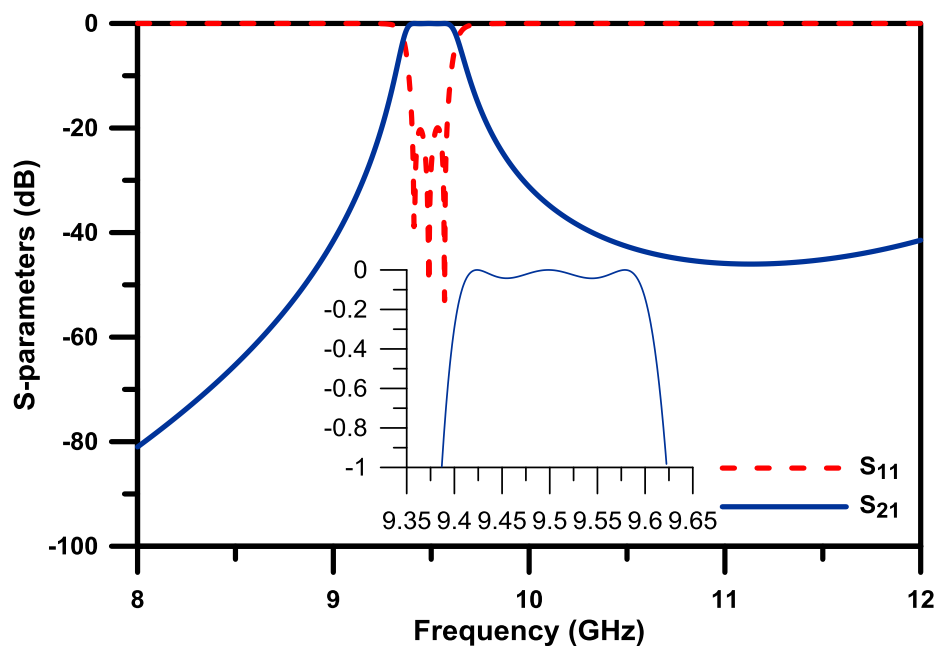


Figure 1.2-2: Frequency response of a 3rd order E-plane rectangular waveguide filter.

There are several attempts that have been made in previous work in order to address the performance and size related issues that plague the conventional E-plane filters. The first method utilises periodical structures embedded within the conventional E-plane resonator, and the phenomenon known as slow wave effect has been used to explain the miniaturisation achieved. The periodic elements are formed by equally spaced metallic ridges [1-19]. Slow wave effect is a well established method for achieving size reduction of resonators and is famous among planar resonator structures. To put simply, the method reduces the phase velocity of the fundamental mode of the resonator. This in turn minimises the resonator size in order to support the reduced guided resonant wavelength. It has been shown in [1-19] that this method can achieve a size reduction of roughly 50%. The authors attempt to further improve the stopband performance by introducing a low pass element prior to the band pass filtering module [1-20]. This method completely suppresses the spurious resonance due to the periodically placed structures. But due to the additional lowpass element, the size of the filter increases drastically.

Another method that makes use of the slow wave effect was proposed in [1-21]. In this article the authors present two structures. The first utilises high impedance surfaces on both the top and bottom planes of the resonant sections. The high impedance surface is constructed out of a dielectric substrate with an array of small square shaped metal patches etched on the surface and each of the metal patches are connected to the ground plane through drilled copper via posts. Their second approach utilises a Split ring resonator (SRR) placed within the centre of a conventional E-plane resonator where both the septa and the SRR are etched on to a dielectric substrate. Both the structures are capable of reducing the guided wavelength of the conventional E-plane resonators, thus achieving miniaturisation of the overall filter. Similar configurations of filters using embedded S-shape, T-shape and quarter wavelength resonators, which also generates transmission zeros to improve upper stopband selectivity has been proposed in [1-22]-[1-24]. For all cases, the theory of extracted pole sections has been applied to facilitate the design of these resonators and filters; where the design procedure for such filters based on extraction of generalised coupling coefficients can be found on [1-24].

In order to augment both the upper and lower stopband performance of the conventional E-plane filter in terms of selectivity and attenuation, while achieving size reduction of the filter, a cross-coupled filter topology was proposed in [1-25]. In this article, the authors demonstrate a folded 4th order E-plane filter, with source-load coupling as well

as cross coupling between resonators. The cross coupling is achieved through slots in the common wall separating two halves of the filter, which in turn leads to the creation of n number of transmission zeros; with n being the number of resonators. Despite the fact that source-load coupling can create filters with improved slope selectivity compared to all pole filters due to generation of transmission zeros, the locations of transmission zeros are very sensitive small changes in the dimensions, therefore making the filter more sensitive to manufacturing tolerances. In article [1-25] the authors propose a similar configuration of the filter, but with only cross-coupling between two resonators. Thus creating a single transmission zero which can be arranged to be either on the upper, lower or both sides of the stopband, depending on the type of cross-coupling (electric or magnetic), which in this case is determined by the position of the coupling slot. However considering the benefit that these filters give in terms of improved selectivity and attenuation, the size of the filters are still considerably large. This is due to the fact that even if the length of the structure is halved due to folding, the width of the structure now doubles its size.

A more compact E-plane doublet structure using source-load coupling has been proposed in [1-26]. This structure uses a couple of hair pin resonators etched on one side of a dielectric substrate and a wide septum on the opposite side for source-load coupling. This particular configuration of the hair pin resonators and the wide septum, allows the structure to generate single transmission zero in the upper and the lower stopband, thus improving stopband attenuation. Furthermore the structure is only 25 mm in length and is considerably smaller than the cross-coupled filter approach in [1-25].

1.3 Overview of Past Research work in Reconfigurable Rectangular Waveguide Filters

Research in tuneable and reconfigurable microwave filters has gained popularity in recent years due to the recent technological advancements in multifunctional communication systems. In comparison to using fixed filters, tuneable and reconfigurable filters are capable of providing greater functionality as well as compactness for these multifunctional systems [1-1]. Typically a filter can be made to change its central frequency by attaching uniformly controlled reconfigurable elements to each resonator which forms the filter. Examples of these reconfigurable elements include PIN diodes, micro electro mechanical systems (MEMS) and the Optical switch.

Examples of tuneable elements include the varactor diodes, ferromagnetic materials and liquid crystals.

PIN and varactor diodes are generally used in implementing reconfigurable and tuneable planar microwave antennas and filters [1-9]-[1-11]. Their reliability, versatility in circuit implementation and the extreme low cost of production makes them an attractive solution for such planar microwave devices. However, their high power consumption during ON state and poor quality factors makes them inappropriate for high frequency applications. Furthermore, the need for biasing circuits increases the design complexity of structures utilising PIN diodes, as they cause interference with the rest of the circuit and therefore need to be accounted for during the design process. Due to the above reasons no real applications of the PIN diode as a reconfigurable element in waveguide filters have been reported in literature.

MEMS based switches essentially behave similar to voltage controlled actuators. They can either be used as a switch or a variable capacitor. Switches based on MEMS technology are capable of providing a good isolation, have low power consumption, high linearity, reduced insertion loss and higher quality factors compared to PIN diodes [1-4]. Due to these reasons, research on the application of RF-MEMS for implementing reconfigurable waveguide filters has gained an increasing attention. In [1-27] the authors propose a tuneable waveguide cavity resonator using capacitive RF-MEMS cantilever switches, covering a tuneable frequency range from 5.5 to 4.3 GHz. The prototype of the resonator also reports Q factors between from 425 to 528 for the tuneable frequency range; which according to the authors, are the highest Q factor reported for a RF-MEMS based tuneable waveguide resonator at this point. The authors have also extended this approach to a tuneable waveguide cavity filter demonstrated in [1-18]. E-plane reconfigurable waveguide resonators and filters at K-band using RF-MEMS cantilever switches have been demonstrated in [1-28]. The switches are used to connect printed metallic lines and placed on to an inner side-wall of the waveguide. The activation of the switches leads to the realisation of an equivalent movable inner wall which causes a shift in the resonance frequency. The proposed filter has been shown to produce a frequency shift of 730 MHz with measured unloaded quality factors of 750 and 1450 in the ON and OFF states respectively.

1.4 Aims and Objectives of the Thesis

Due to the nature and the construction of waveguides transmission lines using metallic housing, rectangular waveguide filters suffer from increased size and cost of production. Therefore, the core aim of this thesis is to investigate and develop compact rectangular waveguide filters with improved stopband performance for wireless applications. The investigation will be carried out in the following stages.

Since planar circuit mounted E-plane strip is a cost effective means of realising inline waveguide resonators and filters, the initial stage of the research work carried out will contemplate on improving the current range of such E-plane resonators and filters. Resonators are the building blocks of filters. Therefore the first step in achieving compactness of waveguide filters will concentrate on developing a method of miniaturising the corresponding resonators. Special attention will be given to the waveguide extracted pole section (EPS), as it is capable of generating a single pole and a single transmission zero to improve upper stopband selectivity, while achieving a considerable size reduction through the use of non resonating nodes (NRN) [1-23].

A new compact inline E-plane wave guide resonator will be developed. The structure will be based upon the principle operation of the EPS, but will be required to provide improved performance and size reduction in comparison to the conventional product. An electrical equivalent circuit will be constructed and a comprehensive analysis of the structure will be conducted, which will include the origin of the generated transmission zeros and the resonances. The effects of the physical dimensions on the transmission characteristics will also be studied. Next improved highly compact filters with transmission zeros in both the upper and lower stopbands will be designed and constructed based on the aforementioned compact resonators. Experimental verification of such highly compact resonators and filters will be provided in order to validate the simulated results.

Cross-coupled filters are an attractive method for filter design as they are capable of producing transmission zeros to improve both selectivity and stopband performance. Therefore as the second objective, the application of cross-coupled resonators with regards to the design of compact filters with transmission zeros in conventional rectangular waveguides using all metal inserts will be conducted. The first step, while taking into consideration of the design constraints, will be to determine the type of resonator that would be most suitable and the coupling scheme that can be realised for

implementing within the rectangular waveguide. The second step will be to develop a suitable procedure for determining the initial dimensions of the proposed cross-coupled filters which might involve extraction of the model parameters from simulation results. Experimental verification of such compact cross coupled filters will be provided to validate the accuracy of the design process.

The third objective of this investigation will be to focus on the development of compact tuneable waveguide resonators and filters. The possibility of tuneable filters for achieving size reductions to RF front-end of a communication system, has enthused a growing research interest in this area. This in turn, has led to development of some novel tuneable elements. The investigation will, for the first time, concentrate on the possible application of an N-type silicon dice doped with phosphorus as a switching element for a tuneable waveguide resonator. The functioning of the silicon dice as a switch will depend on optical illumination. A prototype of a novel optically tuneable waveguide resonator will be designed, fabricated and tested.

1.5 Outline of The Thesis

This section summarizes the contents of the thesis which present work carried out for a period from 2011-2014 which is organized into six chapters.

The Chapter 2 present a brief introduction to the background material that is relevant to the research work undertaken. The chapter commence with a brief discussion of rectangular waveguides and several of its important properties that make this technology very attractive for filter implementation. Basic filter theory and the design of band pass filters through synthesis of filter prototypes for both direct coupled and cross coupled filters have been presented. It also brings into attention the importance of non-resonating node and the extracted pole section in the design of compact filters.

Chapter 3 present the development of compact high performance E-plane waveguide filters. The chapter begins with an introduction to the conventional E-plane waveguide resonators and filters as it is the most basic level of the structures that will be discussed in this thesis. It also demonstrate the realisation of an E-plane extracted pole section and how cascading several of such sections can lead to the creation of compact high performance waveguide filters. Expanding on this, the chapter finally present a novel ultra compact E-Plane waveguide filter which is approximately 65% more compact than filters formed out of the traditional E-plane extracted pole sections.

Chapter 4 demonstrate the development of highly compact E-plane cross coupled filters using all metallic inserts within a rectangular waveguide. Two separate filtering modules known as the singlet and the doublet are introduced, where the first has the capability to produce a single pole and a transmission zero either in the upper or lower stopband and the latter generates a transmission zero in both upper and lower stopbands. The chapter then introduces the new configuration of the E-plane insert that can realise both the aforementioned modules. Next two highly compact experimental filters which implement the proposed singlet and doublet sections in cascade with extracted pole sections are proposed. Extraction of generalized coupling coefficients from the EM-simulated responses for symmetric singlet and doublet filtering blocks has been presented in order to facilitate the development of these filters.

Chapter 5 details an implementation of an optically reconfigurable E-plane waveguide resonator. The photoconductive properties of silicon and the advantages it offers in terms of high power handling capabilities, high switching speeds and due to the fact that

they do not require any biasing circuits, make it a very attractive option for implementing in waveguide filters. The chapter gives a brief overview of the phenomenon that takes place within a dice of silicon when illuminated with light of appropriate wavelength that consent to it being used as a switching element. This is followed by the E-plane waveguide resonator structure and how it is modified to include the optical switch in order to achieve frequency switching characteristics. Measurement results of a fabricated prototype will be provided in order to validate the performance of the proposed tuneable E-plane waveguide resonators. Taking into consideration of the measured results of the reconfigurable resonator, simulated results for an optically reconfigurable E-plane filter is also provided.

Finally in Chapter 6, the main conclusion of the work presented in this thesis is given a summary of the contribution of this work and suggestions for future work are highlighted.

A list of achievements of the research work conducted and presented in this thesis is summarised in Table 1.5-1.

1.	The development of a novel direct coupled ultra-compact E-plane waveguide filter with improved upper and lower stopband performance in comparison to conventional E-plane waveguide filters has been conducted. Experimental verification of the structure has been provided. A size reduction of approximately 85% can be achieved.
2.	The thesis presents the development of novel compact modular E-plane cross-coupled waveguide filters. Filtering modules known as the singlet and the doublet have been physically realised and implemented using dual metallic inserts placed within the E-plane of WR90 (WG16) rectangular waveguide housing. In order to tackle the problem with sensitivity due to dimension variations, which increase significantly with higher order filters with source-load coupling, a modular cross-coupled topology has been realised using dual metallic inserts.
3.	For the first time, the implementation of optically reconfigurable E-plane waveguide resonators and filters using a photoconductive switch has been presented.

Table 1.5-1: Table of achievements.

1.6 References

- [1-1] R. J. Cameron, C. M. Kudsia, and R. R. Mansour, *Microwave filters for communication systems: fundamentals, design, and applications*. Hoboken, New Jersey: John Wiley & Sons, 2007.
- [1-2] G. L. Matthaei, L. Young and E. M. T. Jones, *Microwave filters, impedance matching networks, and coupling structures*, Dedham, MA: Artech House, 1964.
- [1-3] M. N. S. Swamy and K.-L. Du, *Wireless Communication Systems: From RF Subsystems to 4G Enabling Technologies*, New York: Cambridge University Press, 2010.
- [1-4] F. Ellinger, *Radio Frequency Integrated Circuits and Technologies*, Berlin: Springer, 2007.
- [1-5] R. Wenzel, "Synthesis of combline and capacitively loaded interdigital bandpass filters of arbitrary bandwidth," *IEEE Trans. Microwave Theory Tech.*, vol. 19, no. 8, pp. 678–686, Aug. 1971.
- [1-6] Ali E. Atia and Albert E. Williams, "Narrow-Bandpass Waveguide Filters", *IEEE Trans. Microwave Theory Tech.*, vol. 20, no. 4, pp.258-265, April 1972.
- [1-7] S. Amari and U. Rosenberg, "New building blocks for modular design of elliptic and self-equalized filters," *IEEE Trans. Microwave Theory Tech.*, vol. 52, no. 2, pp. 721–736, Feb. 2004.
- [1-8] S. B. Cohn, "Microwave filters containing high-Q dielectric resonators," *IEEE Trans. Microwave Theory Tech.*, vol. 16, no. 4, pp. 218–227, Apr. 1968.
- [1-9] K. Rabbi and D. Budimir, "Highly Selective Reconfigurable Filter for UWB Systems," *Microwave and Wireless Components Letters, IEEE*, vol. 24, no.3, pp. 146,148, March 2014.
- [1-10] L. Athukorala and D. Budimir, "Open-loop tunable resonators and filters with constant bandwidth," *Microwaves, Antennas & Propagation, IET*, vol. 6, no. 7, pp. 800,806, May 16 2012.

- [1-11] L. Athukorala and D. Budimir, "Compact Second-Order Highly Linear Varactor-Tuned Dual-Mode Filters With Constant Bandwidth," *Microwave Theory and Techniques, IEEE Transactions on*, vol. 59, no. 9, pp. 2214,2220, Sept. 2011.
- [1-12] J. Uher and W.J.R. Hoefer, "Tunable microwave and millimeter-wave band-pass filters," *Microwave Theory and Techniques, IEEE Transactions on*, vol. 39, no. 4, pp. 643-653, Apr 1991.
- [1-13] P. Bernardi and F. Valdoni, "Fundamentals of a new class of magnetically tunable waveguide filters," *Magnetics, IEEE Transactions on*, vol. 2, no. 3, pp. 264-268, Sep 1966.
- [1-14] Sang-June Park, I. Reines, C. Patel and G.M Rebeiz, "High-Q RF-MEMS 4–6 GHz Tunable Evanescent-Mode Cavity Filter," *Microwave Theory and Techniques, IEEE Transactions on*, vol. 58, no. 2, pp. 381-389, Feb. 2010.
- [1-15] Winter Dong Yan and R.R Mansour, "Tunable Dielectric Resonator Bandpass Filter with Embedded MEMS Tuning Elements," *Microwave Theory and Techniques, IEEE Transactions on*, vol. 55, no. 1, pp. 154-160, Jan. 2007.
- [1-16] G. M. Rebeiz and J. B. Muldavin, "RF MEMS switches and switch circuits," *Microwave Magazine, IEEE*, vol. 2, no. 4, pp. 59-71, Dec 2001.
- [1-17] D. Budimir, *Generalized Filter Design by Computer Optimization*, Artech House, 1998.
- [1-18] Y. Konishi and K. Uenakada, "The Design of a Bandpass Filter with Inductive Strip Planar Circuit Mounted in Waveguide," *IEEE Trans. Microwave Theory Tech.*, vol. 22, no. 10, pp. 869-873, Oct.1974.
- [1-19] G. Goussetis and D. Budimir, "Novel periodically loaded E-plane filters," *Microwave and Wireless Components Letters, IEEE*, vol. 13, no. 6, pp. 193-195, June 2003
- [1-20] G. Goussetis and D. Budimir, "Compact ridged waveguide filters with improved stopband performance," in *IEEE MTT-S Int. Microw. Symp. Dig.*, vol. 2, pp. 953–956, Jun 2003.

- [1-21] A. Shelkovnikov and D. Budimir, "Miniaturized Rectangular Waveguide Filters," *Int. J. RF and Microwave CAE*, vol. 17, no. 4, pp. 398-403, 2007.
- [1-22] N. Suntheralingham and D. Budimir, "Enhanced Waveguide Bandpass Filters Using S-shaped Resonators," *Int. J. RF and Microwave CAE*, vol. 19, no. 6, pp. 627-633, 2009.
- [1-23] O. Glubokov and D. Budimir, "Extraction of Generalized Coupling Coefficients for Inline Extracted Pole Filters With Nonresonating Nodes," *Microwave Theory and Techniques, IEEE Transactions on*, vol. 59, no. 12, pp. 3023-3029, Dec. 2011.
- [1-24] O. Glubokov (2011). *Development of Waveguide Filter Structures for Wireless and Satellite Communications*. PhD. Thesis. University of Westminster: UK.
- [1-25] E. Ofli, R. Vahldieck and S. Amari, "Novel E-plane filters and diplexers with elliptic response for millimeter-wave applications," *Microwave Theory and Techniques, IEEE Transactions on*, vol. 53, no. 3, pp. 843-851, March 2005.
- [1-26] O. Glubokov and D. Budimir, "Compact E-plane doublet structures for modular filter design," *Microwave Conference (EuMC), 2010 European*, pp.1253,1256, 28-30 Sept. 2010.
- [1-27] S. J. Park, I. Reines and G. Rebeiz, "High-Q RF-MEMS tunable evanescent-mode cavity filter," *Microwave Symposium Digest, 2009. MTT '09. IEEE MTT-S International*, pp.1145-1148, 7-12 June 2009.
- [1-28] L. Pelliccia, F. Cacciamani, R. Sorrentino, P. Farinelli, P. Ligander and O. Persson, "High-Q MEMS-tunable waveguide filters in K-band," *Microwave Conference (EuMC), 2012 42nd European*, pp. 273-276, 29 Oct. 2012-1 Nov. 2012.

CHAPTER 2

BACKGROUND

The following chapter concisely highlight some of the basic knowledge that is requisite and relevant to the subject of this thesis. In section 2.1, a brief discussion of the advantages and disadvantages of microwave filters formed of waveguides will be provided, followed by several of their important properties that make this technology suitable for filter implementation. Section 2.2-2.6 will detail the basic filter theory and the design of bandpass filters through synthesis of filter prototypes for both direct-coupled and cross-coupled filters. Section 2.7 emphasise the importance of extracted pole section in the design of compact filters, where as the use of non-resonating nodes for modular design of elliptic filters will be highlighted in section 2.8.

2.1 Rectangular Waveguides

Rectangular waveguides are hollow metallic tubes which are widely used as a conduit for transferring electromagnetic waves between two points. Their introduction and applications have a history dating back to the late 19th century. Widely used in many microwave and millimetre wave communication systems, these structures have a unique set of advantages over transmission lines mediums, like the microstrip, stripline and coaxial. These advantages include high power handling capability and high Q factors which are revealed by waveguide cavities and are important for communication systems such as radar, satellite and in mobile base stations. However, conventional waveguide filters are bulky and take up a large amount of space, which in turn can increase the cost of wireless systems. This has enthused scientists and engineers to research on waveguide miniaturisation.

Due to the nature of its construction, the aforementioned transmission line mediums, tend to suffer from relatively high loss from dielectric and radiation losses. And these losses increase rapidly at higher frequencies due to the unavailability of low loss dielectric materials. It is at these frequencies that waveguides become practical due to their unique advantages.

Unlike microstrip, stripline and the coaxial transmission lines, waveguides are modelled as a single enclosed conductor as it typically consist of just one propagating path. Waveguides do not support Transverse Electromagnetic (TEM) modes as no solution exists for the Maxwell's equations that satisfy the boundary condition for the TEM mode to occur [2-1]. However, waveguides support Transverse Electric (TE) and Transverse Magnetic (TM) modes. Due to this reason, waveguides are also limited by their cut-off frequency of the dominant TE_{10} mode. This phenomenon that pertains to waveguides can be well described through solving Maxwell's equations and a detailed analysis of the structure can be found in [2-1].

A diagram of a hollow metallic rectangular waveguide structure is given in Figure 2.1-1. The waveguide is assumed to be homogeneous, vacuum filled and have zero conductor losses. It is also oriented in such a way that the electromagnetic waves propagate along the Z direction.

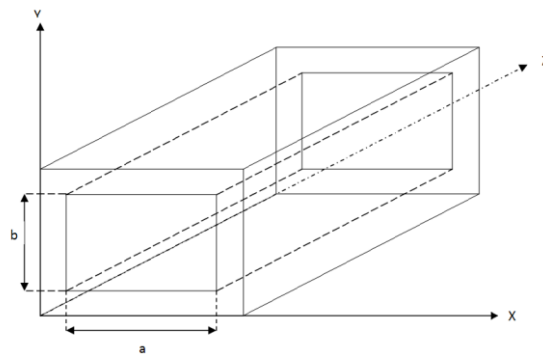


Figure 2.1-1: Conventional rectangular waveguide configuration.

The electromagnetic fields within a waveguide always have some specific form. If just a cross section of the waveguide is taken into consideration, the half sinusoidal variations of the electromagnetic field distribution patterns along dimensions 'a' and 'b' of a waveguide can be recognised as waveguide modes. These modes are assigned to two categories, TE (electric field is orthogonal to the direction of propagation) and TM (magnetic field is orthogonal to the direction of propagation). The number of these half sinusoidal variations along the cross dimensions represents the order of the mode. I.e. if we consider TE_{mn} modes, the subscript 'm' represent number of half sinusoidal waveforms across dimension 'a' where as 'n' represent that across dimension 'b'. A graphical illustration of some of the different types of modes that can be supported by a waveguide can be found in [2-1].

The cut-off frequency of a rectangular waveguide is a geometrical parameter that depends on the cross-dimensions of the structure. The larger these dimensions are, the lower is the cut off frequency of the waveguide and also the range of recommended operating frequencies. The cut-off frequency for a rectangular waveguide is given in (2.1.1), where c is the speed of light, μ and ε represents the permeability and permittivity respectively of the materials that fill the waveguide, m and n are integers that represent the order of the TM or TE mode. It is evident that as the order of the mode reduces, so does the cut-off frequency. If TM modes are considered, where the longitudinal component of the magnetic field is zero, but the longitudinal component of the electric field exists, through solving Maxwell's equations and by applying the correct boundary conditions in order to satisfy this condition, it can be proven that the order of the lowest TM mode is TM_{11} [2-1].

$$f_c = \frac{1}{2\pi\sqrt{\mu\varepsilon}} \cdot \sqrt{\left(\frac{m\pi}{a}\right)^2 + \left(\frac{n\pi}{b}\right)^2} \quad (2.1.1)$$

Similarly by applying the boundary conditions for TE mode of propagation, it can be proven that either m or n can be zero at one point, however not both at the same time, and that the lowest cut-off wave mode is the TE_{10} mode. For this mode, the cut-off frequency reduces down to:

$$f_c = \frac{1}{2\pi\sqrt{\mu\varepsilon}} \cdot \sqrt{\left(\frac{\pi}{a}\right)^2} = \frac{v}{2\pi} \cdot \frac{\pi}{a} \quad (2.1.2)$$

Where $v = \frac{1}{\sqrt{\mu\varepsilon}}$ is the velocity of light in a dielectric medium and since $v = f\lambda$, then dimension 'a' can be written as:

$$a = \frac{\lambda_c}{2} \quad (2.1.3)$$

Figure 2.1-2 below presents the cut-off frequencies of the TE and TM modes for WG16 (WR90) waveguide with inner dimensions $a = 22.86$ mm and $b = 10.16$ mm. Due to the infinite amount of modes the structure support, only the first few are presented.

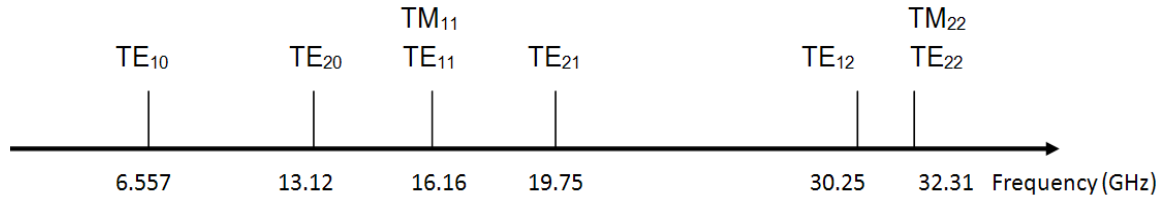


Figure 2.1-2: Cut off Frequencies of TE and TM Modes of a conventional rectangular waveguide.

At frequencies $f > f_c$, the propagation constant is purely imaginary and is called phase constant β [2-1]. In this case, in terms of the cut-off frequency, it is given by:

$$\beta = 2\pi f \sqrt{\mu\epsilon} \cdot \sqrt{1 - \left(\frac{f_c}{f}\right)^2} \quad (2.1.4)$$

The guided wavelength is defined as the distance in the z-direction of propagation required for a phase change of 2π . Hence for each propagating mode at operating frequency f_0 , this is given as:

$$\lambda_g = \frac{2\pi}{\beta} = \frac{\lambda_0}{\sqrt{1 - \left(\frac{f_c}{f}\right)^2}} \quad (2.1.5)$$

As mentioned before, the fundamental propagating mode of a rectangular waveguide cavity occurs when $m = 1$ and $n = 0$, i.e. TE₁₀. The wave impedance for the TE₁₀ mode is given as [2-1]:

$$Z_{TE} = \frac{\eta}{\sqrt{1 - \left(\frac{f_c}{f}\right)^2}} \quad (2.1.6)$$

Where $\eta = \sqrt{\frac{\mu}{\epsilon}}$ is known as the intrinsic wave impedance of a plane wave propagating in an unbounded medium.

2.2 Bandpass Filter Theory

Microwave filters play a key role in modern wireless communication systems by providing a means for frequency band separation. These essential components are constituted either of lumped elements (inductors, capacitors and resistors) or distributed elements (waveguide sections, microstrip, fin-line or any other medium). The elements of the filters are arranged in a particular topology, such that it allows the desired signal to pass within a specified range of frequencies with minimum attenuation, while suppressing (attenuating) all undesired frequencies. In an ideal sense, the filter networks should be able to provide perfect transmission for all frequencies in the desired passband, whereas in the stopband, it should provide infinite attenuation. Electrical filters can be distinguished into four different types according to their filtering properties. These are known as lowpass, highpass, bandpass, and bandstop. Ideal filter responses are shown in Figure 2.2-1, where it shows the transmission of signals outside of the desired passband are completely rejected. However in practice, ideal filter responses are not feasible. Practically, no actual filter can ever operate over an unlimited frequency range as all filters exhibit spurious responses and all filter elements have losses associated with them.

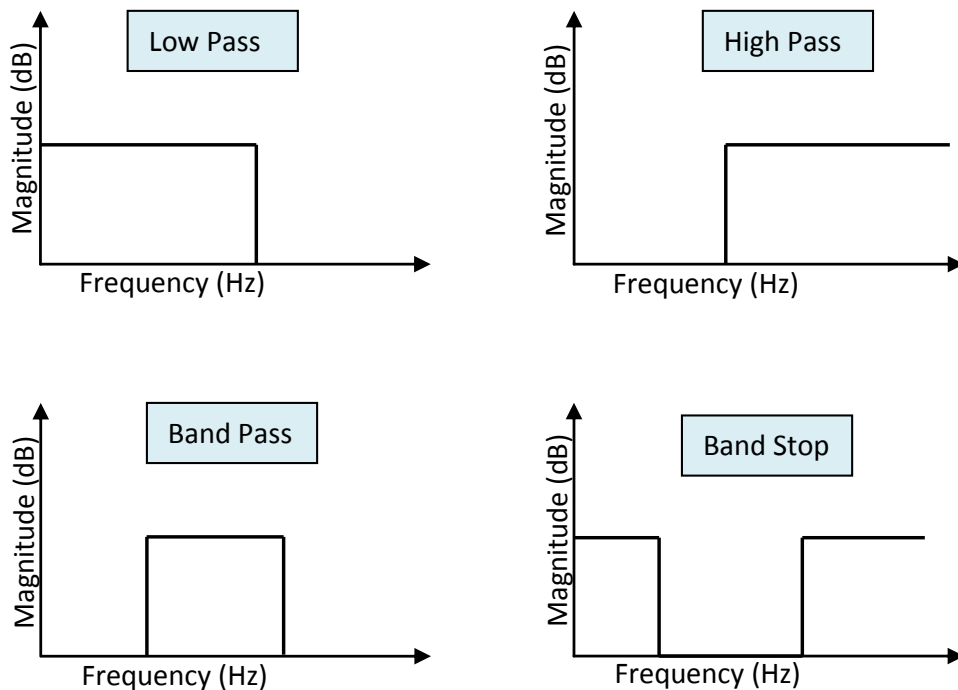


Figure 2.2-1: Typical frequency response of a rectangular waveguide.

There are several different well known characteristic functions that can be used to approximate the ideal responses that are shown in Figure 2.2-1. They are known as Butterworth, Chebyshev, and Elliptic functions. Each one of them can be used during filter design procedure, depending on the specification and characteristics of the frequency response required from the circuit under consideration. Filter design procedure generally starts off with the approximation of one of the abovementioned filter transfer functions in order to synthesise a lowpass prototype filter network, after which scaling and transformation of the network to the required filter type will be carried out. The transformed network can then be realised physically through either lumped or distributed elements. Lumped elements are used to realise filters operating at low frequencies where physical dimensions of the circuit are a lot less than that of the operating wavelength. Due to the ease of construction of these components, they are easy to mass produce and are convenient for realising low cost filters. However at higher frequencies, the physical dimensions of the circuits become comparable to the operating wavelength and their frequency behaviour becomes more complex. Therefore, filter design in this case is carried out using distributed elements and methods to design and implement microwave filters with distributed elements is well described in [2-2]

A doubly terminated lossless transmission network which may be used to represent a lossless bandpass filter is illustrated in Figure 2.2-2. Assuming that the input power to be transmitted is represented as P_{in} , the power received at the load is P_{out} , and since P_{out} can never exceed P_{in} in passive circuits, it can be denote that:

$$\frac{P_{in}}{P_{out}} = 1 + |K(s)|_{s=j\omega}^2 \quad (2.2.1)$$

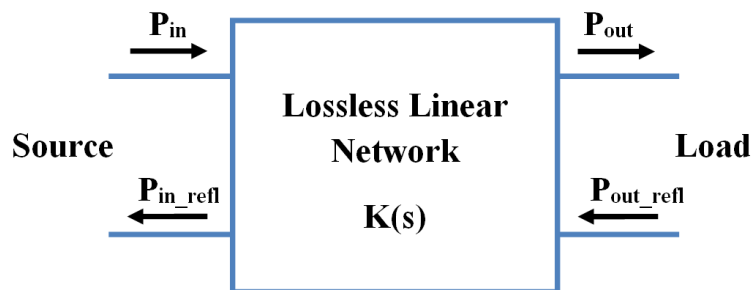


Figure 2.2-2: A doubly terminated lossless linear network.

Here $K(s)$ is known as the characteristic function and the inverse of the power ratio in equation (2.2.1) shows the squared magnitude of the transmission coefficient. This in

transmission line theory is known as the scattering parameter $S_{21}(s)$ [2-3] and is given in equation (2.2.2).

$$|S_{21}(s)|_{s=j\omega}^2 = \frac{1}{1 + |K(s)|_{s=j\omega}^2} \quad (2.2.2)$$

The reflected power is characterised by the reflection coefficient or by the scattering parameter $S_{11}(s)$. For lossless networks this parameter is related to $S_{21}(s)$ through the following expression [2-3]:

$$|S_{11}(s)|^2 + |S_{21}(s)|^2 = 1 \quad (2.2.3)$$

It is shown in [2-3] that for a linear time invariant networks, $S_{11}(s)$ and $S_{21}(s)$ can be represented as a ratio of two of the corresponding polynomials $F(s)$, $E(s)$ and $P(s)$ where $s = j\omega$. These polynomials are also known as characteristic polynomials and the characteristic function $K(s)$ can also be represented by using these polynomials for which the expressions are given in equations (2.2.4-2.2.6).

$$S_{11}(s) = \frac{F(s)}{E(s)} \quad (2.2.4)$$

$$S_{21}(s) = \frac{P(s)}{\varepsilon \cdot E(s)} \quad (2.2.5)$$

$$K(s) = \varepsilon \cdot \frac{F(s)}{P(s)} \quad (2.2.6)$$

The constant ε in (2.2.5) and (2.2.6) is known as the ripple factor and is used to normalise the maximum amplitude in the passband of the filter response, by normalising the characteristic polynomials $F(s)$ and $P(s)$ [2-3]. The following subsections will briefly outline properties of some of the well known characteristic functions, such as the Butterworth or maximally flat, Chebyshev and generalized Chebyshev (pseudo-elliptic), in terms of the characteristic polynomials.

2.2.1 Butterworth Approximation

The Butterworth, also known as maximally flat is the simplest approximation available and it is used for describing lowpass filters designed to have a maximally flat frequency response as possible in the passband. This is an all pole filter function and the approximation is defined by [2-3]:

$$K(\omega) = \varepsilon \cdot \omega^n \quad (2.2.1.1)$$

Where n is the order of the polynomial and represent the degree of the prototype network and ε is the ripple factor. The above approximation suggests that the characteristic polynomials $P(s) = 1$ and $F(s) = s^n$ and the S-parameters of a filter prototype can be determined as:

$$|S_{21}(s)|_{s=j\omega}^2 = \frac{1}{1 + \omega^{2n}} \quad (2.2.1.2)$$

$$|S_{11}(s)|_{s=j\omega}^2 = \frac{\omega^{2n}}{1 + \omega^{2n}} \quad (2.2.1.3)$$

Consequently, the coefficients of the polynomial $E(s)$ can be derived from the following expression [2-3]:

$$s_k = \begin{cases} \exp\left[\frac{j\pi}{2n}(2k-1)\right], & \text{for } n \text{ even} \\ \exp\left(\frac{j\pi k}{n}\right), & \text{for } n \text{ odd} \end{cases} \quad (2.2.1.4)$$

where $k = 1, 2, \dots, 2n$. As an example, the calculated maximally flat prototype responses corresponding to several circuit orders are illustrated in Figure 2.2-3.

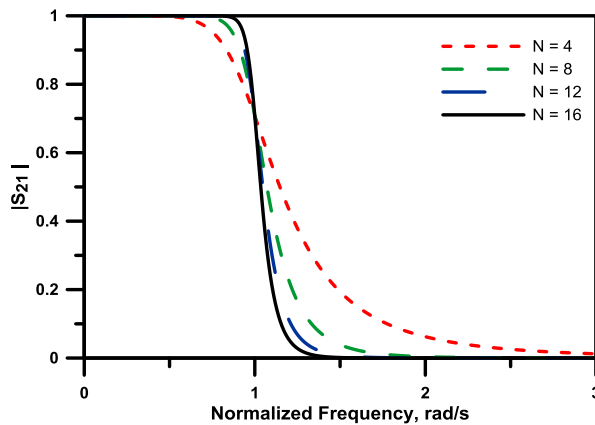


Figure 2.2-3: Frequency response of the maximally flat filter for various filter orders N .

2.2.2 Chebyshev Approximation

The Chebyshev approximation is capable of producing sharper roll-offs (transition slopes) for lower order filters in comparison to maximally flat approximation. However, due to the equidistant spacing of the location of poles within the passband of the filter, Chebyshev filters exhibit an equi-ripple response in the passband [2-3]. The Chebyshev characteristic function is defined as:

$$K(\omega) = \varepsilon \cdot T_n(\omega) \quad (2.2.2.1)$$

Where $T_n(\omega)$ is a Chebyshev polynomial of degree n . Hence we can observe that characteristic polynomials $P(s) = 1$ and $F(s) = T_n(s/j)$ and the expressions for the S-parameters yield:

$$|S_{21}(s)|_{s=j\omega}^2 = \frac{1}{1 + \varepsilon^2 T_n^2(\omega)} \quad (2.2.2.2)$$

$$|S_{11}(s)|_{s=j\omega}^2 = \frac{\varepsilon^2 T_n^2(\omega)}{1 + \varepsilon^2 T_n^2(\omega)} \quad (2.2.2.3)$$

The following trigonometric expression can be used to define the Chebyshev polynomials [2-3]:

$$T_n(x) = \cos(n \cdot \arccos(x)) \quad (2.2.2.4)$$

The characteristic polynomial $E(s)$ can be derived from the product of the left half plane roots $s_k = \sigma_k + j\omega_k$, i.e. $\sigma_k < 0$, where σ_k and ω_k can be calculated as [2-3]:

$$\sigma_k = \pm \sinh\left(\frac{1}{n} \cdot \sinh^{-1} \frac{1}{\varepsilon}\right) \sin \frac{\pi}{2} \cdot \frac{2k-1}{n}, \quad (2.2.2.5)$$

$$\omega_k = \cosh\left(\frac{1}{n} \cdot \sinh^{-1} \frac{1}{\varepsilon}\right) \cos \frac{\pi}{2} \cdot \frac{2k-1}{n}, \quad (2.2.2.6)$$

Where $k = 1, 2, \dots, 2n$.

A typical frequency response of a Chebyshev filter prototype is presented in Figure 2.2-4.

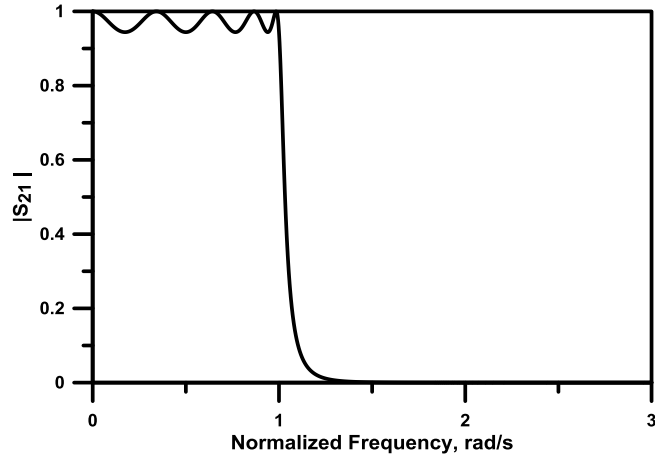


Figure 2.2-4: Chebyshev Lowpass filter prototype frequency response.

2.2.3 The Generalised Chebyshev Approximation

The Generalised Chebyshev, also known as pseudo-elliptic approximation, allows for realisation of filters with an equi-ripple characteristic in the passband region and designer pre-defined transmission zeros in the stopband region. The advantage this provides is that it allows for highly selective filters with sharp transition bands and asymmetrical frequency responses. Furthermore, the locations of the transmission zeros generated are not restricted to just occur at real frequencies only. The Generalized Chebyshev characteristic function is defined as [2-3]:

$$K(\omega) = \varepsilon \cdot C_N(\omega) \quad (2.2.3.1)$$

Where

$$C_N(\omega) = \cosh \left(\sum_{n=1}^N \cosh^{-1}(x_i(\omega)) \right) \quad (2.2.3.2)$$

And

$$x_i(\omega) = \frac{\omega - \frac{1}{\omega_{Tzi}}}{1 - \frac{\omega}{\omega_{Tzi}}} \quad (2.2.3.3)$$

It is to be noted that, ω is the angular frequency variable, whereas ω_{Tzn} represent the location of the n^{th} transmission zero.

Therefore the transmission coefficient S_{21} is represented as follows [2-3]:

$$|S_{21}(s)|_{s=j\omega}^2 = \frac{1}{1 + \varepsilon^2 C_N^2(\omega)} \quad (2.2.2.4)$$

Taking into consideration of equation (2.2.6), it is possible to write the filtering function $C_N(\omega)$ as a ratio of two polynomials:

$$C_N(\omega) = \varepsilon \cdot \frac{F_N(\omega)}{P_N(\omega)} \quad (2.2.2.5)$$

Where the characteristic polynomial $P_N(\omega)$ can be composed directly out of the transmission zeros, while polynomial $F_N(\omega)$ is generated using a recursive technique [2-3]:

$$F_N(\omega) = \frac{1}{2} [G_N(\omega) + G'_N(\omega)] \quad (2.2.2.6)$$

$$G_N(\omega) = \prod_{i=1}^N \left[\left(\omega - \frac{1}{\omega_{Tzi}} \right) + \omega' \sqrt{\left(1 - \frac{1}{\omega_{Tzi}^2} \right)} \right] \quad (2.2.2.7)$$

$$G'_N(\omega) = \prod_{i=1}^N \left[\left(\omega - \frac{1}{\omega_{Tzi}} \right) - \omega' \sqrt{\left(1 - \frac{1}{\omega_{Tzi}^2} \right)} \right] \quad (2.2.2.8)$$

where $\omega' = \sqrt{\omega^2 - 1}$.

An example of a generalized Chebyshev filter prototype response is given in Figure 2.2-5

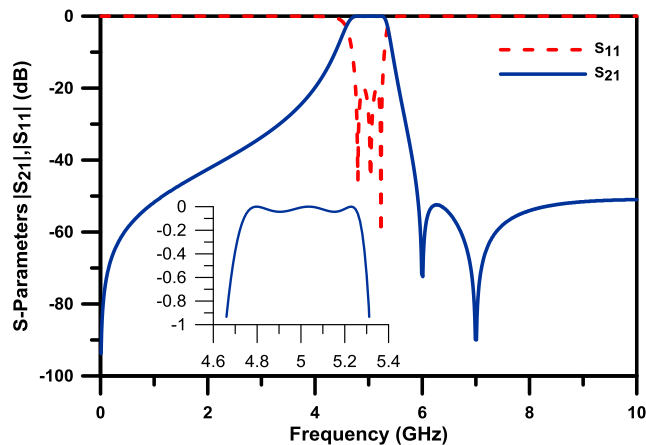


Figure 2.2-5: Generalized Chebyshev (psudeo-elliptic) response of a third order filter with two prescribed transmission zeros in the upper stopband.

2.3 Filter Prototypes

Once the approximation process for the characteristic polynomials has been completed, the next step is to synthesis a suitable equivalent filter prototype network that satisfies the given specification. The prototype network acts as link between the theoretical filtering function and the physical structure to be realised. Generally, the lowpass filter prototype networks are chosen initially. Thereafter, desired network transformation procedures are applied depending on whether a bandpass, bandstop or highpass filter network is required. The maximally flat and Chebyshev lowpass filter responses can be realised by prototype network comprising of capacitors and inductors in shunt and series configuration, as illustrated in Figure 2.3-1. For odd order filters, the ladder network is symmetrical, else asymmetrical for even order network. The element values of the ladder network are normalised so that the input and output impedances are set to unity and the total number of elements required are determined by the degree of the polynomial.

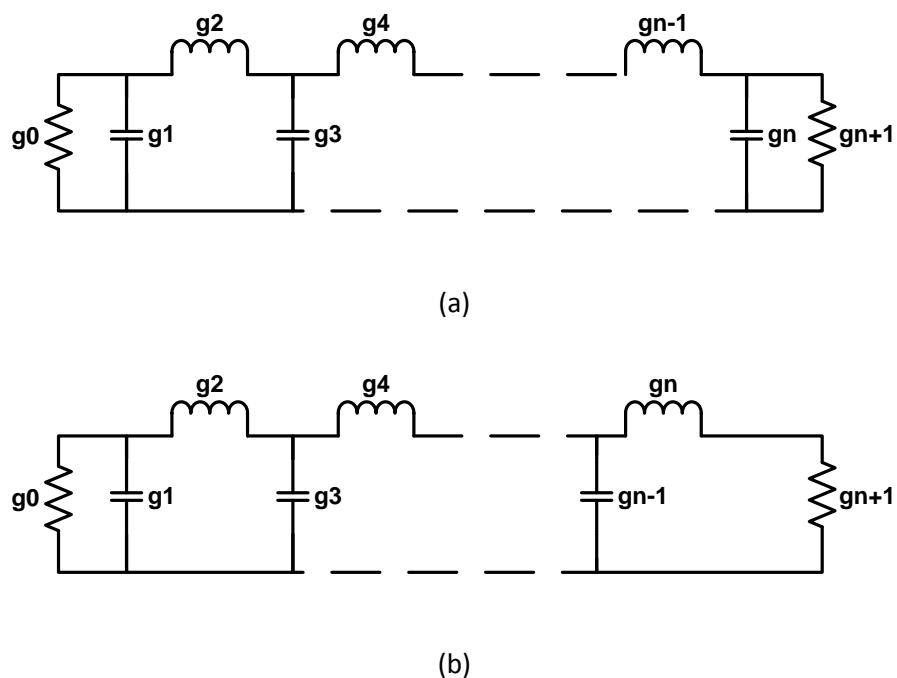


Figure 2.3-1: Lumped element lowpass prototypes: (a) Odd order filter network; (b) Even order filter network.

There exists a well established ladder network synthesis technique that can be used to calculate the element values g_n of the lowpass prototype (inductive if it's a series element and capacitive if it is a shunt element) [2-4]. Alternatively for large values of n , currently available tables can be used to gain the element values.

The lowpass filter prototypes which consist of shunt and series elements may not always be suitable for microwave and millimetre-wave applications due to realisation difficulties of the filter network. A more practical filter design would be to use either shunt or series elements spaced by immittance inverters [2-4]. This is because at such high frequencies, as mentioned earlier, filter structures are realised through distributed parameters and it becomes convenient to transform the ladder network to the circuit shown in Figure 2.3-3.

Immittance inverters (as shown in Figure 2.3-2) are lossless two port networks that can be either admittance inverters (J -inverters) or impedance inverters (K -inverters), where both types are frequency independent and have a unique property. That is, in the case of an impedance inverter, if impedance Z_L is terminated at one port, then the input impedance (Z_{in}) looking from the other port is defined as [2-4]:

$$Z_{in} = \frac{K^2}{Z_L} \quad (2.3.1)$$

Whereas for the admittance inverter, the input admittance (Y_{in}) looking from one port for an admittance Y_L terminated at the other is [2-4]:

$$Y_{in} = \frac{J^2}{Y_L} \quad (2.3.2)$$

Impedance inverters can be used to design bandpass filters consisting of just series connected elements, whereas admittance inverters can be used to design bandpass filters consisting of just shunt connected elements. The replacement of shunt or series connected elements with inverters for design of bandpass filters can be found in [2-3], where a comprehensive synthesis procedure for such prototype networks is provided.

In distributed circuits, an admittance/impedance inverter can be realized as a discontinuity separating two homogeneous sections of transmission lines, or even as a quarter wavelength section of transmission line (also known as a quarter wavelength transformers). Further information on the realisation of impedance and admittance inverters can be found in [2-2].

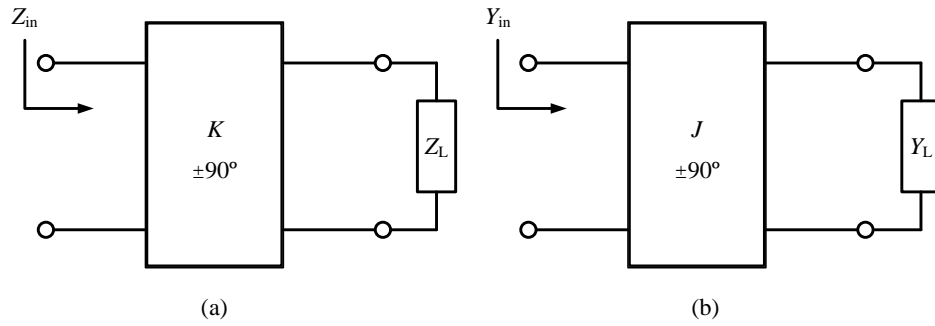


Figure 2.3-2: Imittance inverters: (a) Impedance (K) inverter; (b) Admittance (J) inverter.

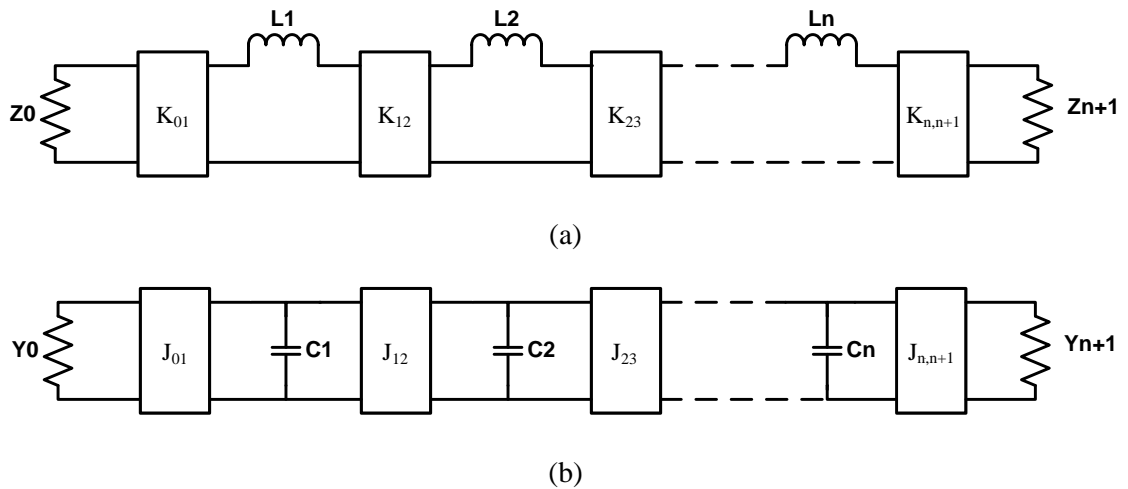


Figure 2.3-3: Impedance inverter lowpass lumped element prototype.

The two passive circuits in Figure 2.3-3 are time invariant and belong to a class of linear and lossless networks. Ladder networks also consist of just a single path where energy can propagate between source and load. Hence they are also minimum phase networks and are limited for realising all pole filters such as Butterworth and Chebyshev type responses, where no transmission zeros are generated.

In order to synthesise filter responses, such as the generalised Chebyshev, which consist of finite position transmission zeros, networks that consist of cross-couplings (coupling between non-adjacent resonators) must be used [2-5]. Here, transmission zeros are generated due to the availability of more than one path for the signal to navigate between source and load, which can lead to the interaction of signals at the load with opposite phase shifts that can cancel each other [2-6]. Alternatively, a more advanced lowpass filter prototype network is available [2-3], where the synthesis of these types of networks are carried out by a method known as the extracted pole technique [2-7].

2.4 Lowpass To Bandpass Frequency Transformation

The lowpass filter prototype networks briefly considered earlier, are normalised such that their source and load resistance/conductance are set to unity and has an angular cutoff frequency $\omega'_c = 1$. However, these values are impractical for use in real applications and the network needs to be transformed in order to gain acceptable solutions for required specifications. Although there exist transformation from lowpass to lowpass, lowpass to highpass, lowpass to bandstop and lowpass to bandpass [2-4], only the latest is briefly outlined here as the thesis mainly consider filters with bandpass responses. The bandpass filter prototype is derived by applying the frequency transformation given according to equation (2.4.1). It is performed such that the normalised angular cutoff frequency ($\omega'_c = 1$) of the lowpass prototype corresponds to the two bandstop angular edge frequencies ω_1 and ω_2 of the bandpass filter.

$$\omega' = \frac{\omega'_c \omega_0}{\omega_2 - \omega_1} \left(\frac{\omega}{\omega_0} - \frac{\omega_0}{\omega} \right) \quad (2.4.1)$$

The centre frequency ω_0 of the passband relates to the centre frequency ($\omega' = 0$) of the prototype and is calculated as $\omega_0 = \sqrt{\omega_1 \omega_2}$. When the transformation is applied to the inductive elements of the lowpass prototype, they become series *LC* resonant circuits with the new element values calculated as [2-4]:

$$L_{res} = \frac{\omega'_c L}{\omega_2 - \omega_1} \quad (2.4.2)$$

$$C_{res} = \frac{1}{\omega_0^2} \cdot \frac{\omega_2 - \omega_1}{\omega'_c L} \quad (2.4.3)$$

Whereas when the transformation is applied to capacitive elements of the lowpass prototype, they become parallel *LC* resonant circuits bearing the new element values calculated as [2-4]:

$$C_{res} = \frac{\omega'_c C}{\omega_2 - \omega_1} \quad (2.4.4)$$

$$L_{res} = \frac{1}{\omega_0^2} \cdot \frac{\omega_2 - \omega_1}{\omega'_c C} \quad (2.4.5)$$

From (2.4.4-2.4.5) it can be seen that the resonant circuit has the resonance frequency $\omega_0 = \frac{1}{\sqrt{L_{res} C_{res}}}$.

2.5 Multiple Coupled Resonators

The multiple coupled resonator bandpass prototype was introduced by Atia and Williams in 1970s in order to facilitate the development of symmetric cross-coupled networks [2-5], [2-9] and the proposed model is presented in Figure 2.5-1, which consists of N resonators coupled by transformers. Each resonator is formed by series arrangement of a single capacitor with a capacitance of 1 F and a single inductor with self inductance of 1 H respectively within a loop. Therefore all individual resonators have a centre frequency of 1 rad/s and the couplings are all normalized for a bandwidth of 1 rad/s. Additionally each loop is theoretically coupled to every other loop through cross-coupling between the inductors. This circuit is limited to support filter prototypes with symmetrical responses only.

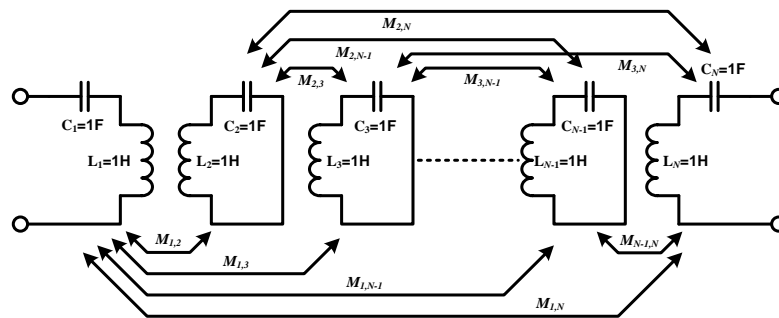


Figure 2.5-1: Model of the general coupled-resonator filter.

The above model has been further modified by Cameron [2-3] by the inclusion of hypothetical frequency invariant reactance elements (FIR), inserted in series with the capacitor and inductor within each loop, in order to account for resonant frequency shift of each individual resonator [2-8]. This in turn, allows the circuit to model asymmetric frequency behaviours. The circuit proposed by Cameron is shown in Figure 2.5-2.

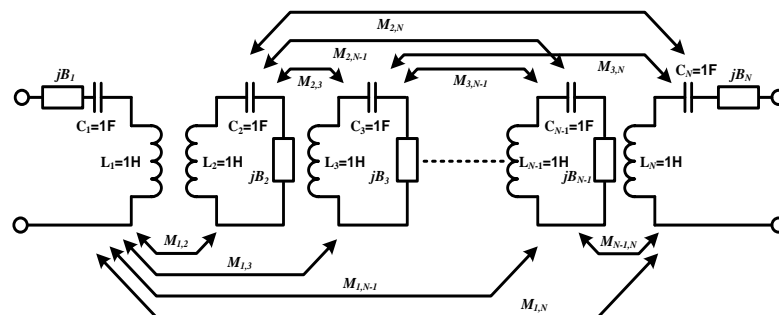


Figure 2.5-2: Cameron's modified model of the general coupled-resonator filter.

The multiple coupled bandpass filter prototype depicted in Figure 2.5-2 can be represented as a lowpass prototype network [2-3]. The lowpass equivalent prototype network is shown in Figure 2.5-3. In this model, the mutual couplings between each resonator, which are assumed to be frequency invariant, are replaced by inverters of the same values. The series capacitances disappear due to the transformation from bandpass to lowpass. Consequently, only the FIR elements appear in series with the inductors.

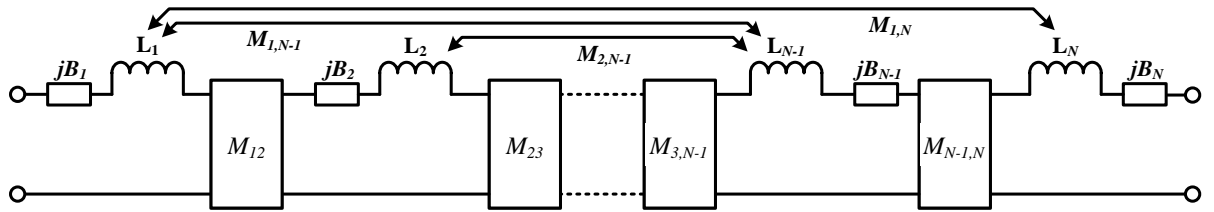


Figure 2.5-3: The lowpass prototype of the multiple coupled resonator filter.

2.6 The General $N \times N$ and $N + 2$ Coupling Matrix

Consider the two port network in Figure 2.6-1, which operates between a voltage source generating E volts with internal impedance of R_s ohms and load impedance of R_L ohms. The equations derived as a means of applying Kirchoff's equations for each loop, may be written in the following matrix representation [2-3].

$$[Z] \cdot [i] = [E] \quad (2.6.1)$$

Matrix $[Z]$ is an impedance matrix of the network with N loops including its terminations and the above equation can be expanded in to the following:

$$[\mathbf{R} + s\mathbf{I} + j\mathbf{M}] \cdot [i_1, i_2, i_3, \dots, i_N]^t = E \cdot [1, 0, 0 \dots 0]^t \quad (2.6.2)$$

Here \mathbf{R} represents the termination impedance matrix whose only non-zero matrix entries include R_{11} and R_{NN} . \mathbf{I} is an identity matrix and s represent the complex frequency variable ($s = j\omega$); and \mathbf{M} represents the coupling matrix that contains all the mutual couplings between the resonators. The entries on the main diagonal of the coupling matrix (values of the FIR elements) are known as self couplings, whereas couplings numbered sequentially such as $M_{N,N+1}$, are referred to as mainline couplings, and non-sequentially numbered couplings are known as cross-couplings. An example of the coupling matrix \mathbf{M} is given in equation (2.6.3).

$$\mathbf{M} = \begin{bmatrix} B_1 & M_{12} & \cdots & M_{1,N-1} & M_{1,N} \\ M_{21} & B_2 & \cdots & M_{2,N-1} & M_{2,N} \\ \vdots & \vdots & \ddots & \vdots & \vdots \\ M_{N-1,1} & M_{N-1,2} & \cdots & B_{N-1} & M_{N-1,N} \\ M_{N,1} & M_{N,2} & \cdots & M_{N,N-1} & B_N \end{bmatrix} \quad (2.6.3)$$

The circuit in Figure 2.5-2, can be analysed for the full coupling matrix which includes both source and load terminals, as represented by equation (2.6.1) and (2.6.2).

$$[i] = [Z]^{-1} \cdot [E] \quad (2.6.4)$$

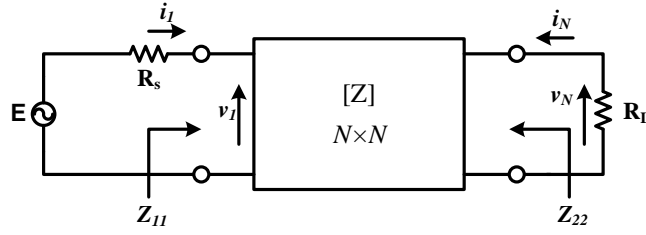


Figure 2.6-1: The multiple coupled resonator filter including source E with impedance R_s and load impedance R_L .

By referring to Figure 2.6-1 and from equation (2.6.4), it can be observed that:

$$i_1 = [Z]_{11}^{-1} \times E \quad (2.6.5)$$

$$i_N = [Z]_{N1}^{-1} \times E = \frac{v_N}{R_L} \quad (2.6.6)$$

Substituting equation (2.6.6) into the definition of transmission coefficient S_{21} for a two port network as given in [2-2], the following can be obtained:

$$S_{21} = 2 \sqrt{\frac{R_s}{R_L}} \times \frac{v_N}{E} = 2 \sqrt{\frac{R_s}{R_L}} \times R_L [Z]_{N1}^{-1} = 2 \sqrt{R_s R_L} \times [Z]_{N1}^{-1} \quad (2.6.7)$$

For a two port network, the reflection coefficient at the input port can be obtained as:

$$S_{11} = \frac{Z_{11} - R_s}{Z_{11} + R_s} = 1 - \frac{2R_s}{Z_{11} + R_s} \quad (2.6.8)$$

From Figure 2.6-1, it can be observed that the input impedance Z_{11} looking into the network at the input port can be calculated as $Z_{11} = v_1/i_1$, where the potential divider at the port gives v_1 and i_1 is defined by equation (2.6.5).

$$Z_{11} = \frac{E \times Z_{11}}{Z_{11} + R_S} \cdot \frac{1}{[Z]_{11}^{-1} \times E} \quad (2.6.9)$$

$$[Z]_{11}^{-1} = \frac{1}{Z_{11} + R_S} \quad (2.6.10)$$

Therefore, by substituting equation (2.6.10) into (2.6.8) to solve for S_{11} , the following expression can be obtained:

$$S_{11} = 1 - 2R_S[Z]_{11}^{-1} \quad (2.6.11)$$

The source and load terminations of circuit in Fig. 2.6-1 can be normalised to unity by the inclusion of an impedance inverter M_{S1} and M_{NL} with values of $\sqrt{R_S}$ and $\sqrt{R_L}$ respectively at either end [2-3]. The inverters can be absorbed into the $[Z]$ matrix, thus changing the format of the matrix to $(N + 2) \times (N + 2)$. The $N + 2$ cross-coupled network with parallel resonators is shown in Figure 2.6-2, together with the corresponding coupling matrix given in equation (2.6.12).

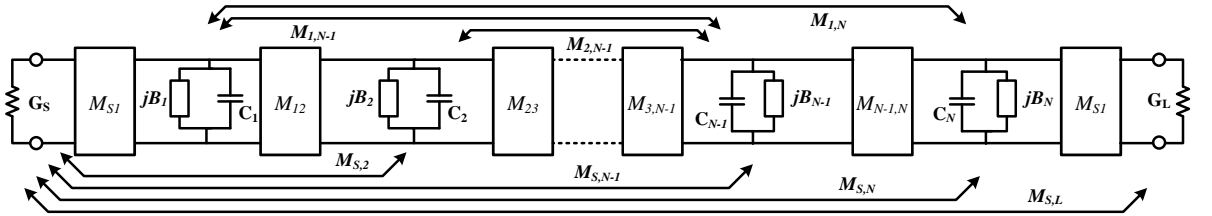


Figure 2.6-2: The $N+2$ multiple coupled resonator network.

$$M = \begin{bmatrix} M_{S,S} & M_{S1} & M_{S1} & \cdots & M_{S,N-1} & M_{S,N} & M_{S,L} \\ M_{1S} & B_1 & M_{12} & \cdots & M_{1,N-1} & M_{1,N} & M_{1,L} \\ M_{2S} & M_{21} & B_2 & \cdots & M_{2,N-1} & M_{2,N} & M_{2,L} \\ \vdots & \vdots & \vdots & \ddots & \vdots & \vdots & \vdots \\ M_{N-1,S} & M_{N-1,1} & M_{N-1,2} & \cdots & B_{N-1} & M_{N-1,N} & M_{N-1,L} \\ M_{N,S} & M_{N,1} & M_{N,2} & \cdots & M_{N,N-1} & B_N & M_{N,L} \\ M_{L,S} & M_{L,1} & M_{L,2} & \cdots & M_{L,N-1} & M_{L,N} & M_{L,L} \end{bmatrix} \quad (2.6.12)$$

2.7 Extracted Pole Filters

The coupled filter networks described previously are capable of producing finite frequency transmission zeros in the complex frequency variable due to cross-coupling between non-adjacent resonators. Generally, the couplings in the network can be of positive, negative sign or mixed. From a practical point of view, it is easier to realise filters with couplings of the same sign. However if the transmission zeros generated are due to mixed couplings, then it can pose difficulties in physical implementation. To address this issue, Rhodes and Cameron introduced the extracted pole filter network which is synthesised using the extracted pole procedure described in [2-7] or [2-10].

The synthesis procedure begins with the removal of the transmission zeros (which are represented by bandstop sections) before paying attention to the remainder or main body of the network and the remaining network would not need any cross-coupling with opposite signs to the mainline couplings [2-3]. The bandstop section consists of a lowpass resonator represented as an inductor in series with an FIR element [2-11], and is shown in Figure 2.7-1.

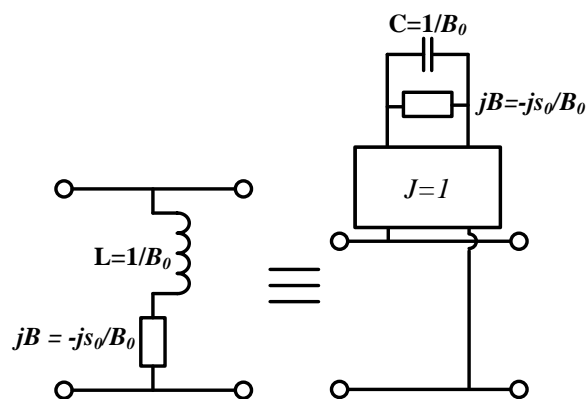


Figure 2.7-1: Schematic representation of a bandstop section.

The bandstop section is extracted from the $[ABCD]$ matrix of the overall filter network, which can be composed from the know polynomials of the filtering function. The procedure to obtain the overall $[ABCD]$ matrix can be found in [2-3]. Initially the two port network is considered as a transmission line cascaded with a remainder $[ABCD]_1$ matrix which represents the rest of the network as show in Figure 2.7-2.

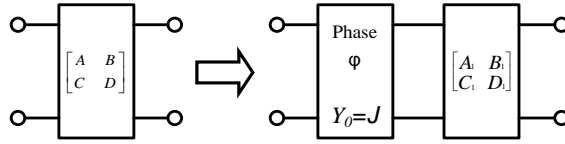


Figure 2.7-2: Deduction of a transmission line section from the filter network.

The entries of the remainder matrix can be calculated as follows [2-3]:

$$\begin{bmatrix} A_1 & B_1 \\ C_1 & D_1 \end{bmatrix} = \begin{bmatrix} A \cos \varphi - j \frac{1}{J} C \sin \varphi & B \cos \varphi - j \frac{1}{J} D \sin \varphi \\ C \cos \varphi - j A J \sin \varphi & D \cos \varphi - j B J \sin \varphi \end{bmatrix} \quad (2.7.1)$$

In the above equation, J is taken as unity for simplification [2-3] and φ can be calculated by:

$$\varphi = \tan^{-1} \frac{A}{jC} \Big|_{s=s_0} \quad (2.7.2)$$

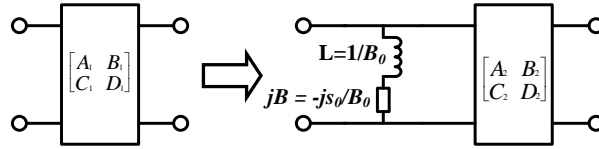


Figure 2.7-3: Extraction of a bandstop section from the remaining network.

The remainder $[ABCD]_1$ matrix after the extraction of the phase length is considered as a bandstop section in series with another two port network described by $[ABCD]_2$ matrix (refer to Figure 2.7-3). Next the residue b_0 of the resonant pair is evaluated as:

$$b_0 = \frac{(s - s_0)D_1}{A_1} \Big|_{s=s_0} \quad (2.7.3)$$

The remainder $[ABCD]_2$ matrix after the extraction of the resonant pair can be calculated as:

$$\begin{bmatrix} A_2 & B_2 \\ C_2 & D_2 \end{bmatrix} = \begin{bmatrix} \frac{A^1}{(s - s_0)} & \frac{B^1}{(s - s_0)} \\ \frac{C^1 - b_0 A^x}{(s - s_0)} & \frac{D^1 - b_0 B^x}{(s - s_0)} \end{bmatrix} \quad (2.7.4)$$

Where

$$A^x = \frac{A^1}{(s - s_0)}, \quad B^x = \frac{B^1}{(s - s_0)} \quad (2.7.5)$$

If the rest of the circuit consists of another bandstop section to be extracted, then the procedure is repeated until all poles are removed from the initial network. A more comprehensive step by step explanation to the procedure with examples can be found in [2-3].

2.8 Non-Resonating Nodes in Filters

The cross-coupled filter networks considered previously are able to generate N number of transmission zeros from N number of resonators if source and load are directly coupled to one another [2-12]-[2-13]. However transmission zeros generated this way are not independently tuneable and are susceptible to manufacturing tolerances, especially for higher order filters, as they depend on all physical parameters in every resonator, thus they lack flexibility. In order to compensate for such tolerances, tuning can be carried out, but it may not always be successful.

The non-resonating node (NRN) is a shunt FIR element introduced within filter prototype networks and allows realisation of networks that can exhibit maximum number of transmission zeros without the need for direct coupling between source and load [2-14].

Another core advantage of using NRNs is that they allow for realisation of compact filters, as strongly detuned resonators with very small dimensions are often used for implementation of NRNs [2-11]. Furthermore, NRNs can also be used for implementing filters with cascaded topologies [2-15]-[2-17], where separately designed modules are interconnected to each other through NRNs to realise the desired filtering functions. The use of separately designed modules has one main advantage, that is, each module has the capability to control its own poles and transmission zero. This intrinsically reduces the sensitivity to manufacturing tolerances that affect cross-coupled filters and simplifies tuning process of the structures [2-14].

During the past years, several well known modules have been introduced which may be cascaded to form higher order filters. The simplest of these modules is called the singlet [2-14], which consists of a single resonator, bypassed due to direct source-load coupling. The scheme is capable of producing a single pole and a single transmission zero, where their locations may vary depending on the signs and values of the three available couplings. The coupling schematic of a singlet is shown in Figure 2.8-1a. A second and more flexible topology is the doublet [2-15], where the schematic is capable

of producing and controlling two poles and two transmission zeros which can be positioned either side of the passband depending on the signs and values of the couplings.

Figure 2.8-1b and 2.8-1c show two possible schematics of the doublet, whereas Figure 2.8-1d shows the schematic of an extended doublet [2-17], which can generate three poles due to the additional shorted resonator and two transmission zeros. In the coupling schemes below, the dark nodes represent resonators in a parallel combination, whereas the dashed nodes represent the source and load for each individual block whereas the lines connecting the nodes are inverters, which are assumed to be frequency independent. Examples of filter implementation using cascaded singlets and cascaded doublets can be found in [2-14]-[2-18].

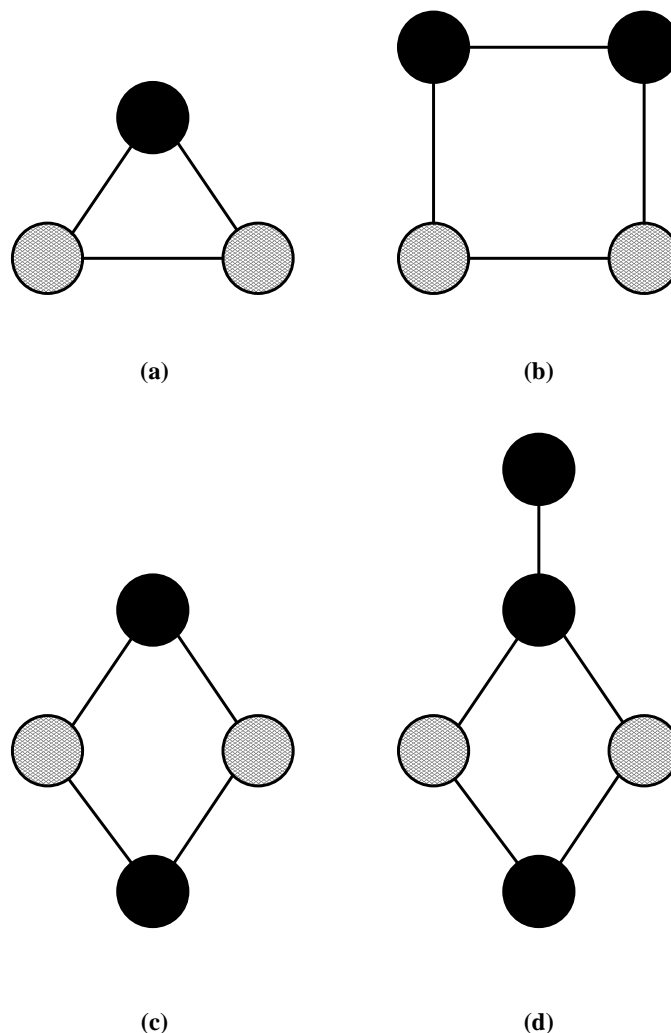


Figure 2.8-1: Modules that are widely used for cascaded filter design: (a) The singlet; (b) The square doublet; (c) The diamond shaped doublet; (d) The extended doublet.

2.9 References

- [2-1] D. M. Pozar, *Microwave engineering*, 3rd edition, New York: John Wiley & Sons, 2004.
- [2-2] G. L. Matthaei, L. Jones and E. M. T. Jones, *Microwave Filters, Impedance Matching Networks and Coupling Structures*, New York: McGraw-Hill, 1964.
- [2-3] R. J. Cameron, C. M. Kudsia, and R. R. Mansour, *Microwave Filters for Communication Systems*, Hoboken, New Jersey, John Wiley & Sons, 2007.
- [2-4] D. Budimir, *Generalized Filter Design by Computer Optimization*, Artech House, 1998.
- [2-5] A. E. Atia and A. E. Williams, "Narrow-Bandpass Waveguide Filters," *IEEE Trans. Microwave Theory Tech.*, vol.0, no. 4, pp. 258–265, Apr. 1972.
- [2-6] J. B. Thomas, "Cross-Coupling in Coaxial Cavity Filters – A Tutorial Overview," *IEEE Trans. Microwave Theory Tech.*, vol. 51, no. 4, pp. 1368–1376, Apr. 2003.
- [2-7] J. D. Rhodes, and R. J. Cameron, "General Extracted Pole Synthesis Technique With Applications to Low-Loss TE₀₁₁ Mode Filters," *IEEE Trans. Microwave Theory Tech.*, vol. 28, no. 9, pp. 1018-1028, Sept. 1980.
- [2-8] R. F. Baum, "Design of Unsymmetrical Band-Pass Filters", *IRE Trans. Circuit Theory*, vol. 4, no. 2, pp. 33-40, June 1957.
- [2-9] A. E. Atia and A. E. Williams, "New Types of Bandpass Filters for Satellite Transponders", *COMSAT Tech. Rev.*, vol. 1, pp. 21-43, 1971.
- [2-10] S. Amari and G. Macchiarella, "Synthesis of Inline Filters With Arbitrary Placed Attenuation Poles by Using Nonresonating Nodes," *IEEE Trans. Microwave Theory & Tech.*, vol. 53, no. 10, pp. 3075–3081, Oct. 2005.
- [2-11] O. Glubokov (2011). *Development of Waveguide Filter Structures for Wireless and Satellite Communications*. Ph.D. Thesis. University of Westminster: U.K.

- [2-12] S. Amari, "On the Maximum Number of Finite Transmission Zeros of Coupled Resonator Filters With a Given Topology," *IEEE Microwave Wireless Components Lett.*, vol. 9, no. 9, pp. 354-356, Sept. 1999.
- [2-13] S. Amari and J. Bornemann, "Maximum Number of Finite Transmission Zeros of Coupled Resonator Filters With Source/Load Multi-Resonator Coupling and a Given Topology," *Microwave Conference 2000 Asia Pacific*, pp. 1175-1177, Dec. 2000.
- [2-14] S. Amari, U. Rosenberg and J. Bornemann, "Singlets, Cascaded Singlets, and the Nonresonating Node Model for Advanced Modular Design of Elliptic Filters," *IEEE Microwave and Wireless Components Letters*, vol. 14, no. 5, pp. 237-239, May 2004.
- [2-15] S. Amari and U. Rosenberg, "The Doublet: A New Building Block for the Modular Design of Elliptic Filters," in *Eur. Microwave Conf.* Milan, Italy, vol. 2, pp. 123-125, 2002.
- [2-16] S. Amari and U. Rosenberg, "A Universal Building Block for Advanced Modular Design of Microwave Filters," *IEEE Microwave and Wireless Components Letters*, vol. 13, no. 12, pp. 541-543, Dec. 2003.
- [2-17] S. Amari and U. Rosenberg, "New Building Blocks for Modular Design of Elliptic and Self-Equalized Filters," *IEEE Trans. Microwave Theory Tech.*, vol. 52, no. 2, pp. 721-736, Feb. 2004.
- [2-18] O. Glubokov and D. Budimir, "Compact E-plane Doublet Structures for Modular Filter Design," in *Eur. Microwave Conf.*, Paris, France, pp. 1253-1256, 2010.

E-PLANE EXTRACTED POLE WAVEGUIDE FILTERS

3.1 Introduction

Due to the rapid growth in commercial success in microwave and millimetre wave systems, key components such as high performance waveguide filters with low insertion loss, wide stopbands and high selectivity, while maintaining a reduced cost and a compact size are becoming more in demand for satellite communication systems and mobile wireless systems [3-1]-[3-2]. Such demands have previously resulted in the development of dual-mode waveguide filters [3-3]-[3-5] and dielectric resonator loaded filters [3-6]-[3-7]. Both these well established technologies are capable of achieving a size reduction, but at the cost of high design complexities. Since filters for satellites must be extremely reliable to operate in space, they also suffer from high manufacturing costs. Furthermore, designs of filters using dielectric resonators are limited to narrowband applications.

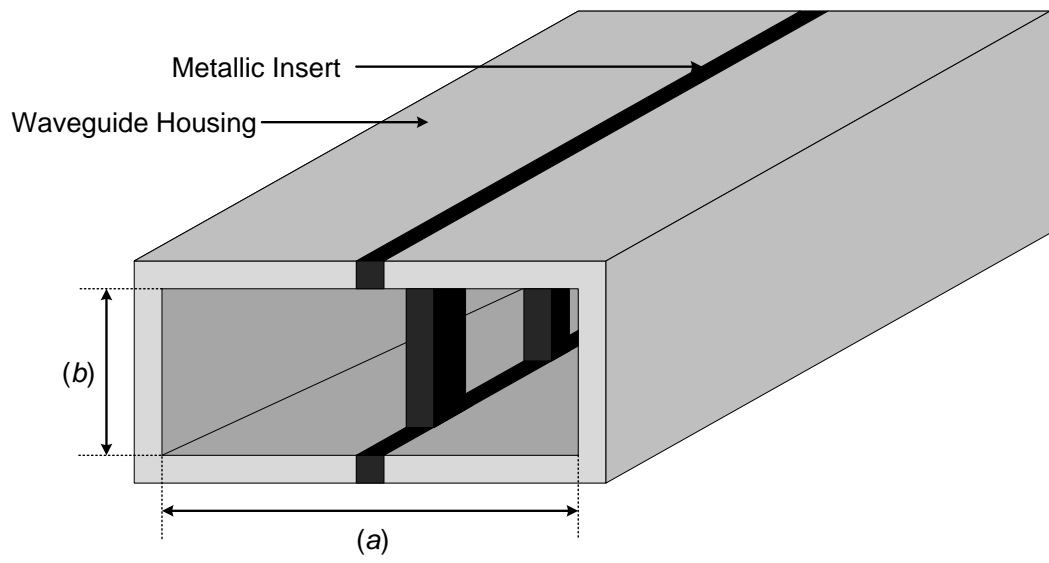
In order to address the drawback of high manufacturing costs that relates to waveguide filters, Konishi and Uenakada introduced the planar circuit mounted E-plane strip [3-8]. Due to the simplistic construction of the structure, filters formed from this technology are regarded as being highly suitable for mass manufacturing. Some of the earliest research and developments in this technology can be found in [3-9]-[3-13]. However, the conventional E-plane waveguide filters using periodically located inductive obstacles can be quite bulky and thus making them unsuitable for space applications [3-1]. The following chapter will be dedicated to the development of compact high performance E-plane waveguide filters. The chapter will commence with a brief discussion on the conventional E-plane waveguide filters and their implementation in section 3.2. This will be followed by section 3.3 that describes the design and realisation of an E-plane extracted pole section (E-plane EPS) and high performance filters implemented by cascading several of such sections. Expanding on this, section 3.4 will present a novel ultra-compact E-Plane waveguide filter which is approximately 85% more compact than filters formed from using conventional E-plane resonators.

3.2 Conventional E-Plane Waveguide Filters

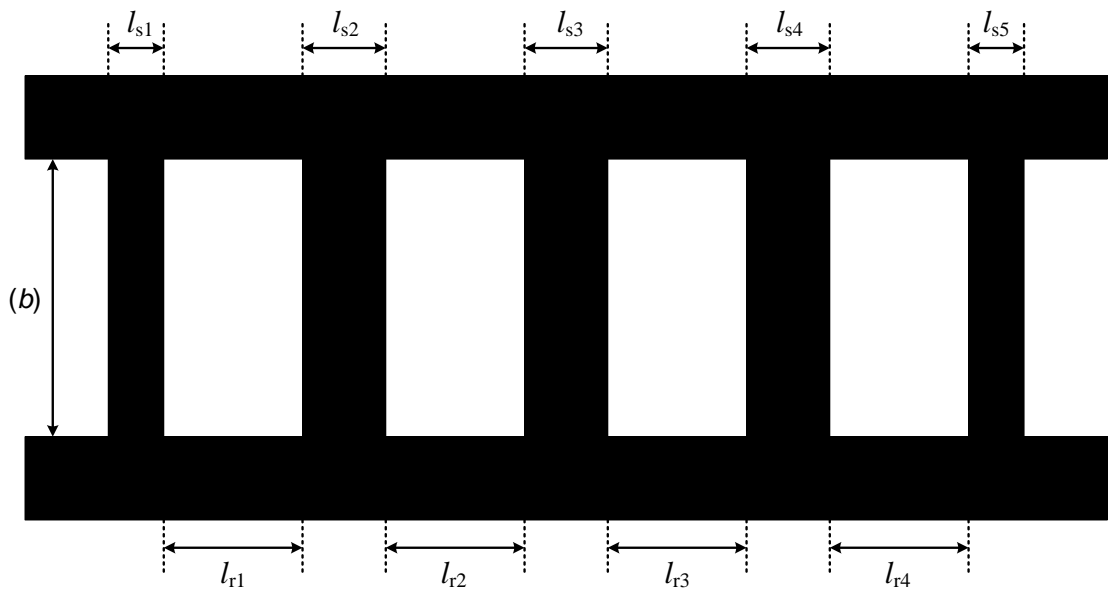
An E-plane resonator or filter commonly refers to a rectangular waveguide which consists of an insert placed in a parallel plane to the narrow wall of the waveguide, where the first mode of the E -field is present. The inserts placed within the waveguide can be composed of either all metal or metallo dielectric (printed circuits). Although E-Plane bandpass filters formed from all metallic inserts are considered to be the simplest approach, both aforementioned methods of realising E-plane filters are regarded as being highly cost efficient. E-plane inserts supported using dielectric materials have the advantage of being slightly compact, but with the disadvantage of incurring additional losses.

The geometry of a conventional E-plane rectangular waveguide filter is illustrated in Figure 3.2-1. Such structures consist of longitudinally oriented inductive strips, also known as metallic septa, in the E-plane of the waveguide in such a manner that it forms half wavelength resonators between each of them. Consequently the structure can be viewed as a series of homogeneous waveguides, each performing as electromagnetic resonators (represented by the lengths l_r in the figure), which are coupled directly to each other inductively [3-14]. The lengths l_s represent the lengths of the individual inductive septa.

The technique of designing and implementing conventional E-plane waveguide filters has been investigated thoroughly in previous works and is now well established [3-14]. It has been proven that the performance of these structures are mainly determined and controlled by the pattern of the metallisation insert. The size (l_s) and the number of the metal septa are parameters that determines the bandwidth of the filter, whereas the resonant frequency of the filter is determined by the length of the half wavelength resonators (l_r) formed by the insert. From a practical point of view, the structure can be realised by employing split block waveguide housing. For the fabrication of the metal insert, techniques such as metal etching or stamping methods for thicker sheets can be used. The techniques allows for low cost and mass fabrication of these structures. However in terms of physical dimensions, selectivity and stopband performance of these structures, it is still an area for improvements and is the main objective of this work.



(a)



(b)

Figure 3.2-1: Conventional rectangular E-plane waveguide configuration: (a) E-plane filter; (b) Metal insert for a 4th order E-plane filter.

The conventional direct coupled E-plane waveguide filters as shown in Figure 3.2-1 can be synthesised using a network-circuit based approach. The procedure commence with the bandpass distributed filter prototype which is realised with the consideration that the lumped element resonant circuits of the inverter coupled bandpass lumped element prototype are equivalent to the distributed line elements (also known as unit elements). A distributed filter will consist of n such unit elements, each of which would correspond to a resonator. In the case of conventional E-plane filters, the uniform sections of waveguides between the reflective discontinuities, known as metallic septa, in Figure 3.2-1, exhibits resonating behaviour. The length of each unit element is considered to be half the guided wavelength of the waveguide line section at the centre frequency ($\lambda_{g0}/2$).

Cascading of unit elements with different impedances will affect propagation of the electromagnetic waves through the line, yielding reflected waves between them; which in turn can lead to resonance. However if we consider a waveguide with a uniform cross section, in order to achieve a similar effect, some form of discontinuity must be loaded [3-14]. In the conventional E-plane filter operating in TE_{10} mode, such discontinuities are realized by the presence of metallic septa and are characterised by shunt inductive behaviour, which can also be represented by K inverters [3-14]. Therefore, the conventional E-plane filter can be realised as a cascade of half wavelength resonators with K inverters. The direct coupled distributed filter prototype network is shown in Figure 3.2-2b. The analytical procedure for calculating the values of impedance inverters and unit elements as well as a comprehensive design procedure for the conventional E-plane filters can be found in [3-14].

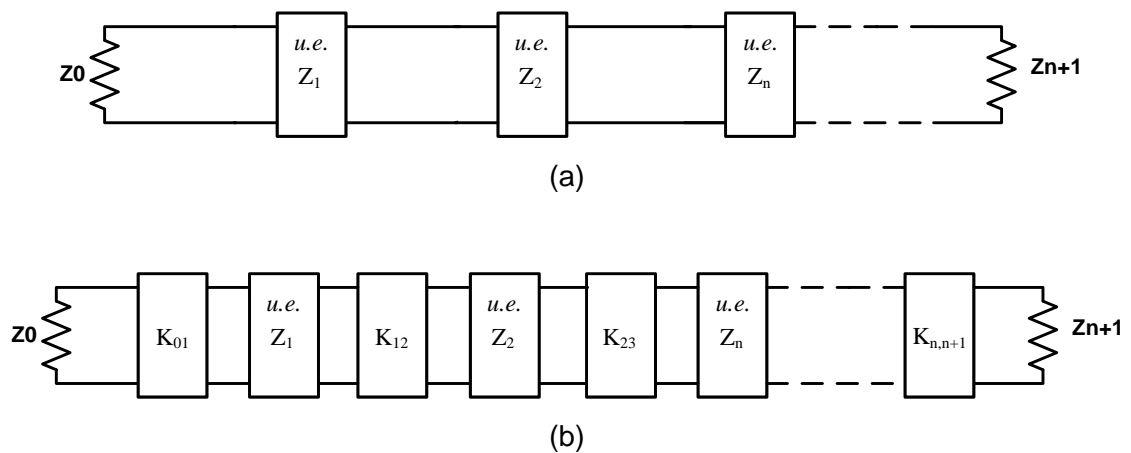


Figure 3.2-2: Bandpass distributed filter prototypes: (a) Unit Element Filter; (b) Prototype for direct couple half wavelength resonator waveguide filter.

3.3 E-plane Extracted Pole Waveguide Filters

Extracted pole filters have gained popularity in filter applications due to their capability to realise the maximum number of transmission zeros equal to that of the filter order without having to directly couple source to load. The filters are also inherently modular, as each extracted pole section (EPS) is capable of generating and controlling its own transmission zero simply by adjusting its own individual parameters.

Extracted pole filters in rectangular waveguide technology were widely implemented by the use of resonating and non-resonating cavities [3-15]-[3-17]. However, due to the disadvantages that this approach provides in terms of excessive time as well as resource consumption during fabrication, a more design flexible approach using E-plane inserts was proposed in [3-18]. Extracted pole filters designed in this manner reaps the benefits of E-plane technology due to their simplicity during fabrication, inexpensiveness and the fact that a variety of different filter responses can be realised by the utilisation of the same waveguide housing.

During the past few years, several investigations into achieving miniaturisation of conventional E-plane resonators and filters as well as making improvements towards stopband performance were conducted. It was demonstrated that S-shaped resonators [3-19] and split ring resonators (SRR) [3-20]-[3-21] embedded within a conventional E-plane resonator can shift the fundamental resonance towards lower frequencies, thus allowing a reduction in the length of the conventional resonator. The structures were also able to generate a single transmission zero in the upper stopband. In these works, the phenomenon observed was described in terms of metamaterial effects which occur in periodic lattices composed of SRR or S-shaped resonators. However a more comprehensive theoretical explanation to these effects observed was provided later in [3-22], which describes them using the theory of EPS and non-resonating nodes. It is also well known that one of the benefits of using non-resonating nodes is its ability to provide size reduction, as resonators with small dimensions are generally used for their implementation. In that article, the main properties of the circuit were outlined and an extraction technique for generalised coupling coefficients within and between adjacent EPSs were provided, which aids in the design process of these filters. Some examples of filters realised using EPS in E-plane technology using all metallic inserts can be found in [3-18] and [3-23].

The EPS instigate from the extracted pole filter prototype network as described in section 2.7. The section of transmission line that was extracted at the beginning of the synthesis procedure of these filter networks, can be represented as an equivalent circuit composed of two frequency invariant reactance (FIR) elements connected through an inverter as shown in Figure 3.3-1 [3-2]. This transformation also allows the prototype of the EPS to be represented as an inverter coupled network.

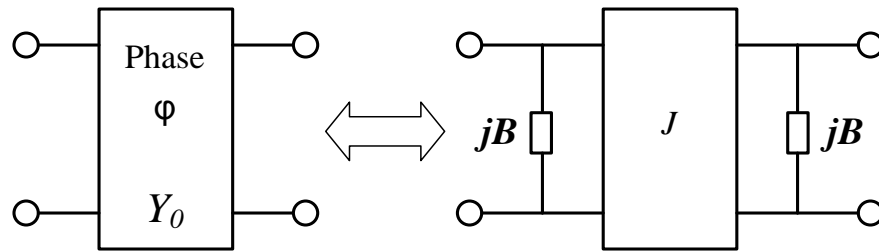


Figure 3.3-1: Transformation of a transmission line section in extracted pole prototypes.

The schematic representation of an EPS consists of a bandstop section connected through an inverter with a FIR element, as shown in Figure 3.3-2a. The shunt FIR element is also referred to as a non-resonating node. In Figure 3.3-2b, an equivalent representation of an EPS is given as a coupling scheme composed of two nodes: resonating and non-resonating. The inverter is presented as a line connecting the nodes.

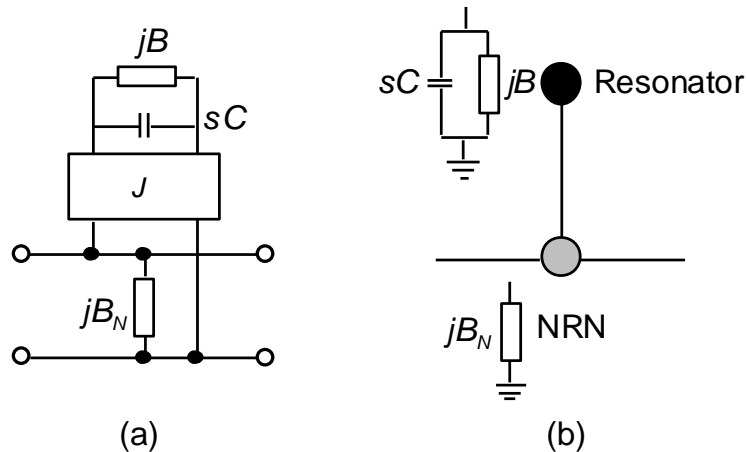


Figure 3.3-2: EPS: (a) Schematic representation; (b) Coupling scheme representation.

An equivalent schematic representation of a doubly terminated EPS is presented in Figure 3.3-3. In this schematic, the resonator is modelled as a FIR in parallel with unit capacitance, whereas the non-resonating node is represented by a single FIR element B_N and J_0 and J_N represent admittance inverters.

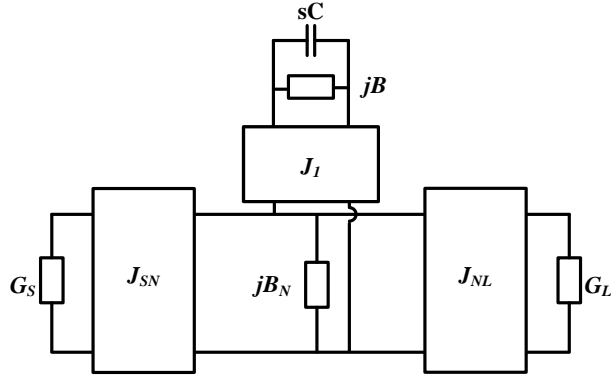


Figure 3.3-3: Schematic representation of a doubly loaded EPS.

Due to the symmetry of the circuit, even and odd mode techniques can be applied to analyse the prototype circuit, which leads to the reflection coefficient that can be calculated as:

$$S_{11} = \frac{1}{1 - j \left(\frac{2J_{SN}^2(\omega' + B)}{B_N \left(\omega' + B - \frac{J_1^2}{B_N} \right)} \right)} \quad (3.3.1)$$

In the above equation, ω' is a lowpass frequency variable which can be obtained through bandpass to lowpass transformation as:

$$\omega' = \frac{1}{FBW} \left(\frac{\omega}{\omega_0} - \frac{\omega_0}{\omega} \right) \quad (3.3.2)$$

Where f_0 is the centre frequency of the filter and FBW is the fractional bandwidth. It can also be shown that the EPS has a pole ω_P and a transmission zero ω_Z described by:

$$\omega_P = -B + \frac{J_1^2}{B_N} \quad (3.3.3)$$

$$\omega_Z = -B \quad (3.3.4)$$

It can be concluded from equation 3.3.3, that in order to place a transmission zero above the passband, the susceptance of the non-resonating node must be negative and in order to place it below, then the susceptance of the non-resonating node must be positive. Higher order direct coupled extracted pole filters can be designed through cascading several of these sections. The synthesis procedure of such networks can be found

explained in detail in [3-24], or by using input impedance or admittance rational functions by applying a direct synthesis technique as explained in [3-25].

In E-plane technology, the EPS can be realised by a strongly detuned conventional E-plane resonator and another resonator embedded within this standard resonator. This type of filter configurations was previously investigated using S-shape resonators, split-ring resonators and quarter wavelength resonators. The S-shape resonators and SRRs can be implemented by the use of metallo-dielectric slab with the shapes etched onto one side, whereas the quarter wavelength resonators can be implemented by a metallic fin or etched on a metallo-dielectric slab.

From a practical point of view, the quarter wavelength resonators provide a better option for implementing in extracted pole filters, as they tend to take up less space, whereas the size and shape of SRRs and S-shape resonators can vary drastically depending on the operating frequency. For example at high frequencies, the size of SRRs and S-shape resonators will be very small and will require high precision fabrication process and at low frequencies these structures can occupy more space, which in turn, constraint the size of the non resonating node. Furthermore, as E-plane filters can be implemented using split block waveguide housing, it is convenient to connect one end of the metallic fin to one side of this wall. Quarter wavelength type resonators have been widely used in the design and implementation of interdigital filters.

The configuration of this EPS in E-plane technology is presented in Figure 3.3-4. The non-resonating node effect is created by the standard E-plane resonator, which is a small homogeneous waveguide section between the input and output metallic septa that has a self resonance much higher than the intended central frequency of the filter. The bandstop segment of the EPS is realised by the suspended quarter wavelength resonator.

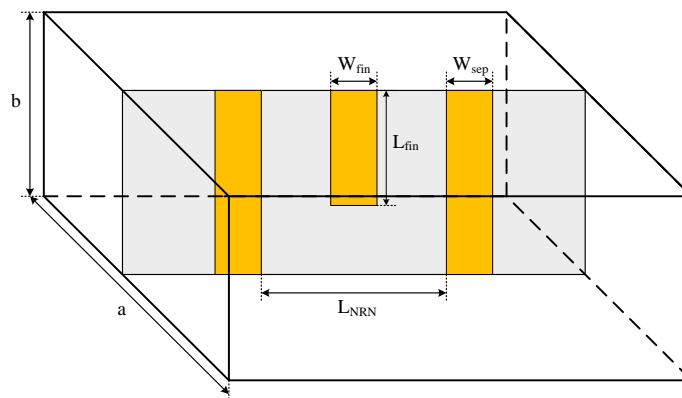


Figure 3.3-4: Configuration of an E-plane EPS within a rectangular waveguide.

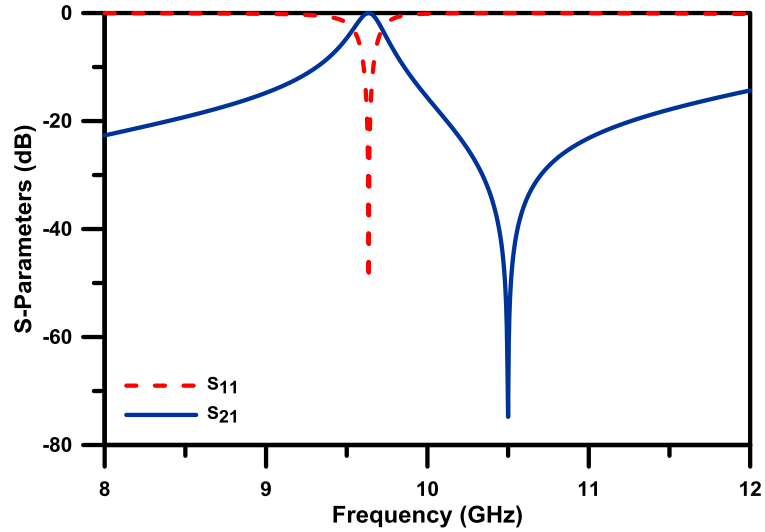


Figure 3.3-5: Simulated S-parameter response of an E-plane EPS with dimensions: $L_{NRN}=5\text{mm}$; $L_{fin}=6.4\text{mm}$; $W_{fin}=1.5\text{mm}$; $W_{sep}=3.5\text{mm}$, inserted in a WG16 (WR90) waveguide housing.

In order to demonstrate the performance of E-plane filters using cascaded EPS, a 4th order direct coupled E-plane EPS filter with four transmission zeros has been designed and simulated for the specifications listed below. The filter has also been measured to validate the performance.

- Centre frequency: 10.0 GHz;
- Ripple passband: 9.9 GHz - 10.2 GHz;
- Ripple level: 0.1dB
- Return loss: 20 dB;
- Transmission zeros: 10.4 GHz, 10.6 GHz, 11.5 GHz, 12.5 GHz.

The generalized Chebyshev approximation has been applied for the above specifications, which leads to the following filter polynomials:

$$S_{11}(s) = \frac{F(s)}{E(s)}; \quad S_{21}(s) = \frac{P(s)}{\varepsilon \cdot E(s)} \quad (3.3.5)$$

$$P(s) = s^4 - j29.7s^3 - 281s^2 + j978s + 1093 \quad (3.3.6)$$

$$F(s) = s^4 - j0.462s^3 + 0.913s^2 - j0.337s + 0.082 \quad (3.3.7)$$

$$\varepsilon \cdot E(s) = 815(s^4 + (2.175 - j0.462)s^3 + (3.276 - j1.191)s^2 + (2.529 - j1.822)s + (0.713 - j1.139)) \quad (3.3.8)$$

Extraction of admittance inverters' and FIS' values from the derived characteristic polynomials leads to the coupling structure presented in Figure 3.3-6 with the following values of the denoted elements: $J_{s1} = 1$, $B_{N1} = -8.72$, $J_1 = 8.71$, $B_1 = -9.06$, $J_{12} = 1$, $B_{N2} = -3.03$, $J_2 = 2.39$, $B_2 = -2.29$, $J_{23} = 1$, $B_{N3} = -6.11$, $J_3 = 4.86$, $B_3 = -4.2$, $J_{34} = 1$, $B_{N4} = -12.44$, $J_4 = 13.49$, $B_4 = -14.73$, $J_{4L} = 1$.

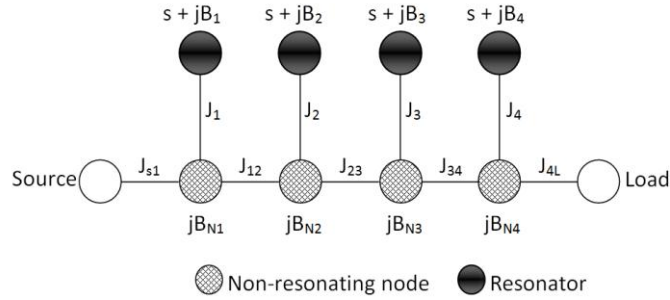


Figure 3.3-6: Coupling schematic of the 4th order EPS filter.

The filter has been designed and simulated in CST Microwave StudioTM. It has been implemented using the standard E-plane technology with an all-metal insert within a rectangular waveguide. Configuration of the insert for the filter is shown in Figure 3.3-7. Initial dimensions of the insert can be calculated by GCC extraction technique as described in [3-18]; final dimensions obtained by optimisation are presented in Table 3.3-1.

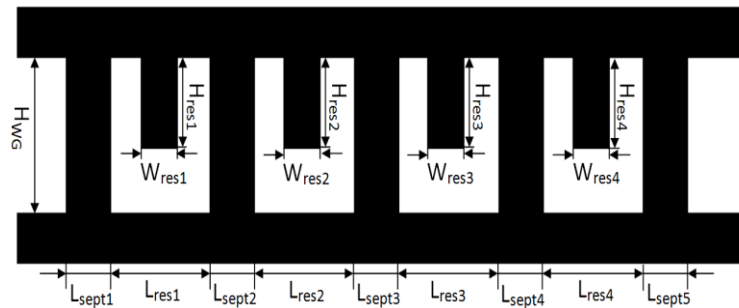


Figure 3.3-7: Layout of the E-plane insert for the 4th order EPS filter.

Parameters	Values (mm)	Parameters	Values (mm)
L_{sept1}	1.7	L_{res3}	4.2
L_{sept2}	5.02	L_{res4}	8.6
L_{sept3}	4.87	H_{res1}	5.8
L_{sept4}	6.64	H_{res2}	6.55
L_{sept5}	2.5	H_{res3}	6.3
L_{res1}	6.2	H_{res4}	5.2
L_{res2}	3.1	$W_{resi}, i=1...4$	1.6

Table 3.3-1: Dimension of the E-plane insert for the designed 4th order EPS filter.

In order to validate the simulated results, the filter structure was realised using the standard E-plane technology, where the insert was plotted on a copper foil ($\sigma = 5.8 \times 10^7 \text{ S/m}$) with thickness of $T = 0.1 \text{ mm}$. The inserts were placed in a channel within the standard waveguide housing WG-90 ($22.86 \times 10.16 \text{ mm}^2$) constructed out of brass. A photograph of the fabricated inserts together with the housing used is shown in Figure 3.3-8. The fabricated filter was then measured using an Agilent E8361A vector network analyser and a comparison of the results obtained with the simulated response has been presented in Figure 3.3-9. It can be observed from the measured results, that all four transmission zeros are visible and are within their intended locations. However, an insertion loss at the centre frequency of about 1.22 dB and slight shift in the poles can also be observed. This is mainly due to the tolerances encountered during fabrication, which is mainly due to the imitations in accuracy of the fabrication device used. Although it is possible to conclude that there is a good agreement between simulated and measured results taking into consideration the tolerances encountered.

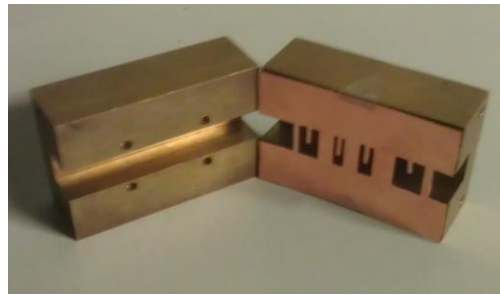


Figure 3.3-8: Photograph of the fabricated insert for the 4th order EPS filter, placed within a channel of a split block waveguide housing.

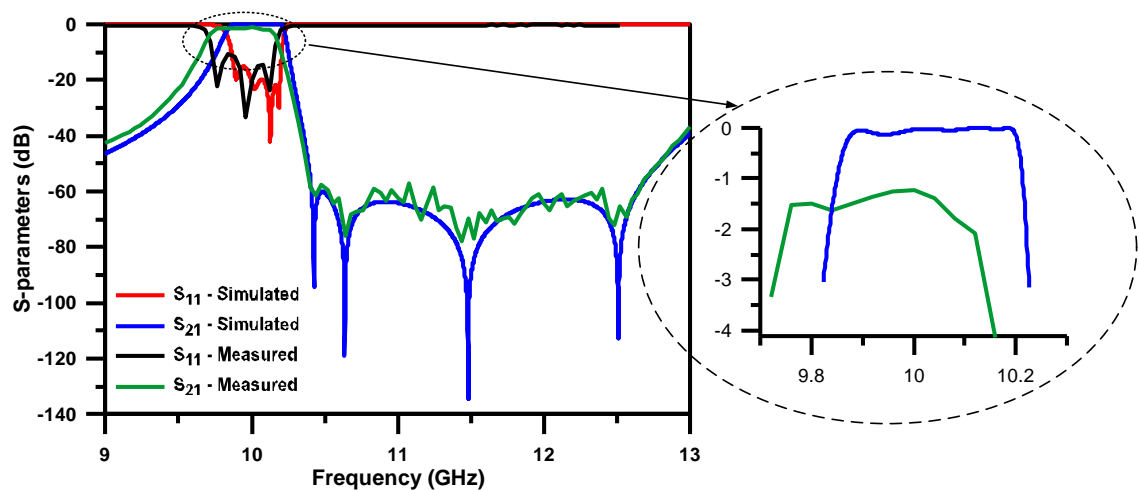


Figure 3.3-9: Comparison between simulated and measured results of the fabricated 4th order EPS filter.

3.4 Two Pole E-plane Extracted Pole Sections and Filters

It is well known that for a given filter order, dual mode filters are able achieve a size reduction of at least half of conventional filters of the same order [3-4]-[3-5]. Most of these unique filter structures were realised using waveguide cavities which exploit multiple resonant modes within each of the cavities. However due to the necessity of high precision fabrication facilities, these structures tend to suffer from high manufacturing costs. On the other hand, a type of filter, that has the ability to generate two poles from a single EPS, implemented using planar mounted E-plane inserts, can reap benefits offered by E-plane technology and address the cost related drawbacks. This section will describe the development of such an E-plane filter, using a modified EPS.

It has been shown in section 3.3 that an E-plane EPS is capable of generating a transmission zero in the upper stopband. Enlarging the length of the NRN of the E-plane EPS (distance between the two septa), it was found, that the structure is capable of exhibiting a frequency response with two poles and a transmission zero in the lower stopband. Therefore, this section will first present the analysis of an E-plane EPS in order to obtain its natural frequencies.

Prior to analysing and obtaining the natural frequencies of an E-plane EPS with an embedded quarter wavelength resonator, an examination of the natural frequencies of a conventional E-plane resonator which is weakly coupled to the input and output through the wide metallic septa has been conducted. The configuration of this resonator is given in Figure 3.4-1. Typical layout of a conventional E-plane filter formed by cascading such resonators was given in Figure 3.2-1.

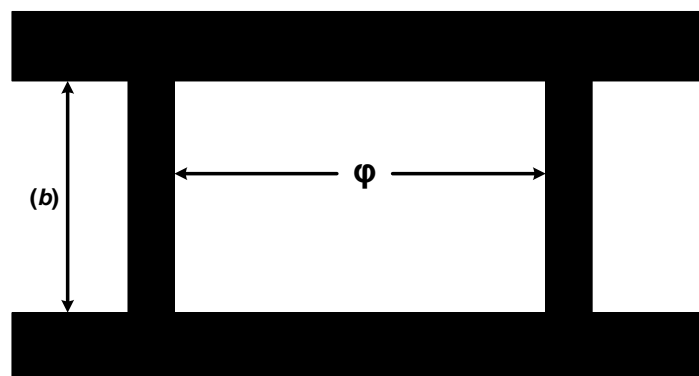


Figure 3.4-1: Configuration of a conventional E-plane resonator.

A two port network that is represented by its ABCD matrix, can be described by the following set of equations:

$$V_1 = A \cdot V_2 + B \cdot I_2 \quad (3.4.1)$$

$$I_1 = C \cdot V_2 + D \cdot I_2 \quad (3.4.2)$$

The entries A , B , C and D in this case, represent components of the chain matrix of a transmission line section. By applying the condition $V_1 = V_2$, it is possible to obtain the natural frequencies of the circuit shown in Figure 3.4-1. To satisfy this condition, it is clear that A must be equal to 1 and B equal to zero.

Taking into consideration that the circuit is reciprocal, we have $A \cdot D - B \cdot C = 1$ and this will reduce to $A \cdot D = 1$, since $B = 0$. Also assuming that the circuit is symmetrical, this will reduce to $A^2 = 1$. This, in turn, means resonance occurs when $\cos\varphi = \pm 1$ or $\tan\varphi = 0$, which is true when φ is equal to $k\pi$, where $k = 1, 2, 3 \dots$ Therefore, $\varphi = \beta l$ or $k\pi = \beta l$, where $\beta = \frac{2\pi}{\lambda}$, thus $l = \frac{k\lambda}{2}$. Here φ is the phase length, β is the phase constant, l is the physical length of the transmission line section and λ is the wavelength at centre frequency f_0 .

The same procedure can be applied in order to analyse the E-plane EPS. Figure 3.4-3 presents the schematic model of the EPS (its physical configuration is shown in Figure 3.4-2), taking into consideration the input and output septa as inverters, as a system of three cascaded 2-port networks.

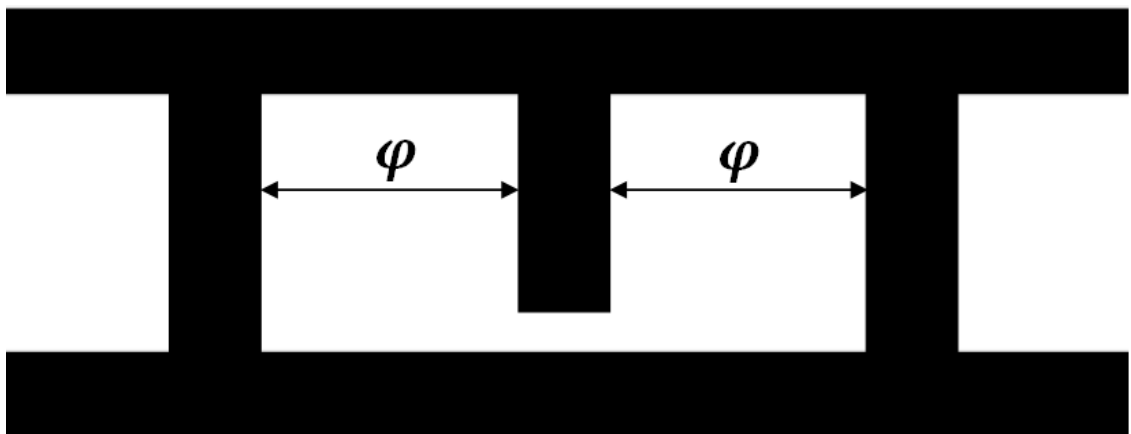


Figure 3.4-2: Configuration of the E-plane EPS.

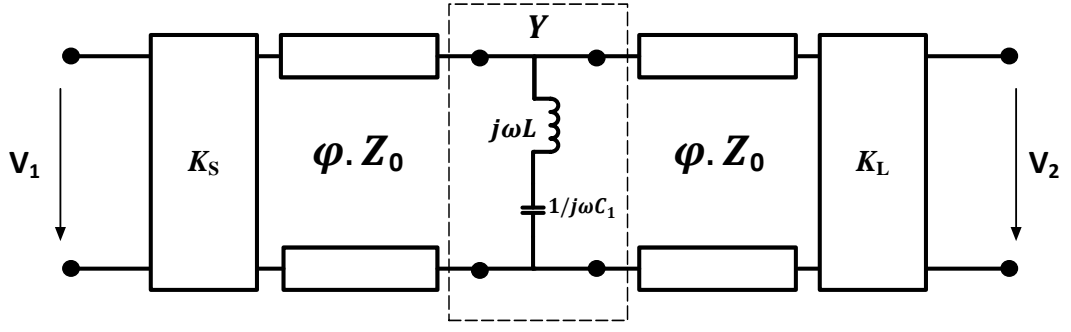


Figure 3.4-3: Circuit schematic representation of an E-plane EPS.

The φ -blocks represent the transmission line sections with the phase length φ , while a Y -block represents the fin as a series resonator. Their $ABCD$ -matrices are given as follows:

$$\begin{bmatrix} A & B \\ C & D \end{bmatrix}_{TL} = \begin{bmatrix} \cos \varphi & jZ_0 \sin \varphi \\ j \sin \varphi / Z_0 & \cos \varphi \end{bmatrix} \quad (3.4.3)$$

$$\begin{bmatrix} A & B \\ C & D \end{bmatrix}_{Fin} = \begin{bmatrix} 1 & 0 \\ Y & 1 \end{bmatrix} \quad (3.4.4)$$

where, $Y = 1/j\omega L \left(\frac{\omega^2 - \omega_0^2}{\omega^2} \right)$. Consequently, the $ABCD$ -matrix of the entire circuit can be obtained as:

$$\begin{bmatrix} A & B \\ C & D \end{bmatrix}_{EPS} = \begin{bmatrix} \cos 2\varphi + j \frac{Z_0 Y_1}{2} \sin 2\varphi & jZ_0 \sin 2\varphi - Z_0^2 Y_1 \sin^2 \varphi \\ \frac{j \sin 2\varphi}{Z_0} + Y_1 \cos^2 \varphi & \cos 2\varphi + j \frac{Z_0 Y_1}{2} \sin 2\varphi \end{bmatrix} \quad (3.4.5)$$

Once again, by applying the condition $V_1 = V_2$, it is possible to obtain the natural frequencies of the E-plane EPS shown in Figure 3.4-3. Therefore to satisfy this condition, it is clear that B must be equal to 0, consequently $A \cdot D = 1$. Thus the following set of equations is obtained:

$$jZ_0 \sin 2\varphi - Z_0^2 Y_1 \sin^2 \varphi = 0 \quad (3.4.6)$$

$$\left(\cos 2\varphi + j \frac{Z_0 Y_1}{2} \sin 2\varphi \right)^2 = 1 \quad (3.4.7)$$

After several manipulations of the above set of equations, two solutions can be obtained:

$$\tan \varphi = -2\omega L_1 \left(\frac{\omega^2 - \omega_o^2}{\omega^2} \right) \quad (3.4.8)$$

$$\varphi = \pi k \quad (3.4.9)$$

The derived equations state that poles of the structure occur when $\tan \varphi = -2\omega L_1 \left(\frac{\omega^2 - \omega_o^2}{\omega^2} \right)$ and when $\tan \varphi = 0$ for $\varphi = k\pi$, where $k = 1, 2, 3, \dots$ or $\beta l = k\pi$

where $\beta = \frac{2\pi}{\lambda}$ which means $l = \frac{k\lambda}{2}$. Figure 3.4-4 shown below has been utilised in order to demonstrate this.

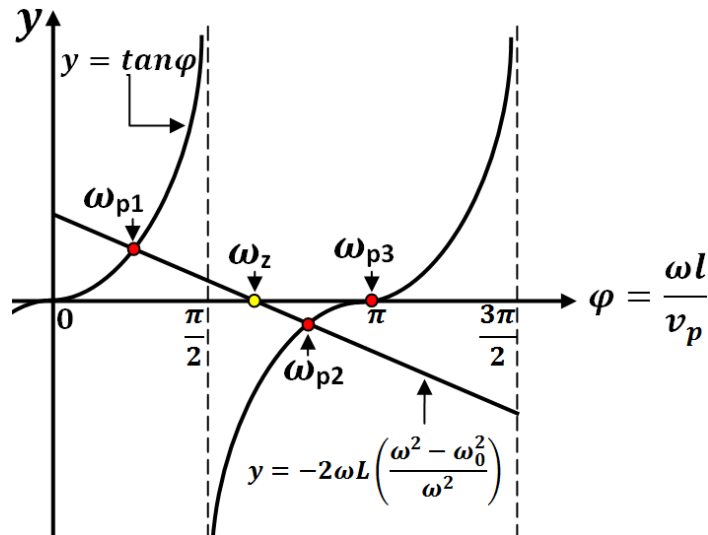


Figure 3.4-4: Graphical illustration of the poles and zeros of an E-plane EPS.

The locations of the poles for the circuit in Figure 3.4-3, determined by the set of equations (3.4.8) and (3.4.9) are illustrated by the Figure 3.4-4 and are denoted in the graph as ω_{p1} , ω_{p2} and ω_{p3} . Here ω_{p1} and ω_{p2} are determined by the intersection between $y = \tan \varphi$ and $y = -2\omega L((\omega^2 - \omega_0^2)/\omega^2)$. The third pole ω_{p3} is determined by the condition $\tan \varphi$ is equal to zero. By keeping the values of the series resonator constant (which can be achieved by keeping the dimensions of the metallic fin constant) and for very small sections of transmission line lengths, roughly $\leq \lambda_g/4$, where λ_g is the guided wavelength, the single pole ω_{p1} and a transmission zero above this pole can be observed. However, ω_{p2} and ω_{p3} will be shifted to much higher frequencies and can be considered as spurious in this case. In this configuration, the circuit is considered to behave as a standard E-plane EPS.

On the other hand, if the transmission line lengths were to be increased roughly by λ_g , then the pole ω_{P1} will be shifted towards very low frequencies and in a waveguide it can be made to occur below the cut-off frequency. With this increase in transmission line lengths the poles ω_{P2} and ω_{P3} will also be shifted towards lower frequencies, but with the appropriate line lengths they can be made to occur within the interested range of frequencies for a chosen waveguide and will be located very close to each other. Such a design can be referred to as a two-pole E-plane EPS. In this case, the transmission zero is located below the poles ω_{P2} and ω_{P3} . Total phase length of the two-pole E-plane EPS usually exceeds $\varphi = 2\pi$ by the width of the fin, however it is still smaller than two standard E-plane resonators weakly coupled through a long septum.

In general, the configuration of the two-pole E-plane EPS is similar to the standard E-plane EPS, but with an enlarged non-resonating node. A comparison of simulated S-parameter response of both a standard E-plane EPS and a two-pole EPS using E-plane inserts is presented on Figure 3.4-5. The first pole ω_{P1} for the two-pole EPS occurs beyond the cut-off frequency of the waveguide and is not shown here.

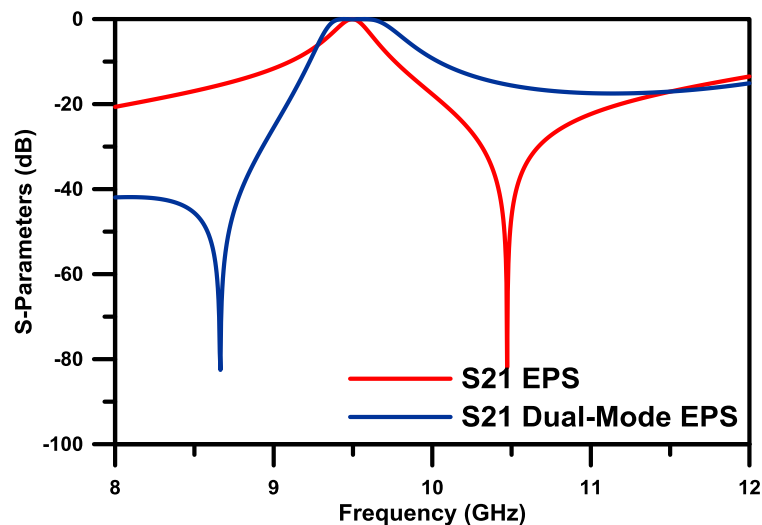


Figure 3.4-5: Comparison of the s-parameter responses between a standard EPS and a two-pole EPS.

By modelling the two-pole E-plane EPS in CST Microwave StudioTM and through investigating the structure by systematically varying the dimensions, it was found that the location of one of the poles can be altered by varying the width of the metallic fin (W_{RES}) as well as the transmission zero, whereas the other pole, which corresponds to the non-resonating node's self resonance, retains its position. The reason for this effect, as shown in Figure 3.4-6, can be explained by the shifting of the internal $\lambda/4$ resonators

resonant frequency due to the modification of its internal inductance and capacitance. A similar effect can be observed by varying the length of the embedded metallic fin (H_{RES}), as shown in Figure 3.4-7. However, it can also be distinguished that the shift in the transmission zero frequency is more than that of the shift in the pole frequency.

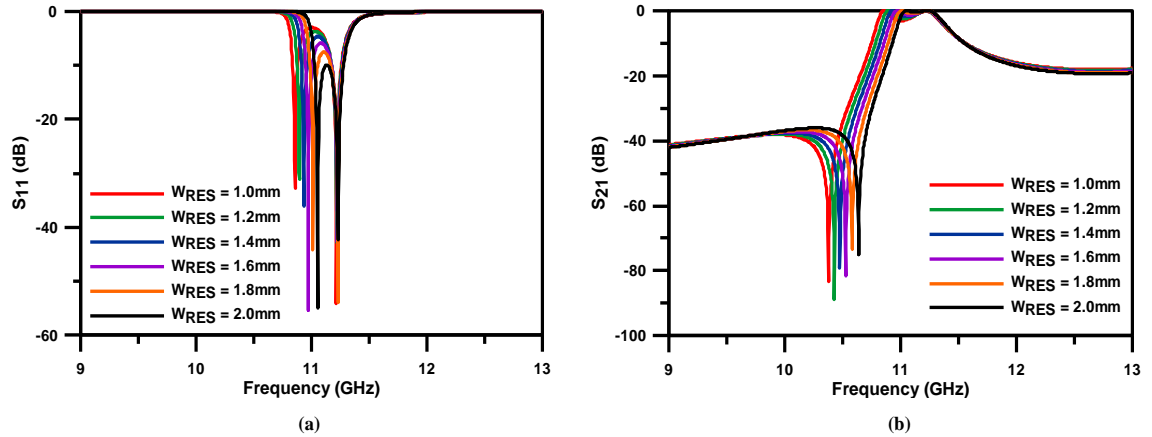


Figure 3.4-6: Effect of varying width of metallic fin (W_{RES}): (a) On S_{11} ; (b) On S_{21} .

By varying the length of the non-resonating node (L_{NRN}), the transmission zero virtually retains its position with just a minor shift towards the pole frequency with the increase in the length (see Figure 3.4-8). This effect may occur due to the slight alteration of the coupling between the septa and the metallic fin. Simultaneously, increasing the length of the non-resonating nodes, results in a down shift of the pole frequencies, but with the effect having a greater emphasis on the second pole which corresponds to the self-resonant frequency of the node. Taking advantage of the observed effects, two-pole E-plane EPS and filters based on them, can be tuned to satisfy a desired specification.

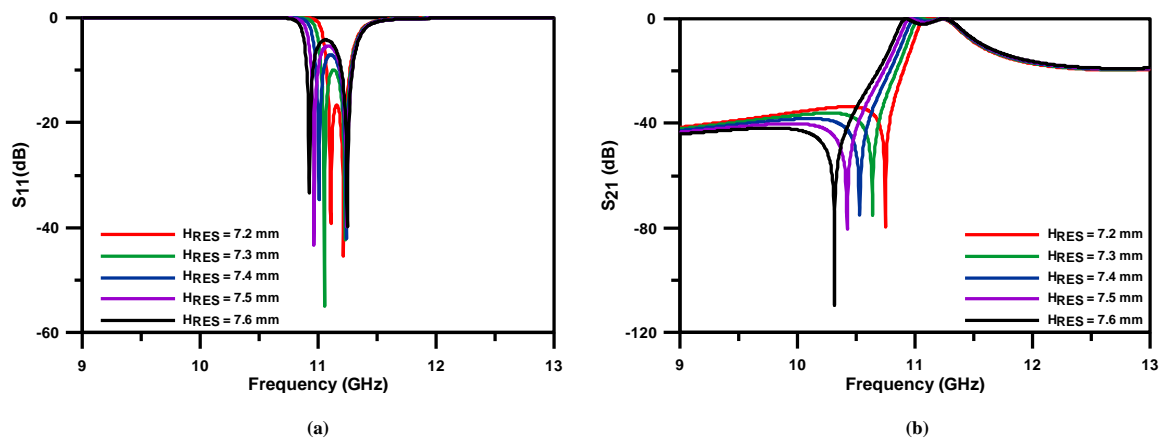


Figure 3.4-7: Effect of varying length of metallic fin (H_{RES}): (a) Effect on S_{11} ; (b) Effect on S_{21} .

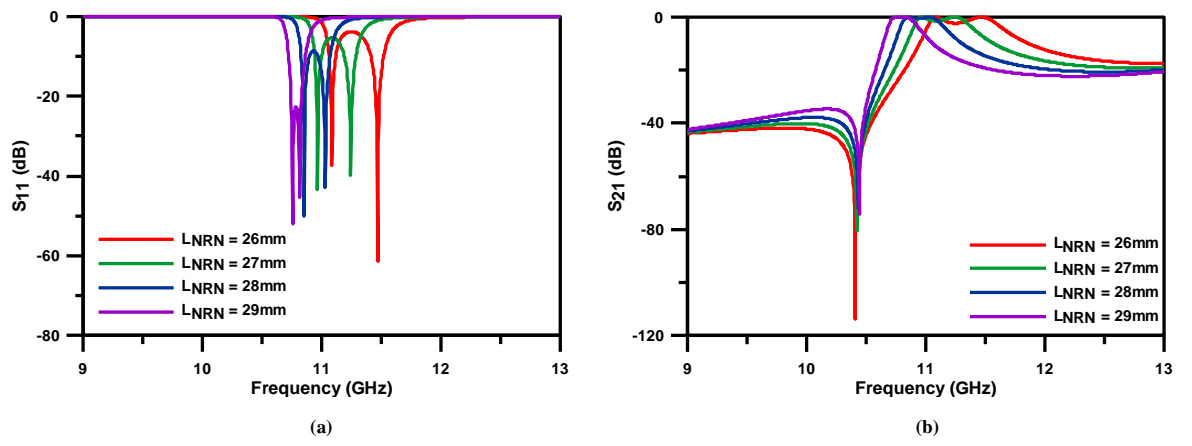


Figure 3.4-8: Effect of varying length of non-resonating node (L_{NRN}): (a) Effect on S_{11} ; (b) Effect on S_{21} .

3.4.1 Filters Implemented using the Two-pole E-plane Extracted Pole Sections

In order to demonstrate the performance of E-plane filters using the two-pole EPS, a 4th order direct coupled filter with two transmission zeros in the lower stopband has been designed and simulated for the specifications listed below. The filter has also been fabricated and tested to validate the performance.

- Centre frequency: 10.5 GHz;
- Ripple passband: 10.4 GHz-10.7 GHz;
- Return loss: 20 dB;
- Transmission zeros: 9.9 GHz, 10.2 GHz.

By ignoring ω_{p1} (as it occur below the cutoff frequency of the waveguide) and taking into consideration of the observed effects in Figures 3.4-6 to 3.4-8, the two-pole E-plane EPS appear to exhibit properties of a standard EPS cascaded with that of another resonator. Hence, a 4th order filter structure using cascaded two-pole EPS can be modelled using a lowpass prototype network with a coupling scheme presented in Figure 3.4-9. However, in order to evaluate initial dimensions, the generalised coupling coefficient extraction procedure as described in [3-18] has not been applied in this case, since it is impossible to distinguish the physical parameters that may be responsible for the couplings. The generalised Chebyshev approximation has been applied for the given specifications, which leads to the following filter polynomials:

$$P(s) = s^4 - j29.7s^3 - 281s^2 + j978s + 1093 \quad (3.3.6)$$

$$F(s) = s^4 - j0.462s^3 + 0.913s^2 - j0.337s + 0.082 \quad (3.3.7)$$

$$\begin{aligned} \varepsilon \cdot E(s) = & 815(s^4 + (2.175 - j0.462)s^3 + (3.276 - j1.191)s^2 \\ & + (2.529 - j1.822)s + (0.713 - j1.139)) \end{aligned} \quad (3.3.8)$$

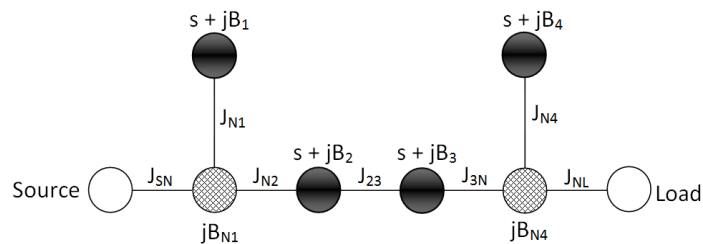


Figure 3.4-9: Coupling scheme of the 4th order filter.

Afterwards, evaluation of admittance inverters' and FIS' values from the calculated characteristic polynomials leads to the coupling structure presented in Figure 3.4-9 with the following values for the denoted elements: $J_{SN} = 1$, $B_{N1} = 4.04$, $J_{N1} = 4.22$, $B_1 = 4.48$, $J_{N2} = 0.88$, $B_2 = -0.07$, $J_{23} = 0.72$, $B_3 = -0.045$, $J_{3N} = 0.88$, $B_{N4} = 1.91$, $J_{N4} = 2.06$, $B_4 = 2.37$, $J_{NL} = 1$. The filter has been designed and simulated in CST Microwave Studio™, using the standard E-plane technology with an all-metal insert placed within a channel in a split block rectangular waveguide housing. Configuration of the insert for the filter is shown in Figure 3.4-10. Final dimensions obtained by means of optimisation are presented in Table 3.4-1.

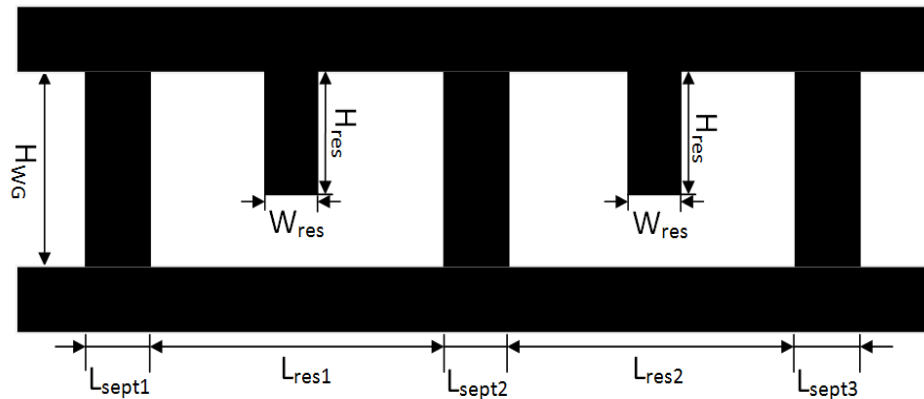


Figure 3.4-10: Configuration of the E-plane insert for the 4th order filter implemented using two cascaded two-pole EPS.

Parameters	Values (mm)	Parameters	Values (mm)
L_{sept1}	3.3	W_{res2}	1.5
L_{sept2}	13.5	H_{res1}	8.0
L_{sept3}	4.0	H_{res2}	7.7
W_{res1}	2.1	L_{res1}	30.0
H_{WG}	10.16	L_{res2}	30.0

Table 3.4-1: Dimension of the E-plane insert for the designed 4th order filter using cascaded two-pole EPS.

In order to validate the simulated results of the filter structure the insert was first plotted on a copper foil ($\sigma = 5.8 \times 10^7 \text{ S/m}$) with thickness of $T = 0.1 \text{ mm}$. Thereafter, the inserts were placed in a channel within the standard waveguide housing WG-90 ($22.86 \times 10.16 \text{ mm}^2$) constructed out of brass. A photograph of the fabricated inserts together with housing used is shown in Figure 3.4-12. The fabricated filter was then measured using an Agilent E8361A vector network analyser and a comparison of the results obtained with the simulated has been presented in Figure 3.4-11. Though the

measurement results show reasonably good agreement with the simulated results, it can be observed that the poles of the filter have shifted slightly towards lower frequencies, as well as the lowest transmission zero. This is mainly due to the high sensitivity of the width of the fins which control the location of the transmission zeros, as well as its influence towards the location of the poles. The measured insertion loss of the filter at its centre frequency after fabrication was found to be 2.52 dB. One explanation for this is the signal leakage that may occur through the imperfect waveguide housing. However, it is possible to improve the measurement results through meticulous use of the available tools.

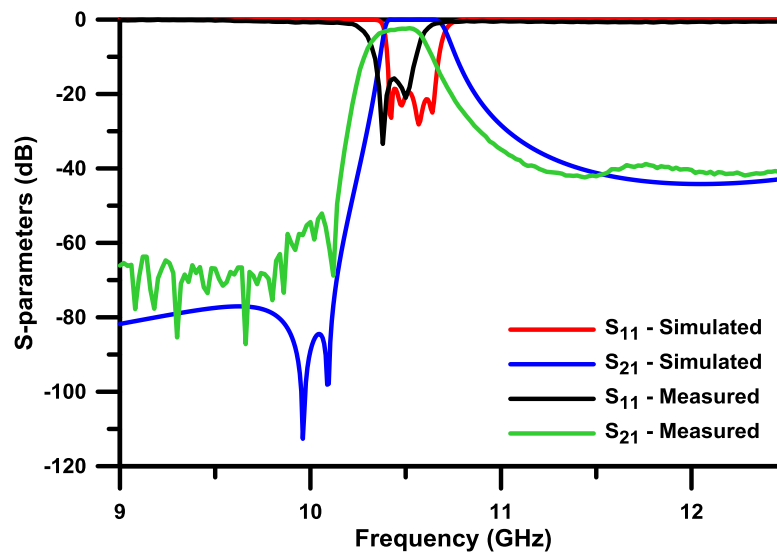


Figure 3.4-11: Comparison between simulated and measured results of the fabricated filter.



Figure 3.4-12: Photograph of the fabricated insert for the 4th order filter.

3.5 Ultra-Compact E-Plane Extracted Pole Waveguide Filters

The two-pole E-plane EPS described in section 3.4 is capable of producing two poles and a transmission zero in the lower stopband. However in order to achieve this trait, the structure has to have an enlarged non-resonating node, thus sacrificing compactness, which is regarded as one of the benefits of using an EPS. Furthermore since the two-pole EPS is only capable of producing a single transmission zero in the lower stopband, it has an inferior upper stopband performance in comparison to the standard E-plane EPS. This section therefore present a solution to this problem by introducing a new structure that is significantly more compact in comparison to the two-pole EPS, while at the same time produces transmission zeros in both the upper and the lower stopbands to improve their attenuation.

3.5.1 Development of the Ultra-compact E-plane Extracted pole filters

Consider the layout of the E-plane extracted pole filter as shown previously in Figure 3.4-2. Extending the length of the non-resonating node displayed the formation of two poles and a single transmission zero in the lower stopband. However filters formed from such a structure suffers from the aforementioned limitations. These limitations can be overcome by the introduction of two additional fins located on either side of the already existing centrally placed metallic fin as depicted in Figure 3.5-1, which improves the performance as well as achieves a significant size reduction.

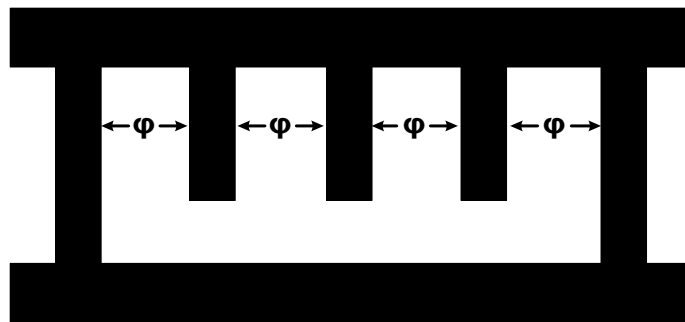


Figure 3.5-1: Configuration of a E-plane insert for realisation of ultra-compact EPS filters.

Figure 3.5-2 shows an equivalent circuit model of the proposed ultra-compact filter, with the input and output septa represented by K inverters. Y-blocks represent fins as series LC resonators which are spaced through sections of transmission lines with a phase length φ and characteristic impedance Z_0 . In order to obtain the natural

frequencies of the schematic, it can be analysed using similar procedure described in section 3.4, as was done for the standard E-plane extracted pole configuration.

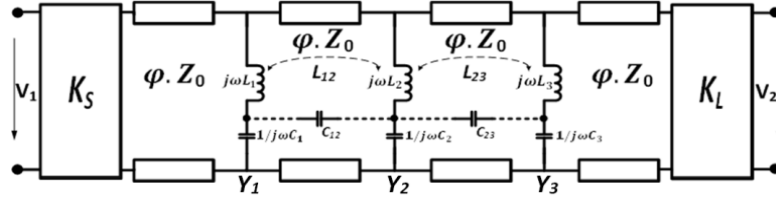


Figure 3.5-2: Equivalent circuit model for the ultra-compact EPS filter.

The $ABCD$ -matrix for a single EPS (Figure 3.4-2) without considering the septa can be computed as a system of cascaded 2-port networks:

$$\begin{bmatrix} A & B \\ C & D \end{bmatrix}_{EPS} = \begin{bmatrix} \cos 2\varphi + j \frac{Z_0 Y_1}{2} \sin 2\varphi & j Z_0 \sin 2\varphi - Z_0^2 Y_1 \sin^2 \varphi \\ \frac{j \sin 2\varphi}{Z_0} + Y_1 \cos^2 \varphi & \cos 2\varphi + j \frac{Z_0 Y_1}{2} \sin 2\varphi \end{bmatrix} \quad (3.5.1)$$

The initial over-all $ABCD$ -matrix of the entire ultra-compact filter can be approximately obtained (without taking into consideration the additional couplings, represented by dashed lines) as:

$$\begin{aligned} \begin{bmatrix} A & B \\ C & D \end{bmatrix}_{Filter} &= \begin{bmatrix} 0 & jK \\ -\frac{j}{K} & 0 \end{bmatrix} \times \begin{bmatrix} A & B \\ C & D \end{bmatrix}_{EPS} \times \begin{bmatrix} 1 & 0 \\ Y_2 & 1 \end{bmatrix} \times \begin{bmatrix} A & B \\ C & D \end{bmatrix}_{EPS} \\ &\times \begin{bmatrix} 0 & jK \\ -\frac{j}{K} & 0 \end{bmatrix} \end{aligned} \quad (3.5.2)$$

where $Y_n = 1/j\omega L_n \left(\frac{\omega^2 - \omega_{0n}^2}{\omega^2} \right)$ and ω_{0n} represent angular frequency of the transmission zero generated by n^{th} fin. The system is considered to be symmetric, therefore $A = D$. As mentioned in section 3.4, to obtain poles of the structure, condition $V_1 = V_2$ is applied to the input and output of the circuit. Therefore, the resonant condition is $B = 0$ and due to reciprocity, $AD - BC = 1$. Thus the following set of equations is obtained:

$$Y_2 \left[-j Z_0 \sin 2\varphi + Z_0^2 Y_1 \sin^2 \varphi \right] + 2 \left[\cos 2\varphi + \frac{j Z_0 Y_1}{2} \sin 2\varphi \right] = 0 \quad (3.5.3)$$

$$\left(\cos 2\varphi + j \frac{Z_0 Y_1}{2} \sin 2\varphi \right) \left(\cos 2\varphi + j \frac{Z_0 Y_1}{2} \sin 2\varphi \right) = 1 \quad (3.5.4)$$

After several manipulations, two sets of solutions to (3.5.3) and (3.5.4) can be found as $\tan\varphi = f_1(\omega)$ and $\tan\varphi = f_2(\omega)$, where:

$$f_1(\omega) = \frac{Z_0 [jY_2 + jY_1] \pm \sqrt{4 - (Z_0^2 (Y_2^2 - Y_1^2))}}{2 + Z_0^2 Y_2 Y_1} \quad (3.5.5)$$

$$f_2(\omega) = \frac{-2\omega L_1 \left(\frac{\omega^2 - \omega_o^2}{\omega^2} \right)}{Z_0} \quad (3.5.6)$$

The locations of the poles determined by equation (3.5.5) and (3.5.6) are illustrated in Figure 3.5-3, where pole frequencies ω_{p1} , ω_{p2} and ω_{p3} correspond to the ω -axis values at the points of intersection of the responses: $y = \tan\varphi$ with that of $f_1(\omega)$ and $f_2(\omega)$. Also, transmission zeros at ω_{z1} - ω_{z3} are determined by the conditions $Z_n = \frac{1}{Y_n} = 0$. The responses in Figure 3.5-3 have been plotted using the relationship between φ and ω : $\varphi = \omega l/v_p$. Here l is the length of the waveguide section and v_p is the phase velocity in the waveguide.

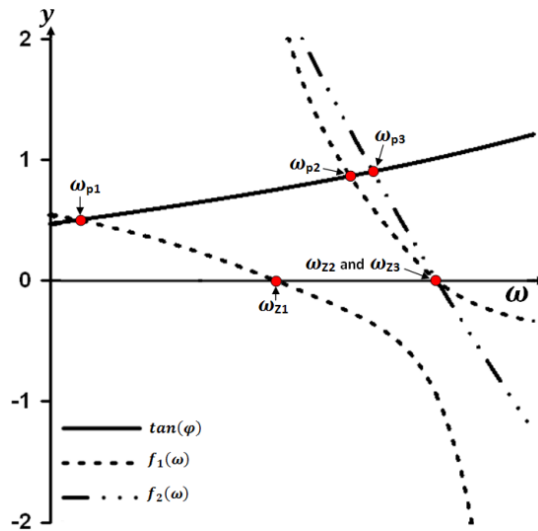


Figure 3.5-3: Graphical illustration of pole and zero locations for the ultra-compact filter.

It can be noticed from Figure 3.5-3 that the poles ω_{p1} , ω_{p2} and ω_{p3} drift with respect to each other depending on parameters of the lines defined by equations (3.5.5) and (3.5.6). From (3.5.5) and (3.5.6), for higher values of L_l it is possible to obtain the poles for smaller values of φ , that is equivalent to significant size reduction, in comparison with the size of the conventional E-plane resonator at the same centre frequency, or the two-pole EPS with an extended non-resonating node length (as demonstrated in section 3.4). Although the two-pole EPS is still comparatively smaller than two standard E-

plane resonators weakly coupled through a long septum.

The two-pole EPS depicted in Figure 3.4-2 can be miniaturized taking advantage of the procedure expressed in this section. For this purpose, each of the two waveguide sections of the phase length $\varphi = \pi$, has been replaced by a single E-plane EPS through the use of extra fins in the middle of both waveguide sections of the standard two pole EPS. Arrangement of the ultra-compact E-plane insert within a split block waveguide housing is presented in Figure 3.5-4.

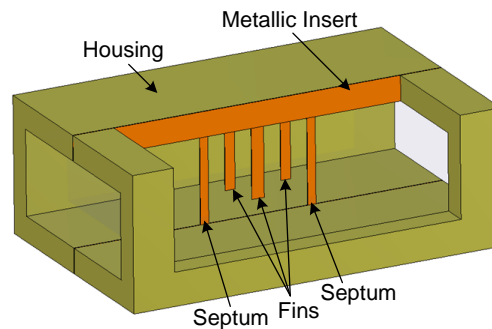


Figure 3.5-4: Arrangement of the E-plane insert for the ultra-compact EPS filters.

In order to illustrate the difference in performance achieved by the proposed structure, the new ultra-compact E-plane filter was compared to the standard two-pole EPS as well as a conventional 2nd order E-plane filter. All three structures were designed to the same specified centre frequency of 9.5 GHz and bandwidth 0.3 GHz. Frequency responses of the structures are compared in Figure 3.5-5.

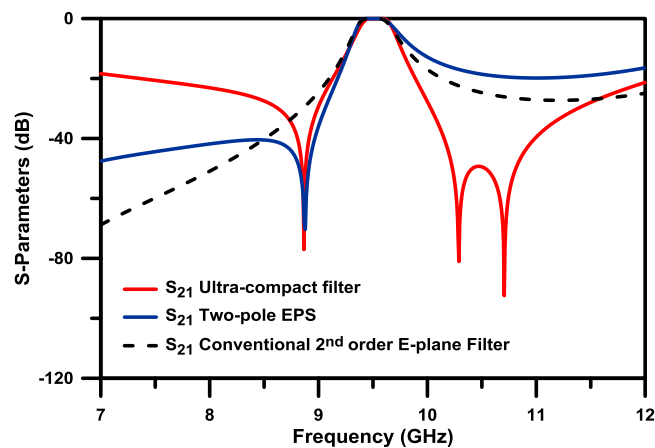


Figure 3.5-5: Comparison of the S-parameter responses of the standard E-plane two pole EPS, the proposed ultra-compact EPS filter and a conventional 2nd order E-plane filter.

As presented in Figure 3.5-5, the proposed structure produces three poles and three transmission zeros. However, the first pole occurs below the waveguide cut-off frequency and is not shown here. Since the fins are placed closely to one another, the capacitive coupling between them (presented in Figure 3.5-2 by capacitance C_{12} and C_{23}) and mutual inductances (L_{12} , L_{23}) result in the splitting of the upper stopband transmission zeros (ω_{Z2} and ω_{Z3}). The equivalent circuit in Figure 3.5-2 has been simulated using Agilent ADS software tool. The frequency response of the circuit is presented in Figure 3.5-6 which takes into account these additional couplings.

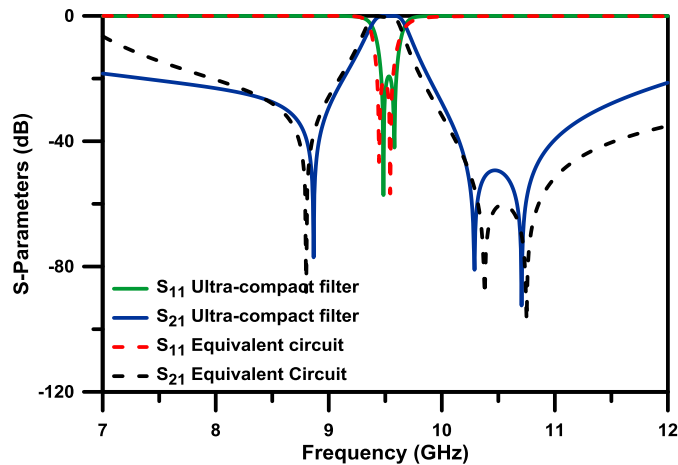


Figure 3.5-6: Comparison of the S-parameter responses of the ultra-compact EPS filter and frequency response of its equivalent schematic.

It is also visible from the comparison that the proposed ultra-compact filter has significantly better upper stopband attenuation. Even considering that both the two-pole EPS and the ultra-compact filter give better performance in terms of selectivity in comparison to the conventional E-plane filter, it is clear that the proposed structure has lower stopband attenuation for the frequency range of 7 GHz to 8.5 GHz. This decrease is due to the shift in ω_{P1} towards higher frequencies after the introduction of the new fins. It is possible to improve this by extending the length of the central metallic fin which creates a shift in ω_{Z1} and ω_{P1} to lower frequencies.

3.5.2 Investigating The Effect of Parametric Variations

This subsection presents the observed effects of dimension variations of the ultra-compact E-plane filter. By modelling and systematically analysing the proposed structure in CST Microwave StudioTM, it was found that the location of the transmission zero in the lower stopband can be controlled independently by varying the length of the central metallic fin (H_{RES2}), which performs as a quarter wavelength ($\lambda/4$) resonator, without having any effect on the locations of the upper stopband transmission zeros. The reason for this effect, as shown in Figure 3.5-7, is due to the shifting of the internal $\lambda/4$ resonator's resonant frequency. Though not shown here, a similar effect, as seen in Figure 3.4-6 for the two pole EPS, can be observed by varying the width of the $\lambda/4$ resonator.

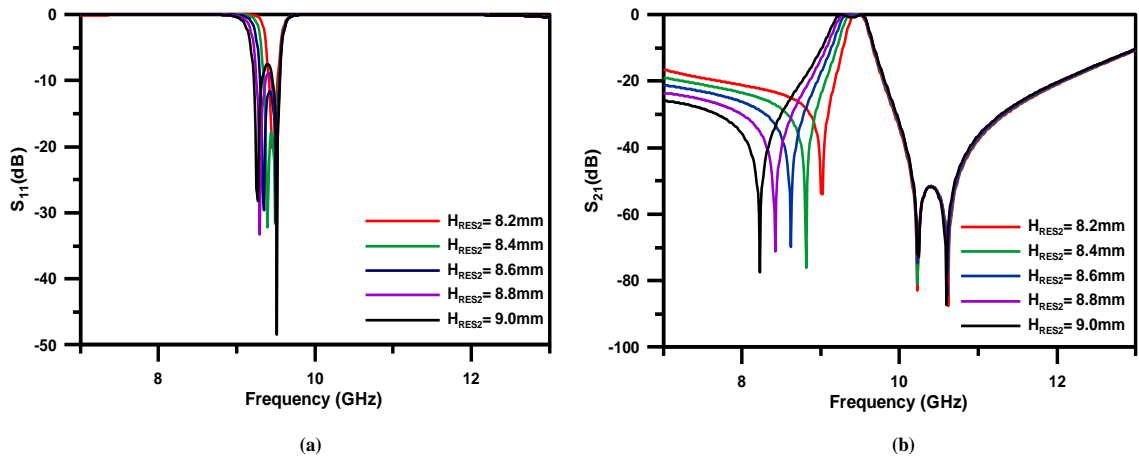


Figure 3.5-7: Effect of varying length of centre metallic fin (H_{RES2}): (a) Effect on S_{11} ; (b) Effect on S_{21} .

By varying the length of the first and last metallic fins (H_{RES1} and H_{RES3}), the upper stopband transmission zeros as well as the two poles (ω_{P2} and ω_{P3}) can be controlled without effecting the location of the lower stopband transmission zero. The observed effect is shown in Figure 3.5-8, and the reason for this shift can be explained again due to the change of the resonant frequency of the two $\lambda/4$ type resonators.

By varying the length of the non-resonating node (L_{NRN}), the lower stopband transmission zero undergoes a minor shift towards the pole frequency with an increase in the length (see Figure 3.4-9). This may be due to the slight alteration of the coupling between the septa and the first and last fins. More noticeably, it is clear that the split in the upper stopband transmission zeros decrease with a reduction in L_{NRN} , which is due

to the tighter coupling between the first and the last fins. Simultaneously, increasing the length of the non-resonating node results in down shift of the pole frequencies. Taking advantage of the observed effects, ultra-compact E-plane filters can be tuned to satisfy a desired specification.

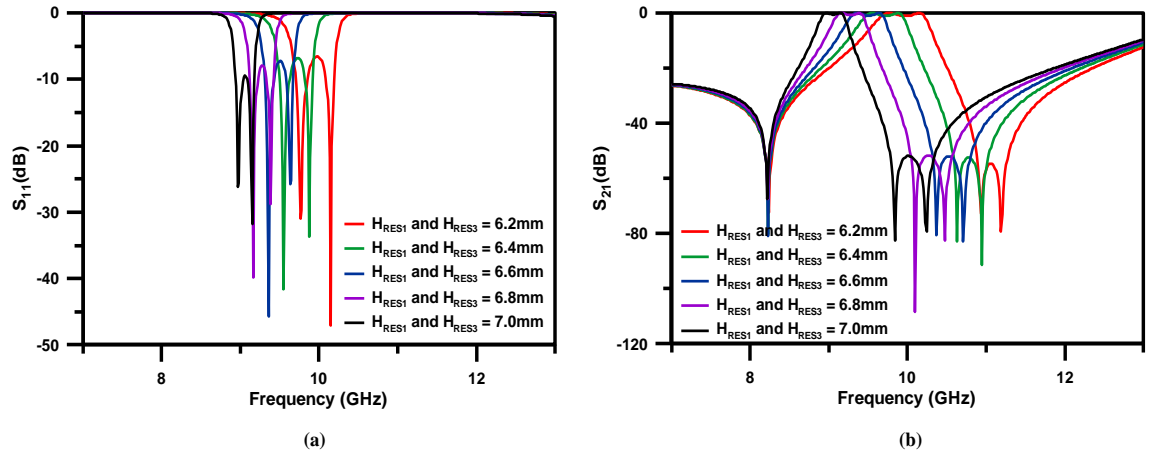


Figure 3.5-8: Effect of simultaneously varying the length of first metallic fin (H_{RES1}) and last metallic fin (H_{RES3}): (a) Effect on S_{11} ; (b) Effect on S_{21} .

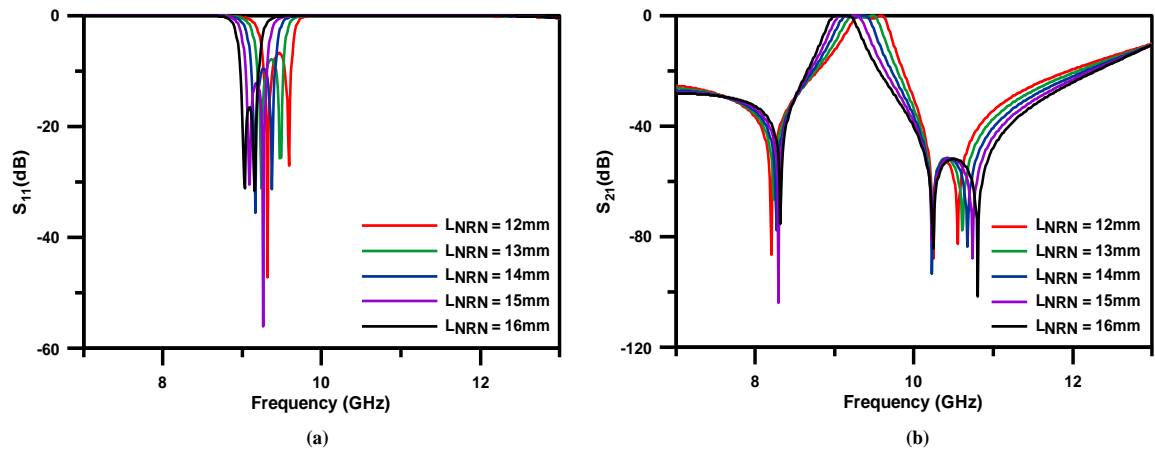


Figure 3.5-9: Effect of varying length of non-resonating node (L_{NRN}): (a) Effect on S_{11} ; (b) Effect on S_{21} .

3.5.3 Simulation and Experimental Verification

In order to demonstrate the performance of the proposed filters, an ultra-compact E-plane filter, with three transmission zeros has been designed and simulated for the specifications listed below.

- Centre frequency: 9.45 GHz;
- Ripple passband: 9.3-9.6 GHz;
- Return loss: 20 dB;
- Transmission zeros: 8.8 GHz, 10.2 GHz, 10.2 GHz.

The filter has been designed and simulated in CST Microwave Studio™. Due to the nature of the filter, where it generates a single pole at lower frequencies than the intended passband, it was not possible to synthesise this type of filter, using the generalised Chebyshev polynomials in order to obtain coupling values for a suitable coupling schematic. Hence the filter has been manually optimized, taking into account the observations made by parametric variations as described in section 3.5.3. The configuration of the E-plane insert is shown in Figure 3.5-10.

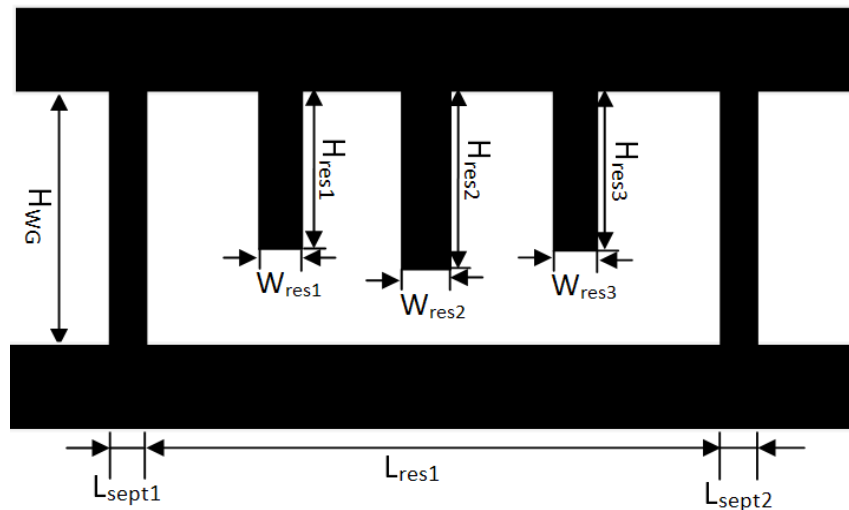


Figure 3.5-10: Configuration of the E-plane insert for the proposed ultra-compact EPS filters.

The length of the fin required for realising the transmission zeros can be found as $\approx \lambda/4$ and the width of the input/output septa as well as the fins were obtained during optimisation process to satisfy filter requirements. Final dimensions of the two E-plane inserts are summarised in Table 3.5-1. It is clear that the proposed structure is 65%

smaller in comparison with the standard two-pole E-plane EPS designed for the same centre frequency.

Standard Dual-mode EPS Filter		Ultra-compact EPS Filter	
Parameters	Values (mm)	Parameters	Values (mm)
L_{sept1}	2.7	L_{sept1}	1
L_{sept2}	2.7	L_{sept2}	1
W_{res1}	1.0	W_{res1}	1
W_{res2}	N/A	W_{res2}	1.4
W_{res3}	N/A	W_{res3}	1
L_{res1}	36.6	L_{res1}	12.7
H_{res1}	8.8	H_{res1}	6.7
H_{res2}	N/A	H_{res2}	8.4
H_{res3}	N/A	H_{res3}	6.7
Total length	42.8	Total length	14.7

Table 3.5-1: Dimension of the E-plane insert for the designed ultra-compact EPS filter.

In order to validate the performance of the simulated structure, the insert has been plotted on a copper foil ($\sigma = 5.8 \times 10^7 \text{ S/m}$) with thickness of $T = 0.1 \text{ mm}$. Subsequently the inserts were then placed in a channel within the standard split block waveguide housing WG-90 ($22.86 \times 10.16 \text{ mm}^2$) constructed out of brass. A photograph of the fabricated inserts together with the housing employed is shown in Figure 3.5-12. The fabricated filter was then measured using an Agilent E8361A vector network analyser and a comparison of the results obtained with the simulated results has been demonstrated in Figure 3.5-11.

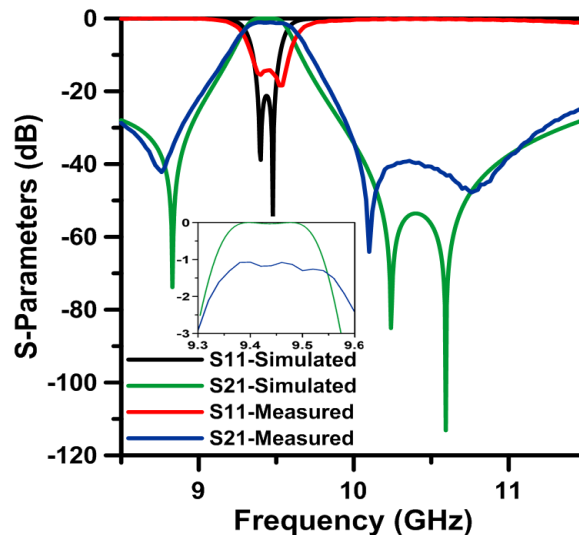


Figure 3.5-11: Simulated and measured S-parameter response of the designed ultra-compact EPS filter.

From Figure 3.5-11, it is clear that the measured results show reasonably good agreement with that of the simulated. However, an insertion loss of the filter of around 1.4 dB can be observed as well as a slightly greater separation of the transmission zeros in the upper stopband. This is mainly due to the tolerances encountered during fabrication process and the limitations to the precision which the plotter can reach, which could have resulted in a decrease in the coupling between the first and last metallic fins. Results can be further improved through meticulous use of the available tools.



Figure 3.5-12: Photograph of the fabricated ultra-compact EPS filter insert placed within a channel of a split block waveguide housing.

Higher order filters based on the proposed structure can be realised through having cascaded sections or by having extra adjacent fins spaced by transmission line sections between the two septa. The designed filter has a length of just 14.7mm. In comparison to a two-pole EPS designed for the same centre frequency and bandwidth, the proposed filter is in the region of 65% more compact. It is also approximately 13% and 85.15% more compact length wise, than a second order EPS filter and a 4th order conventional E-plane filter, designed for the same centre frequency, bandwidth and a comparable upper stopband attenuation, respectively. Table 3.5-3 summarises the insert lengths of the comparable E-plane filters.

E-plane Filter type	Length (mm)
Conventional 2 nd order filter	47.8
Conventional 4 th order filter with comparable upper stopband attenuation to the ultra-compact EPS filter	99.0
2 nd order EPS filter with two transmission zeros in the upper stopband	16.9
Two-pole EPS	42.8
Ultra-compact EPS filter	14.7

Table 3.5-2: Comparison of the ultra-compact EPS filter with that of Conventional E-plane filters, and E-plane EPS filters. All filters are designed for a centre frequency of 9.5 GHz and 0.3 GHz bandwidth.

3.6 Summary

In this chapter, the problem relating to the size of E-plane waveguide filters has been addressed, development of highly compact E-plane filters has been discussed and a novel ultra-compact E-plane filter has been proposed.

In section 3.1 and 3.2, an introduction to the conventional E-plane filters and a brief discussion on such filters has been given. The benefits offered by this technology as well as the drawbacks have been discussed, thus laying the platform for the introduction of highly compact filters with improved performance.

Section 3.3 introduces the E-plane EPS, which has a unique property that allows realisation of compact filters with an improved upper stopband performance. The formation of equivalent lowpass prototype of the EPS with non-resonating node as well as its main properties has been outlined. It is due to the highly detuned E-plane resonator that is used to realise the non-resonating node that leads to a significant size reduction of filters implemented using this technique. In order to demonstrate and validate the performance of these structures, an experimental filter has been designed, simulated and tested.

In section 3.4, an E-plane EPS with an enlarged non-resonating node has been introduced. This modification of the standard E-plane EPS is capable of generating two poles and a single transmission zero in the lower stopband. Analysis of the structure has been carried out to support the observed phenomenon. On the negative aspect, this has in turn, sacrificed the size and due to the lack of transmission zeros in the upper stopband, it also has a poor upper stopband attenuation. To validate the performance of filters formed using these sections, a 4th order filter has been simulated and tested.

In order to address the drawbacks of the two-pole EPS, an ultra-compact EPS filter has been introduced in section 3.5. The proposed structure utilises two additional metallic fins to generate additional transmission zeros in the upper stopband. Thus it exhibits significantly improved upper stopband attenuation in comparison to a two-pole EPS or a 2nd order conventional filter. Analysis of the structure has been carried out to support the observed phenomenon. The introduction of the additional fins also leads to a size reduction of around 65% in comparison to the two-pole EPS, 13% more compact than a second order EPS filter, and 85% more compact than a conventional E-plane filter. The proposed filter has also been fabricated and measured to verify its performance.

3.7 References

- [3-1] V.E. Boria and B. Gimeno, "Waveguide filters for satellites," *Microwave Magazine, IEEE* , vol. 8, no. 5, pp. 60-70, Oct. 2007.
- [3-2] R. J. Cameron, C. M. Kudsia, and R. R. Mansour, *Microwave Filters for Communication Systems*, Hoboken, New Jersey, John Wiley & Sons, 2007.
- [3-3] A.E. Atia and A.E. Williams, "Narrow-Bandpass Waveguide Filters," *Microwave Theory and Techniques, IEEE Transactions on*, vol. 20, no. 4, pp. 258-265, Apr. 1972.
- [3-4] S. Bastioli, C. Tomassoni and R. Sorrentino, "A New Class of Waveguide Dual-Mode Filters Using TM and Nonresonating Modes," *Microwave Theory and Techniques, IEEE Transactions on*, vol. 58, no. 12, pp. 3909-3917, Dec. 2010.
- [3-5] C. Tomassoni, S. Bastioli and R. Sorrentino, "Generalized TM Dual-Mode Cavity Filters," *Microwave Theory and Techniques, IEEE Transactions on*, vol. 59, no. 12, pp. 3338-3346, Dec. 2011.
- [3-6] L. Pelliccia, F. Cacciamani, C. Tomassoni and R. Sorrentino, "Ultra-compact filters using TM dual-mode dielectric-loaded cavities with asymmetric transmission zeros," *Microwave Symposium Digest (MTT), 2012 IEEE MTT-S International*, pp. 1-3, 17-22 June 2012.
- [3-7] Hai Hu and Ke-Li Wu, "A TM_{11} Dual-Mode Dielectric Resonator Filter with Planar Coupling Configuration," *Microwave Theory and Techniques, IEEE Transactions on*, vol. 61, no. 1, pp. 131-138, Jan. 2013.
- [3-8] Y. Konishi, and K. Uenakada, "The Design of a Bandpass Filter with Inductive Strip Planar Circuit Mounted in Waveguide," *IEEE Trans. Microwave Theory Tech.*, vol. 22, no. 10, pp. 869-873, Oct. 1974.
- [3-9] R. Vahldieck, J. Bornemann, F. Arndt and D. Grauerholz, "Optimized Waveguide E-plane Metal Insert Filters For Millimeter-wave Applications," *Microwave Theory and Techniques, IEEE Transactions on* , vol. 31, no. 1, pp. 65-69, Jan. 1983.

- [3-10] Y. C. Shih and T. Itoh, "E-Plane Filters with Finite-Thickness Septa," *Microwave Theory and Techniques, IEEE Transactions on*, vol. 31, no. 12, pp. 1009-1013, Dec. 1983.
- [3-11] F. Arndt, J. Bornemann, R. Vahldieck and D. Grauerholz, "E-Plane Integrated Circuit Filters with Improved Stopband Attenuation (Short Papers)," *Microwave Theory and Techniques, IEEE Transactions on*, vol. 32, no. 10, pp. 1391-1394, Oct. 1984.
- [3-12] V. Postoyalko and D. Budimir, "Design of waveguide E-plane filters with all-metal inserts by equal ripple optimization," *Microwave Theory and Techniques, IEEE Transactions on*, vol. 42, no. 2, pp. 217-222, Feb. 1994.
- [3-13] D. Budimir, "Optimized E-plane bandpass filters with improved stopband performance," *Microwave Theory and Techniques, IEEE Transactions on*, vol. 45, no. 2, pp. 212-220, Feb. 1997.
- [3-14] D. Budimir, *Generalized Filter Design by Computer Optimization*, Artech House, 1998.
- [3-15] J. R. Montejo-Garai, J. A. Ruiz-Cruz, J. M. Rebollar, M. J. Padilla-Cruz, A. Onoro-Navarro and I. Hidalgo-Carpintero, "Synthesis and Design of In-Line N-Order Filters With N Real Transmission Zeros by Means of Extracted Poles Implemented in Low-Cost Rectangular H-Plane Waveguide," *IEEE Trans. Microwave. Theory & Tech.*, vol. 53, no. 5, pp. 1636–1642, May 2005.
- [3-16] G. Macchiarella and Marco Politi, "Use of Generalized Coupling Coefficients in the Design of Extracted-Poles Waveguide Filters with Non-Resonating Nodes," *2009 IEEE MTT-S International Microwave Symposium Dig.*, pp. 1341-1344, June 2009.
- [3-17] M. Fahmi, J. A. Ruiz-Cruz, R. R. Mansur, and K. A. Zaki, "Compact Ridge Waveguide Filters Using Non-Resonating Nodes," *2007 IEEE MTT-S International Microwave Symposium Dig.*, pp. 1137-1340, June 2009.

- [3-18] O. Glubokov and D. Budimir, "Extraction of Generalized Coupling Coefficients for Inline Extracted Pole Filters With Nonresonating Nodes," *Microwave Theory and Techniques, IEEE Transactions on*, vol. 59, no. 12, pp. 3023-3029, Dec. 2011.
- [3-19] N. Suntheralingham and D. Budimir, "Enhanced Waveguide Bandpass Filters Using S-shaped Resonators," *Int. J. RF and Microwave CAE*, vol. 19, no. 6, pp. 627-633, 2009.
- [3-20] A. Shelkovnikov and D. Budimir, "Left-Handed Rectangular Waveguide Bandstop Filters," *Microwave Opt. Technol. Lett.*, Vol. 48, No. 5, pp. 846-848, 2006.
- [3-21] A. Shelkovnikov and D. Budimir, "Miniaturized Rectangular Waveguide Filters," *Int. J. RF and Microwave CAE*, vol. 17, no. 4, pp. 398-403, 2007.
- [3-22] O. Glubokov (2011). *Development of Waveguide Filter Structures for Wireless and Satellite Communications*. PhD. Thesis. University of Westminster: UK.
- [3-23] D. Young and I. C. Hunter, "Integrated E-Plane Filters with Finite Frequency Transmission Zeros," *24th European Microwave Conference, 1994*, vol. 1, pp. 460- 465, 5-9 Sept. 1994.
- [3-24] J. D. Rhodes, and R. J. Cameron, "General Extracted Pole Synthesis Technique With Applications to Low-Loss TE₀₁₁ Mode Filters," *IEEE Trans. Microwave Theory Tech.*, vol. 28, no. 9, pp. 1018-1028, Sept. 1980.
- [3-25] S. Amari and G. Macchiarella, "Synthesis of inline filters with arbitrarily placed attenuation poles by using nonresonating nodes," *IEEE Trans. Microwave Theory Tech.*, vol. 53, no. 10, pp. 3075-3081, Oct. 2005.

CHAPTER 4

E-PLANE CROSS-COUPLED WAVEGUIDE FILTERS

4.1 Introduction

As explained in chapter 3, the conventional E-plane filters are formed through direct coupling of adjacent resonators, which is provided via metallic septa, and therefore provides a single path for signal flow between source and load. Such a configuration of E-plane filters are naturally limited for the realization of all pole frequency responses. On the other hand it has been demonstrated in chapter 3, section 3.2-3.5, that modification of the conventional E-plane resonator to form E-plane extracted pole sections can create filters with enhanced upper and lower stopband performance. In order to achieve this trait, these filters generate transmission zeros due to the presence of embedded resonators forming bandstop sections [4-1]-[4-2], and therefore can be used to realise filters with generalized Chebyshev frequency responses.

Another method to realise filters with generalized Chebyshev type responses, would be to use a cross coupled topology. In such structures, coupling between source-load, non-adjacent resonators or even both simultaneously can be provided, which can allow signals to take more than one path between source and load. In these multi-path structures, transmission zeros are created due to the interaction of signals arriving at the load with opposite phase.

Waveguide cross coupled filters have been widely implemented previously using waveguide resonant cavities [4-3]-[4-6]. However, to present date, apart from couple of notable attempts [4-7]-[4-8], not much work on compact cross-coupled filters using E-plane technology have been conducted. Article [4-7] present E-plane cross-coupled filters which include two identical waveguides combined together through a common wall. Both waveguides consist of a single E-plane insert which forms conventional E-plane resonators. Slots in the common wall are provided in order to create cross-coupling between these non-adjacent resonators. Even though the authors claim a significant size reduction in comparison to the conventional direct coupled E-plane

filters, the volume of the structure will remain the same, as the width of the entire filter structure now nearly doubles its size.

In the second article, the authors have proposed E-plane cross coupled filters using source-load coupling. The authors model the observed behaviour of the structure as a doublet, as it generates two poles and two transmission zeros, one of each at upper and the lower stopbands. The filter has been implemented using a metallo-dielectric insert, in the E-plane of the hollow rectangular waveguide (WR90, $a = 22.86\text{mm}$, $b = 10.16\text{ mm}$). A wide metallic septum is etched on to one side of the dielectric slab, whereas the other side consists of two etched hairpin resonators. The septum acts as an inverter and is used to implement direct source-load coupling. The authors also demonstrate the application of non-resonating nodes in order to cascade several doublet sections to form higher order filters.

In this chapter the idea proposed in [4-8] has been adopted, but it has been modified in order to implement highly compact E-plane cross coupled filters without the need for use of dielectrics, and simply designed using all metallic inserts. In section 4.2, two separate filtering modules are discussed. The first module is known as a singlet [4-9], and has the capability to produce a single pole and a transmission zero either in the upper or lower stopband, whereas the second module is known as a doublet [4-10]. Filters implemented using cascaded singlets and doublets in waveguide technology can be found in [4-8]-[4-12]. Furthermore this section also introduces the new configuration of the E-plane insert for realization of both the aforementioned modules. Section 4.3 briefly discusses the concept of coupling coefficients between two synchronously tuned resonators, and section 4.4 demonstrates the implementation of a compact 3rd order E-plane filter with source-load coupling. In section 4.5, the extraction of generalized coupling coefficients from the EM-simulated responses for symmetric singlet and doublet filtering blocks has been presented. Also two novel highly compact experimental filters which implement the proposed singlet and doublet sections in cascade with extracted pole sections are proposed. Simulation and experimental results are provided in order to demonstrate the performance and feasibility of these filters.

4.2 Cross-Coupled Filtering Modules Using E-plane waveguide Inserts

In this section, the main features and properties of singlets and doublets are highlighted, and novel filtering structures are introduced that implements these basic filtering modules in E-plane technology.

4.2.1 Singlets

The singlet, in its schematic model, is a basic filtering module used for the modular design of generalized Chebyshev type filters. It consists of a single resonator and generates a pole-zero pair due to the bypass coupling between source and load. The coupling schematic of a singlet is given in Figure 4.2-1 which consist of three nodes that represent source, load and the resonator. The couplings (J_{S1} , J_{1L} , J_{SL}) between the nodes are represented by solid lines.

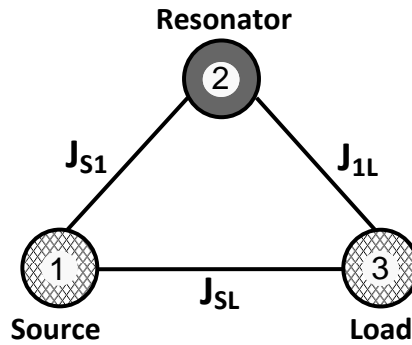


Figure 4.2-1: Coupling schematic representation of singlet.

The module consist of two paths; one that goes from source, through resonator to load; and the other directly between source and load, bypassing the resonator. According to Amari and Bornemann [4-13]-[4-14] it is this reason that leads to the formation of a single real frequency transmission zero. The coupling matrix for a singlet which corresponds to Figure 4.2-1 has the form given in equation (4.2.1), and for a symmetrical singlet, the coupling J_{S1} will equal J_{1L} .

$$M_{singlet} = \begin{bmatrix} 0 & J_{S1} & J_{SL} \\ J_{S1} & jB_1 & J_{1L} \\ J_{SL} & J_{1L} & 0 \end{bmatrix} \quad (4.2.1)$$

By analysing the coupling schematic of in Figure 4.2-1, and assuming that it is symmetric, it can be found that the singlet has a single transmission zero (Ω_Z) and a pole (Ω_P) which can be described in terms of the available couplings, by the following relationship:

$$\Omega_Z = \frac{J_{S1}^2}{J_{SL}} \quad (4.2.2)$$

$$\Omega_P = -\frac{2J_{S1}^2 J_{SL}}{1 - J_{SL}^2} \quad (4.2.3)$$

As can be observed from the set of equations above, the positions of the pole and zero frequency depend entirely on the available couplings. For a symmetrical singlet the location of the pole appear at a real frequency. The transmission zero also occurs at real frequency, regardless of symmetry. When all three couplings are of positive values, the transmission zero is generated above the pass band, provided that the absolute value of J_{SL} is less than 1. In order to position it below, an odd order of negative couplings is required. The difference between pole and zero locations for a singlet at real frequencies can be evaluated as given by equation (4.2.4), which shows the flexibility of transmission zero positioning with respect to the passband.

$$\Omega_Z - \Omega_P = \frac{J_{S1}^2}{J_{SL}} \cdot \frac{1 + J_{SL}^2}{1 - J_{SL}^2} \quad (4.2.4)$$

4.2.2 Physical realization of Singlets using E-plane inserts

A compact E-plane waveguide filter design that can be used to realize generalised Chebyshev filtering functions is shown in Figure 4.2-2. The structure is composed of two metallic inserts inside a waveguide section centred longitudinally and positioned parallel with the central E-plane, also with equal offsets from it. One of the inserts consists of a single wide septum, whereas the other consists of a single fin short-circuited on to either top or bottom broad wall of the waveguide. The wide septum can be used to control the direct source-load coupling. Due to the combination of the wide septum (which acts as a ground plane) and the suspended metallic fin, the resonator itself can be locally modelled as a stripline quarter-wavelength resonator.

Essentially, the structure shown in Figure 4.2-2, is an evanescent-mode filter configuration, since the filter operates below the cut-off frequency of the mid-section of the waveguide, as it has been narrowed by the wide septum. Moreover, even though it has not been implemented here for the sake of ease of fabrication, the path behind the wide septum can be entirely eliminated, leading to characteristic evanescent mode filter cross-sectional size reduction. This inherently will also reduce the weight of the structure.

On the front side of the wide septum, there exist two signal paths. One of the paths passes through the resonators formed between the fin and the wide septum, and is active at the filter's operating frequencies. It also has fundamentally strong coupling with input and output waveguide sections due to it being centrally positioned. The other one is mainly between the fins and the adjacent sidewall.

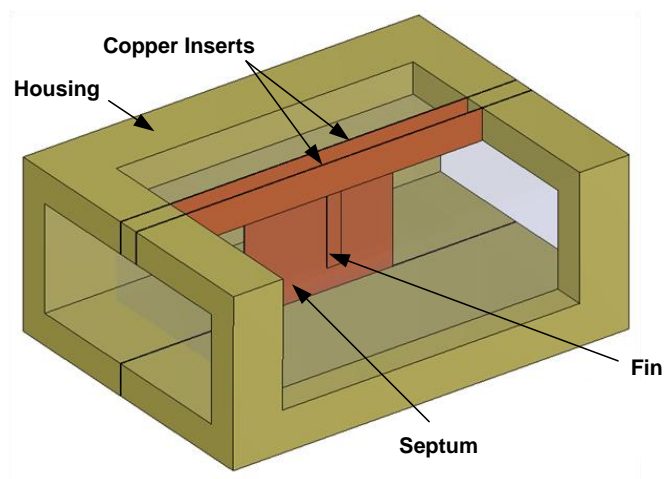


Figure 4.2-2: Configuration of E-plane metallic inserts for the formation of a singlet.

A method introduced by Thomas in 2003 [4-15] demonstrate how it is possible to predict the number of transmission zeros as well as their location (whether upper stopband or lower stopband) for a given cross-coupled topology. The article provides a tutorial overview of how multi-path coupling diagrams can be used to illustrate the phase shifts of different signal paths. By applying the technique shown in this article, the transmission zero appearance of the structures proposed here can be predicted to a certain extent.

The proposed structure, in its current configuration, consists of a positive source-load coupling due to the wide inductive septum. It also has an inductive coupling for both source-resonator and resonator-load couplings due to the H-plane step discontinuity that

connects the input/output terminating waveguide sections into the central evanescent mode waveguide section. Thus, the destructive interference leading towards the formation of the transmission zero occurs above the passband, as shown in Figure 4.2-3. In order to locate the transmission zero below the passband, one of the three available couplings must change sign. Physically it is more convenient to change the bypass coupling to capacitive as it can be achieved easily by changing the wide septum to a wide fin by introducing a gap. As an example, the effect of this simple geometric change in the structure, without altering any other dimensions, is demonstrated by the simulated S-parameter response in Figure 4.2-4.

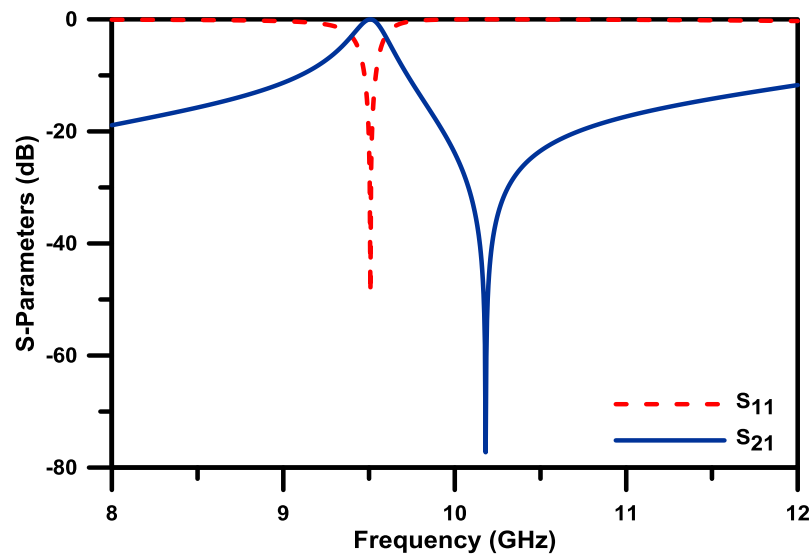


Figure 4.2-3: S-parameter response of the proposed structure with inductive source-load coupling.

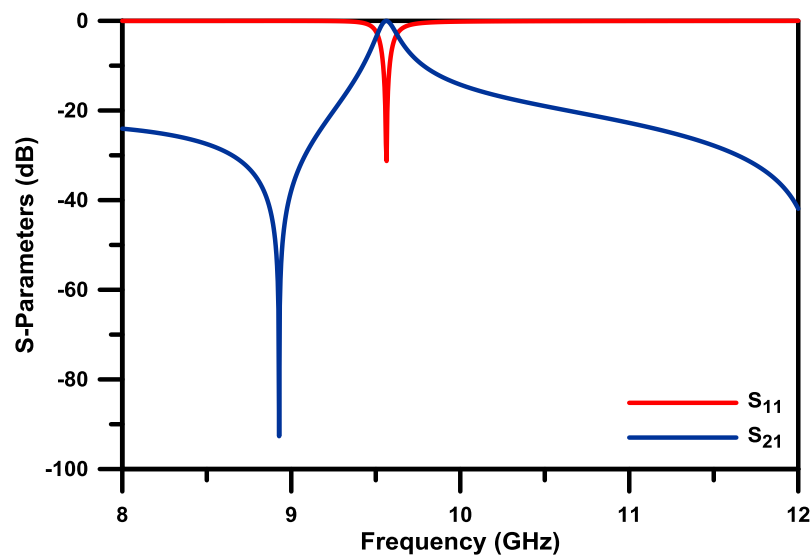


Figure 4.2-4: S-parameter response of the proposed structure with capacitive source-load coupling.

4.2.3 Doublets implemented using E-plane inserts

The doublet is a filtering module proposed by Amari and Uwe for the modular design of elliptic filters [4-10]. The module proposed in their article consists of two paths which contain a single resonator coupled to source and load. This configuration allows the structure to generate two poles and a single transmission zero either on the upper or the lower stopband. A modification of the doublet was proposed in [4-16], which consist an additional direct coupling between source and load. The article demonstrates, that this modification of the classical doublet has the capability to realise Chebyshev, as well as elliptic type frequency responses, depending on the values and sign of the available couplings.

In this section, the implementation of doublets using E-plane inserts is presented. The new configuration of the E-plane structure is shown Figure 4.2-5. Here, one of the inserts consists of two fins separated by a narrow septum, whereas the other consists of a wide fin to form a capacitive bypass coupling between the source and the load.

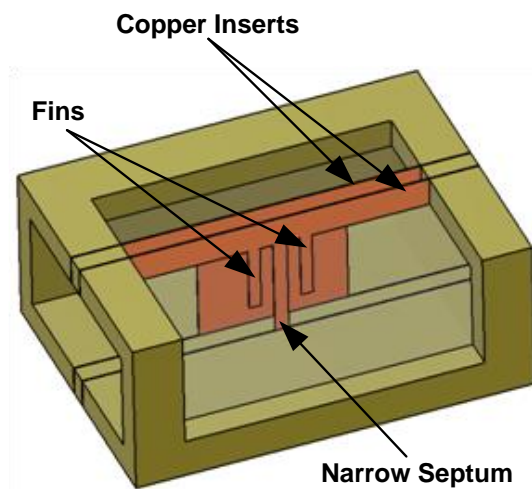


Figure 4.2-5: Configuration of E-plane metallic inserts for the formation of a doublet.

The effect this configuration of metallic inserts creates can be modelled by a doublet, as illustrated by a coupling schematic in Figure 4.2-6. However, unlike the coupling schematic of the classical doublet, the two bypassed resonators are coupled inductively to each other through the inverter J_{12} . This is due to the narrow septum placed between the two fins to reduce the coupling between each other in order to place them closer to one another to reduce overall length.

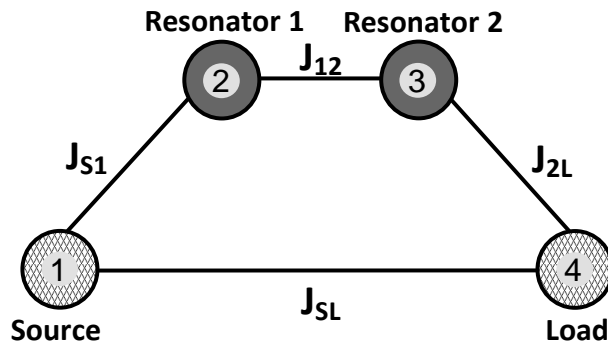


Figure 4.2-6: Coupling schematic representation of the doublet representing filter configuration in Figure 4.2-5.

The proposed structure in Figure 4.2-5, in its current configuration, consists of a negative source-load coupling due to the wide capacitive fin. Again as in the case for the singlet configuration, the structure also have inductive coupling for both source-resonator 1 and resonator 2-load couplings due to the H-plane step discontinuity that connects the input/output terminating waveguide sections into the central evanescent mode waveguide section. The resonators 1 and 2 are coupled inductively to one another through the narrow metallic septum.

By applying the technique shown in [4-15], we can observe that the schematic of the doublet shown in Figure 4.2-6 will generate a single transmission zero above and below the passband, provided that the source-load coupling is negative. The schematic in Figure 4.5-7 which contains the phase shifts the signal undergoes in each path is utilized to demonstrate this.

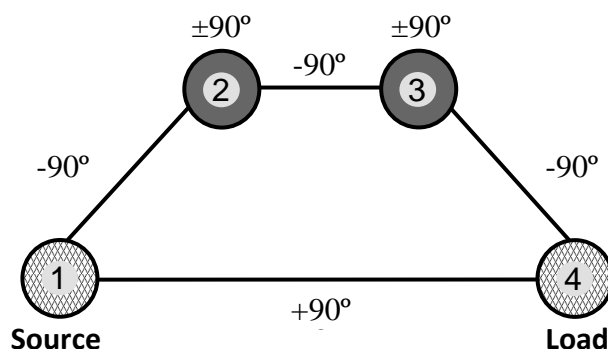


Figure 4.2-7: Coupling schematic representation of the doublet with corresponding phase shifts.

From the schematic in Figure 4.2-7, it is seen that the phase shift on the main path, through the resonators, for frequencies below resonance is -90° ; for frequencies above the passband the total phase shift is -450° . Due to the capacitive coupling, the phase shift provided by the direct source-load coupling is equal to $+90^\circ$. Taking in to consideration of the difference, it is clear that the signals in both paths arrive out of phase at the load both above the resonant and below the resonant. This condition leads to the formation of a single transmission zero in both upper and lower stopbands of the frequency response. If the source load coupling is made inductive (-90°), then we will observe that the signals arrive at the load in phase, both above the resonant and below the resonant. Therefore the schematic in this case provides no transmission zeros.

In order to prove validity of the coupling schematic in Figure 4.2-6 for the proposed configuration of E-plane inserts to form compact doublets, the structure in Figure 4.2-5 has been designed and simulated in CST Microwave StudioTM. A coupling matrix that represents the schematic is given in equation (4.2.5) together with the corresponding entries of the coupling values. The filter specification listed below:

- Centre frequency: 9.5 GHz;
- Ripple passband: 9.4-9.6 GHz;
- Return loss: 20 dB;
- Transmission zeros: 9.0 GHz, 10.0 GHz.

The entry values of the coupling schematic for the filter can be determined either analytically using procedure describe in [4-6], or through optimisation for the given specification.

$$M_{doublet} = \begin{bmatrix} 0 & J_{S1} & 0 & J_{SL} \\ J_{S1} & B_1 & J_{12} & 0 \\ 0 & J_{12} & B_2 & J_{1L} \\ J_{SL} & 0 & J_{1L} & 0 \end{bmatrix} \quad (4.2.5)$$

$$= \begin{bmatrix} 0 & 1.156 & 0 & -0.102 \\ 1.156 & 0 & 1.659 & 0 \\ 0 & 1.659 & 0 & 1.156 \\ -0.102 & 0 & 1.156 & 0 \end{bmatrix}$$

A WG-90 ($22.86 \times 10.16 \text{ mm}^2$) waveguide has been used to house the inserts. Layout and dimensions of the simulated structure are given in Figure 4.2-8 and table 4.2-1. A

comparison of frequency response of the simulated structure and the schematic is provided in Figure 4.2-9.

Compact E-plane doublet	
Parameters	Values (mm)
L_{WG}	40
H_{WG}	10.16
L_{FIN1}	6.82
L_{FIN2}	6.82
W_{FIN1}	1.2
W_{FIN2}	1.2
W_{SEPT}	8.2
W_{SEPI}	1.2
GAP	1.0

Table 4.2-1: Dimensions of the E-plane insert for the compact E-plane doublet.

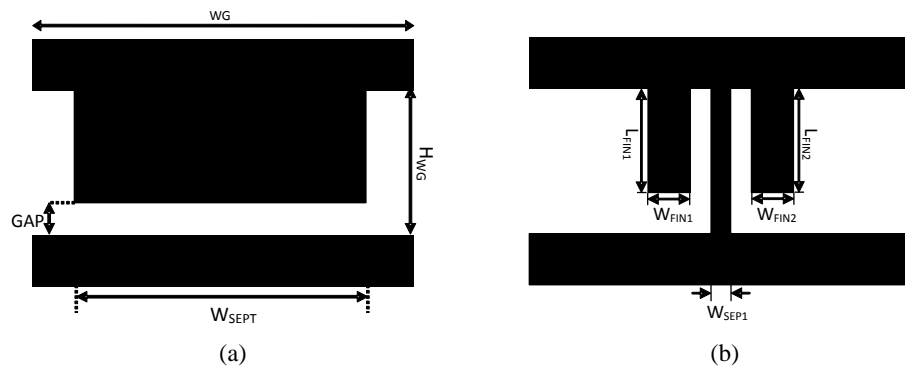


Figure 4.2-8: Layout of the two E-plane inserts for the proposed compact E-plane doublet.

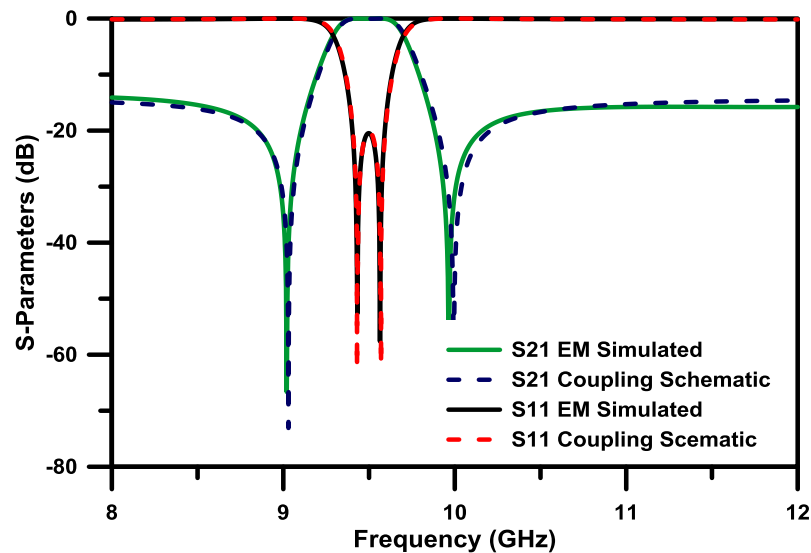


Figure 4.2-9: Simulated S-parameter response of the proposed E-plane doublet structure and the frequency response of the coupling schematic.

4.3 Coupling Coefficients for Filter Design

The low pass filter prototype models discussed earlier in chapter 2, section 2.4 and 2.5, are described by their corresponding coupling matrices for a unity bandwidth and zero centre frequency in terms of normalized angular frequency variable (ω'). Therefore the entries M_{ij} of a coupling matrix represent the degree of interaction between the available resonators in order to satisfy these conditions. However in real life, the filters need to adhere and perform to a set of specifications that contains a particular centre frequency and bandwidth. Therefore in order to provide a link between the model and reality, the coupling values are normalized to a fractional bandwidth FBW , which is defined as BW/f_o . The values obtained by this process are referred to as coupling coefficients. The coupling coefficient between two resonators which are represented in circuit schematic level and connected though an admittance inverter J_{ij} , can be expressed as follows [4-17]:

$$k_{ij} = FBW \cdot \frac{J_{ij}}{\sqrt{B_i \cdot B_j}} \quad (4.3.1)$$

where B_i and B_j represent the susceptances of the i^{th} and the j^{th} resonator.

The external couplings are defined by the external quality factor as:

$$Q_{ext,i} = \frac{G_o}{FBW \cdot J_{0,i}^2} \quad (4.3.2)$$

When developing coupled resonator filters certain techniques are applied that will facilitate in relating values of coupling coefficients obtained from theoretical calculations to that of physical dimensions of the structure that can implement these couplings. For example the coupling between two synchronously or asynchronously tuned resonators can be characterised by two resonant frequencies identifiable through experimental or full wave electromagnetic simulation. Varying particular dimensions of the coupling element, such as gaps or metallic discontinuities, that controls the respective coupling coefficient will allow one to extract the values from the physical structure. Such coupling coefficient extraction procedures for synchronously or asynchronously tuned resonators can be found in [4-18]-[4-19]. It is not the intention of this thesis to repeat the work presented in those references, however a brief summary of how coupling coefficient between two synchronously tuned resonators is provided in this section.

The circuit schematic in Figure 4.3-1 can be used to represent synchronously tuned resonators with mixed couplings. The network consists of two identical resonators with both capacitive and inductive coupling. L , C , C_m , L_m , represent the self inductance, self capacitance, mutual capacitance, and mutual inductance respectively. Due to the symmetry of the circuit, even and odd mode technique can be applied by inserting electric and magnetic walls in the symmetry plane A-A'. As a result of such analysis, two equations representing the resonant frequencies of the circuit can be obtained [4-18]:

$$f_e = \frac{1}{\sqrt{2\pi(L-L_m)(C-C_m)}} \quad (4.3.3)$$

$$f_o = \frac{1}{\sqrt{2\pi(L+L_m)(C+C_m)}} \quad (4.3.4)$$

The coupling between these two resonators represented by coupling coefficient k can be calculated as the superposition of the electric and magnetic components [4-18]:

$$k = \frac{f_e^2 - f_m^2}{f_e^2 + f_m^2} \quad (4.3.5)$$

The expression in equation (4.3.5), can be used for the extraction of coupling coefficient between two synchronously tuned resonators.

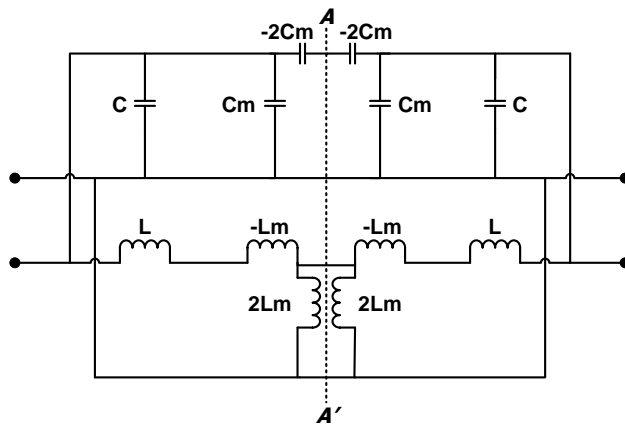


Figure 4.3-1: Circuit representation of two synchronously tuned coupled resonators with mixed couplings.

The external quality factor of a resonator can be determined by its 3dB bandwidth from the frequency response. Consider the equivalent circuit of a doubly-loaded resonator

shown in Figure 4.3-2, where a single resonator has been represented as two identical and symmetrical parts. Plane A-A' represent the symmetry plane.

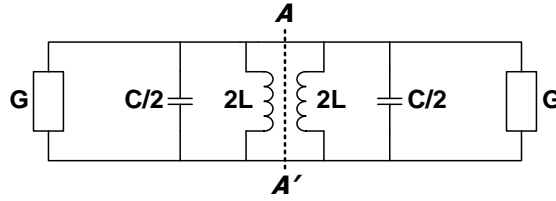


Figure 4.3-2: Circuit representation of a doubly loaded resonator.

By applying even and odd-mode techniques, it has been shown that the following expressions can be obtained for the even and odd-mode reflection coefficients [4-18]:

$$S_{11e} = \frac{1 - jQ_{ext} \Delta\omega / \omega_o}{1 + jQ_{ext} \Delta\omega / \omega_o} \quad (4.3.6)$$

$$S_{11o} = -1 \quad (4.3.7)$$

where $\omega_o = 1/\sqrt{LC}$, and $\omega = \omega_o + \Delta\omega$ with the approximation $\Delta\omega = (\omega^2 - \omega_o^2)/2\omega$. The singly loaded external quality factor is defined by [4-18]:

$$Q_e = \frac{\omega_o C}{G} \quad (4.3.8)$$

After several manipulations the magnitude of the transmission coefficient can be written as follows:

$$|S_{21}| = \frac{1}{\sqrt{1 + (Q_{ext} \Delta\omega / \omega_o)^2}} \quad (4.3.9)$$

From equation (4.3.9) it can be seen that the absolute value of the transmission coefficient becomes 0.707 or -3dB when $Q_e \Delta\omega / \omega_o = \pm 1$. The doubly-loaded external quality factor can be calculated from:

$$Q_{ext} = \frac{\omega_o}{\Delta\omega_{3dB}} \quad (4.3.8)$$

As an example, let us consider the doublet in section 4.2.3. In this structure the two resonators in the main path are coupled to each other via the narrow metallic septa. The structure is also symmetric and the resonators are synchronously tuned, hence

physically identical. Applying the set of equations (4.3.1) and (4.3.2) to the coupling matrix in equation (4.2.5), one can obtain the coupling coefficients as: $k_{12} = 0.0349$, $k_{SL} = 0.002147$, $Q_{ext} = 35.5450$. Next the coupling coefficient k_{12} can be extracted from electromagnetic simulation of the entire structure, and varying the width of the septum that separates the two resonators.

A set of frequency responses used for extraction of coupling coefficient k_{12} is given in Figure 4.3-3a, whereas the extracted values against the dimension varied is given in Figure 4.3-3b. The external quality factor can be evaluated by modelling a single resonator and analyzed as a two port network; where by the expression in equation (4.3.8) can be used for its extraction. It should be mentioned at this point, that this method of obtaining physical dimensions does not necessarily provide the final solution, rather it provides the initial point at which further minor fine tuning will be required to achieve the final result.

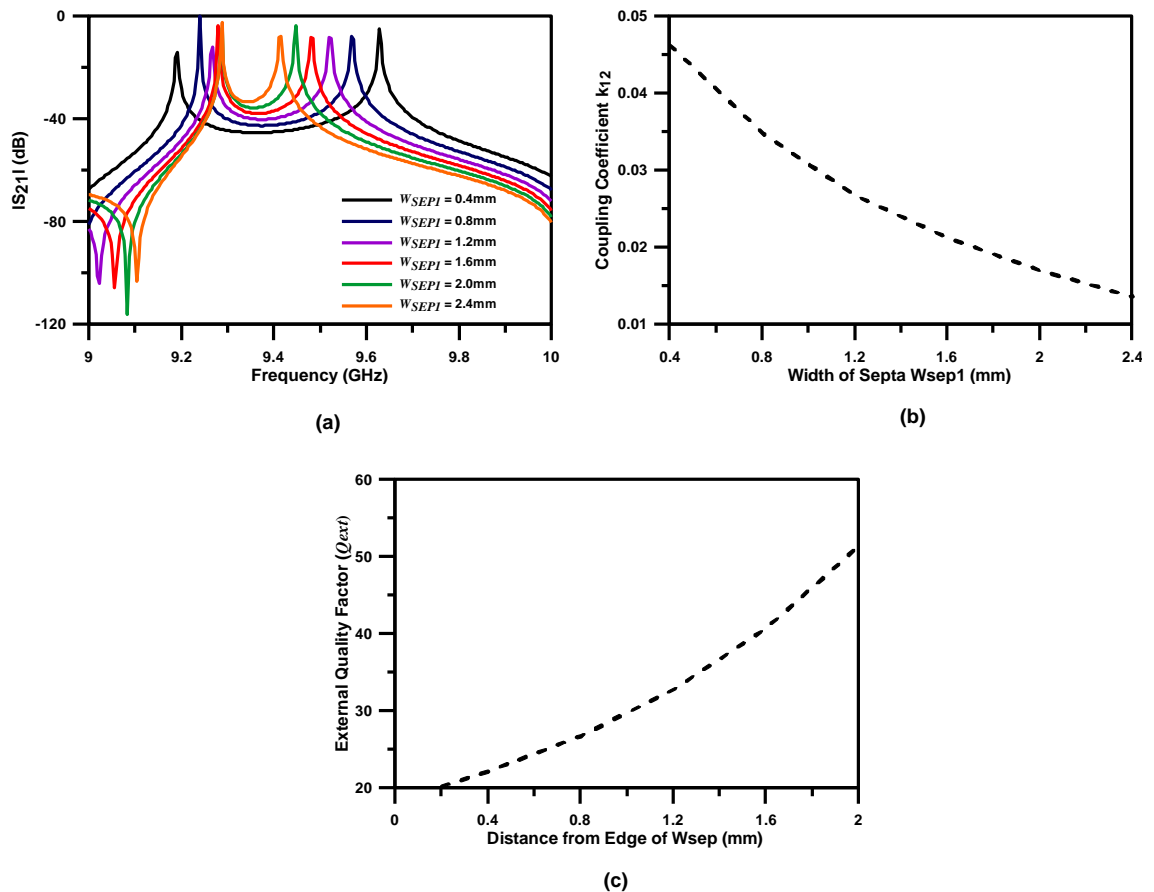


Figure 4.3-3: Extracting k_{12} and Q_{ext} : (a) Simulated frequency responses of the doublet with different septa widths for extraction of coupling coefficient k_{12} ; (b) Extracted coupling coefficient k_{12} for different septa widths; (c) Extracted external quality factor Q_{ext} .

4.4 Compact Higher Order E-plane Cross-Coupled Filters.

It is possible to develop compact higher order filters using the approach described in section 4.2, by placing additional resonators along the main path between source and load. Physically this can be realised by placing more metallic fins spaced by narrow septa. The coupling scheme representation of A 3rd order filter formed this way is shown in Figure 4.4-1.

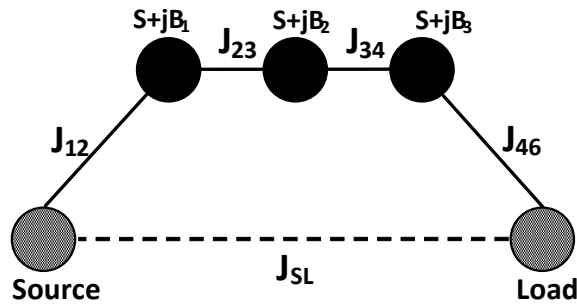


Figure 4.4-1: Coupling Schematic of a 3rd order filter with source-load coupling.

By applying the technique described in [4-15] for the coupling schematic shown above, one can observe that only a single transmission zero above the passband can be realised. Assuming that all the coupling in the main path and the direct source-load coupling is inductive, the phase shift on the main path, through the resonators, for frequencies below resonance is -90° ; for frequencies above the passband the total phase shift is -630° . The direct source-load coupling path also provides a -90° phase shift. Therefore it is clear that the signals travelling through both paths appear out of phase with each other at the load for frequencies above resonance only. The physical representation of the coupling schematic above using a similar configuration discussed in section 4.2 is shown in Figure 4.4.2.

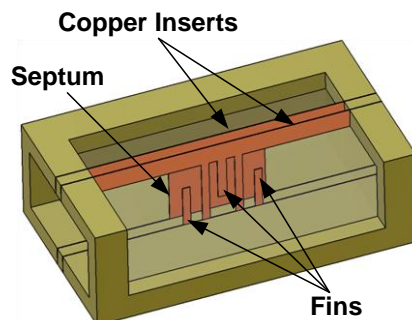


Figure 4.4-2: Configuration of the E-plane inserts for the 3rd order filter with source-load coupling.

The filter is formed by including additional metallic fins which are arranged in alternating directions of interdigital line structures, similar to that of the resonator arrangement in interdigital filters. The fins are also separated by narrow metal septa which contribute towards reducing the unwanted cross coupling between the resonators, which are hard to control. This also results in reducing the direct coupling between the adjacent resonators, thus resonators can now be placed closer to each other, hence shrinking the filter size. A more accurate coupling schematic representation of the 3rd order filter configuration is shown in Figure 4.4-3.

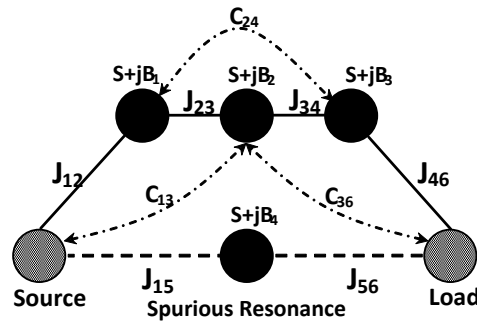


Figure 4.4-3: Coupling Schematic of a 3rd order cross-coupled filter taking into consideration of parasitic couplings and the spurious resonance.

Notations C13, C24, and C36 represent the additional unwanted parasitic couplings that exist within the structure, although they are still significantly low in comparison to the main line couplings. The additional node between the source-load represents higher order spurious resonance [4-11]. As an example a third order filter was designed at the centre frequency of 9.4 GHz with a bandwidth of 0.5 GHz and a transmission zero at 10.4 GHz. The coupling values can be obtained through optimization and the corresponding coupling matrix for the schematic in Figure 4.4-3 is given in (4.4.1).

$$M_{Filter} = \begin{bmatrix} 0 & 0.888 & 0.024 & 0 & 0.145 & 0 \\ 0.888 & 0 & 0.672 & 0.042 & 0 & 0 \\ 0.024 & 0.672 & 0 & 0.672 & 0 & 0.024 \\ 0 & 0.042 & 0.672 & 0 & 0 & 0.888 \\ 0.145 & 0 & 0 & 0 & -14.4 & 0.145 \\ 0 & 0 & 0.024 & 0.888 & 0.145 & 0 \end{bmatrix}. \quad (4.4.1)$$

The additional spurious resonant node could be ignored if only the response surrounding the pass band is of interest [4-11].

The structure has been simulated in CST Microwave Studio™ and a comparison between the simulated s-parameter responses of a conventional 3rd order filter and a 3rd order EPS filter has been provided in Figure 4.4-4. As expected, the EPS filter gives the best upper stopband attenuation as well as steeper upper transition band due to the presence of two additional transmission zeros. However due to the shift of the spurious resonance to higher frequencies, the proposed cross-coupled filter provides good attenuation for a wider range of frequencies. Furthermore, the proposed cross-coupled filter is approximately 70% more compact than a conventional 3rd order E-plane filter and 33% more compact than a 3rd order EPS filter designed for the same centre frequency and bandwidth. In comparison to a conventional filter with similar stopband attenuation, the designed cross-coupled filter is approximately 82% more compact. Table 4.4-1 summarises the total lengths of all three filters.

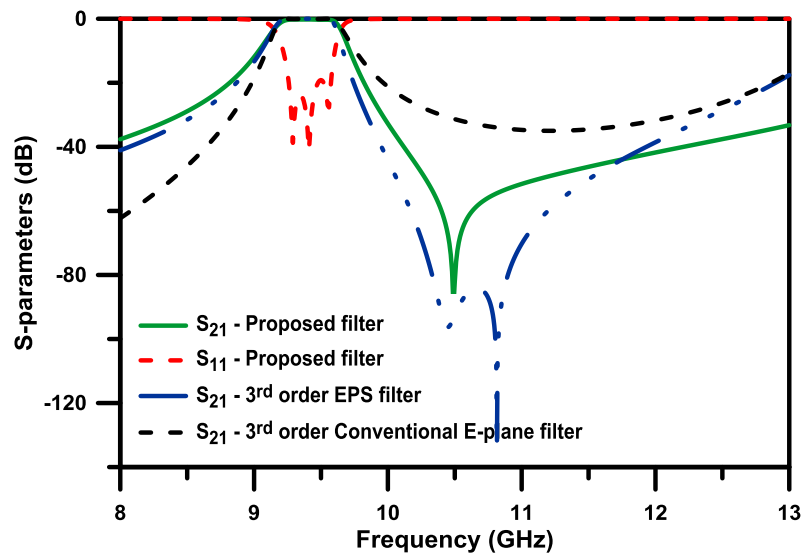


Figure 4.4-4: Comparison between the proposed 3rd order filter with source-load coupling, a 3rd order conventional E-plane filter and a 3rd order EPS filter.

E-plane Filter type	Length (mm)
Conventional 3 rd order filter	67.56
Conventional 5 th order filter with comparable upper stopband attenuation to the ultra-compact EPS filter	116.76
3 rd order EPS filter with three transmission zeros in the upper stopband	30.6
Proposed 3 rd order compact cross-coupled filter	20.5

Table 4.4-1: Comparison of overall length of the compact 3rd order source-load coupled filter with E-plane EPS filter and conventional E-plane filters.

The designed compact cross-coupled filter has been fabricated using the E-plane technology, which utilizes a pair of copper inserts within a standard WG-16 (22.86x10.16 mm²) rectangular waveguide housing. The inserts shown in Figure 4.4-5 with the dimensions given in table 4.4-2 have been plotted on a copper foil with 0.2 mm thickness. S-parameters have been measured using the Agilent E8361A vector network analyzer and shown in Figure 4.4-6 together with the simulated results and that of the frequency response of the coupling schematic.

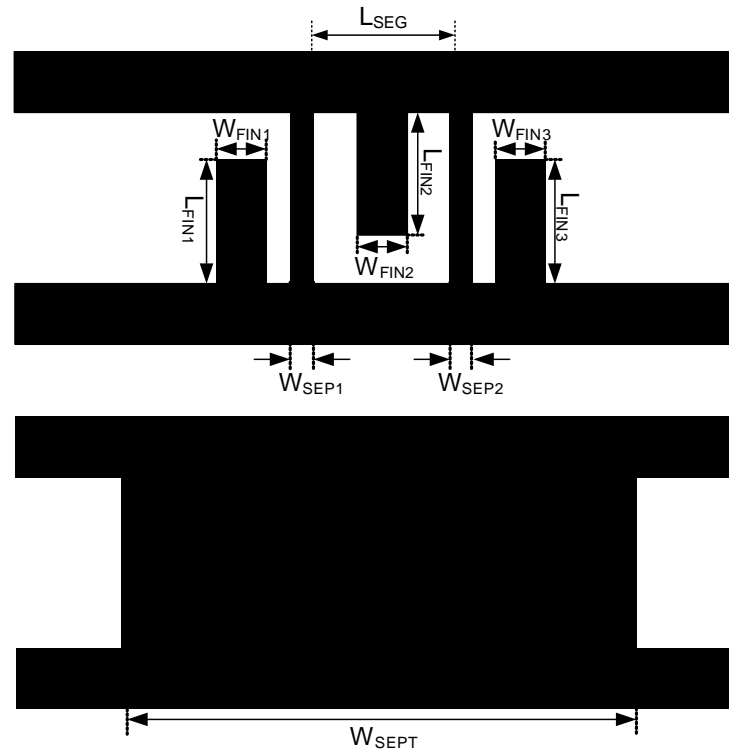


Figure 4.4-5: Layout of the two E-plane inserts for the proposed compact 3rd order source-load coupled filter.

Parameters	Optimised values	Parameters	Optimised Values
L_{FIN1}	6.4	W_{FIN3}	1.6
L_{FIN2}	6.5	W_{SEPT}	20.5
L_{FIN3}	6.4	W_{SEP1}	1.6
W_{FIN1}	1.6	W_{SEP2}	1.6
W_{FIN2}	1.6	L_{SEG}	9.0

Table 4.4-2: Dimensions of the E-plane insert for the compact 3rd order source-load coupled filter.

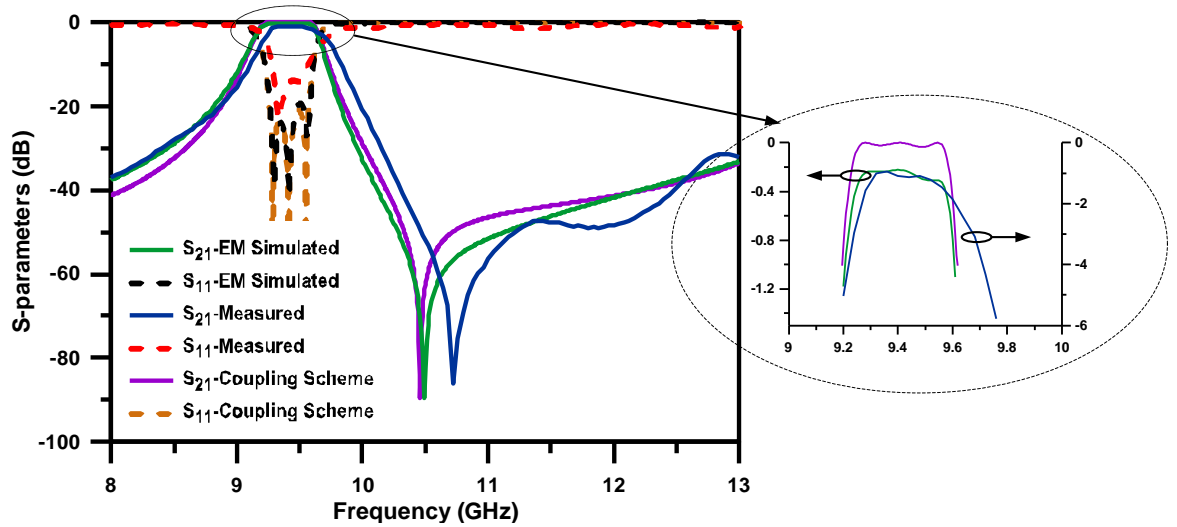


Figure 4.4-6: Comparison between coupling schematic, EM simulation and measurement S-parameter responses of the proposed compact 3rd order filter with source-load coupling.

It can be observed from Figure 4.4-6 that the measured results show reasonably good agreement with that of the simulated. The insertion loss for the filter was found to be around 1.0 dB and is mainly due to signal leakage through the imperfect, custom made waveguide housing. A slight shift in the transmission zeros can also be observed. Further contributions to these are imperfections in alignment of the two inserts within the waveguide housing and tolerances encountered during fabrication process mainly arising from the limitation to accuracy which the plotter reaches. The results can be further improved through meticulous use of the available tools and an accurate construction of the split block waveguide housing. A photograph of the fabricated filter prototype is shown in Figure 4.4-7.



Figure 4.4-7: Fabricated prototype of the compact 3rd order E-plane waveguide filter with source-load coupling.

4.5 Compact Modular Cross-coupled Filters with Cascaded Extracted Pole Sections.

The method of designing higher order cross-coupled filters by simply inserting additional resonant nodes has one major drawback. The transmission zero generated in the frequency response of the structure is due to source-load coupling and the location of it depends on all available couplings in the structure (as evident by equation 4.2.2-4.2.3 for the singlet). This inherently leads to the structure being extremely sensitive to dimension variations of each element within the structure; also it is more susceptible to manufacturing tolerances. Therefore the design process of such higher order filters becomes time consuming and complex process.

On the other hand Singlets and doublets can be used as units for modular filter implementation. Modularity for such filters is achieved by cascading several singlet or doublet blocks in series. Example of such a configuration using cascaded singlets in series is shown in Figure 4.5-1. Each block can generate and control its individual poles and zeros, which in turn allows filtering structures designed in this manner to overcome high sensitivity to manufacturing tolerances. Higher order filters implemented using cascaded singlets and doublets can be found in [4-9] and [4-12].

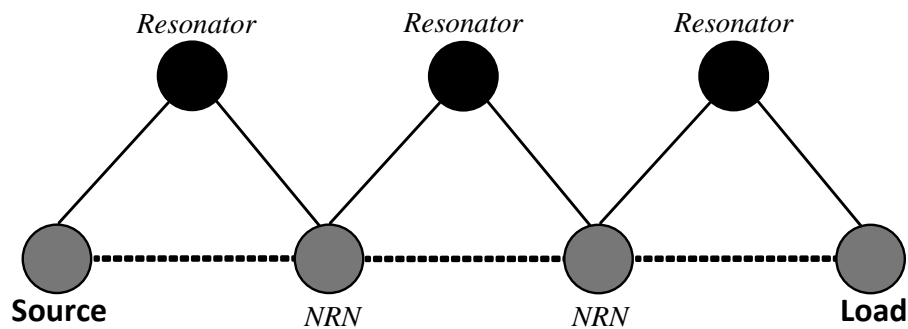


Figure 4.5-1: Cascaded singlet blocks in series to form modular higher order cross-coupled filters.

In this section we present development of two compact higher order waveguide filters exhibiting pseudo-elliptic frequency responses. The filters are implemented using singlet blocks with extracted pole sections cascaded in series on either side and doublet blocks with extracted pole sections cascaded in either sides. Figure 4.5-2 is utilized to illustrate the coupling schematic of such configurations. Each block will generate and control its own respective poles and zeros, thus maintaining modularity. Procedure

based on extraction of Generalized coupling coefficients (GCC) has been utilized In order to facilitate the design of these structures.

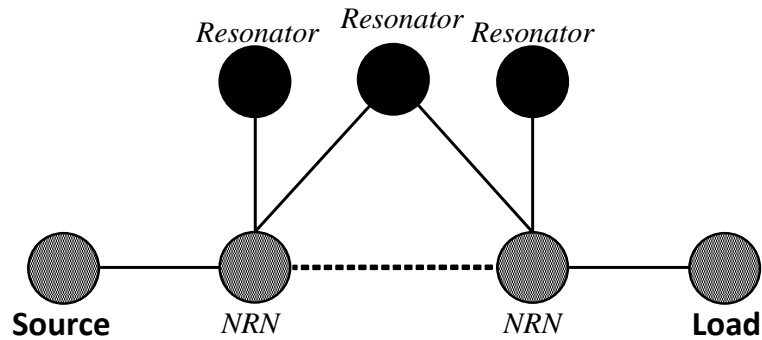


Figure 4.5-2: Singlet block cascaded in series with extracted pole sections.

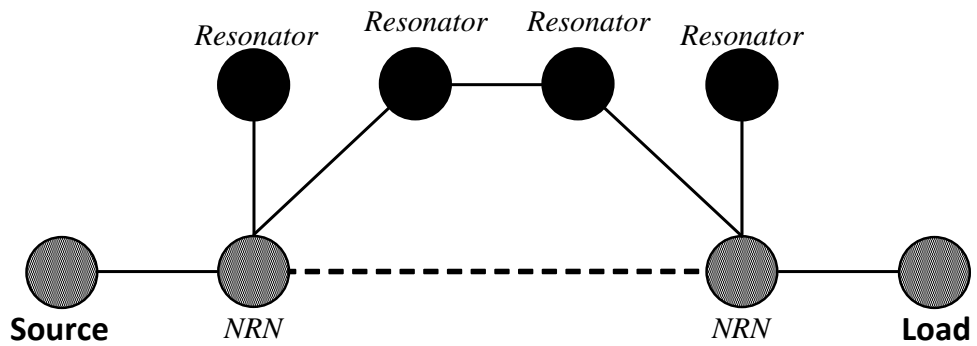


Figure 4.5-3: Doublet block cascaded in series with extracted pole sections.

4.5.1 Extraction of GCCs for Singlets

Consider a symmetric singlet, illustrated by a coupling scheme in Figure 4.5-4, which contains a resonator and two non-resonating nodes connected through admittance inverters. Taking advantage of the symmetry of the schematic, the circuit can be analyzed by using the even-odd mode technique.

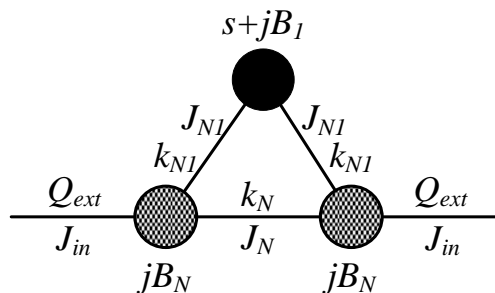


Figure 4.5-4: Coupling schematic of the singlet module with the GCCs denoted by k_N and k_{NI} .

The short and open schematic circuits of the singlet, corresponding to the odd and even modes respectively, are shown in Figure 4.5-5.

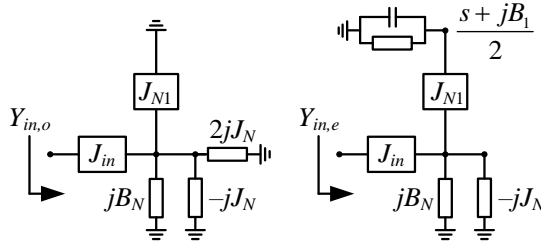


Figure 4.5-5: Analysis of the singlet using even and odd mode technique.

The input admittances for the both cases can be calculated as:

$$Y_{in,o} = -j \frac{1}{Q_o} \quad (4.5.1)$$

$$Y_{in,e} = -j \frac{1}{Q_e} \cdot \frac{\omega - \Omega_{Ze}}{\omega - \Omega_{Pe}} \quad (4.5.2)$$

Here ω is a lowpass prototype frequency variable obtained from the real frequency f by the standard bandpass to lowpass transformation.

The variable entries Q_e , Q_o , Ω_{Ze} , and Ω_{Pe} , can be expressed as:

$$Q_o = \frac{B_N + J_N}{J_{in}^2} \quad (4.5.3)$$

$$Q_e = \frac{B_N - J_N}{J_{in}^2} \quad (4.5.4)$$

$$\Omega_{Pe} = -B_1 + \frac{2 \cdot J_{N1}^2}{B_N - J_N} \quad (4.5.5)$$

$$\Omega_{Ze} = -B_1 \quad (4.5.6)$$

Using even and odd mode admittances, it can be shown that for the doubly loaded singlet module in Figure 4.5-4, has a finite transmission zero at Ω_{TZ} :

$$\Omega_{TZ} = -B - \frac{J_{N1}^2}{J_N} \quad (4.5.7)$$

By combining equation (4.5.3)-(4.5.7) we can obtain the ratios that describe the circuit of interest with a certain scaling factor as given below.

$$\frac{B_N}{J_{in}^2} = \frac{1}{2}(Q_e + Q_o) \quad (4.5.8)$$

$$\frac{J_N}{J_{in}^2} = \frac{1}{2}(Q_e - Q_o) \quad (4.5.9)$$

$$B_1 = -\Omega_{Ze} \quad (4.5.10)$$

$$\frac{J_{N1}^2}{B_N} = \left(\frac{2}{\Omega_{Pe} - \Omega_{Ze}} + \frac{1}{\Omega_{Ze} - \Omega_{Tz}} \right)^{-1} \quad (4.5.11)$$

$$Q_{ext} = \frac{B_N}{J_{in}^2} = \frac{1}{2}(Q_e + Q_o) \quad (4.5.12)$$

The GCC k_N , k_{N1} and Q_{ext} are straightforwardly calculated from the above equations.

4.5.2 Extraction of GCCs For Symmetric Doublets

In order to extract the GCCs for a symmetric doublet the coupling scheme in Figure 4.5-6, which consist of two resonating and two non-resonating nodes connected through admittance inverters, can be analyzed using even and odd mode technique, similar to that done in the case of a singlet. The corresponding open and short circuits are shown in Figure 4.5-7.

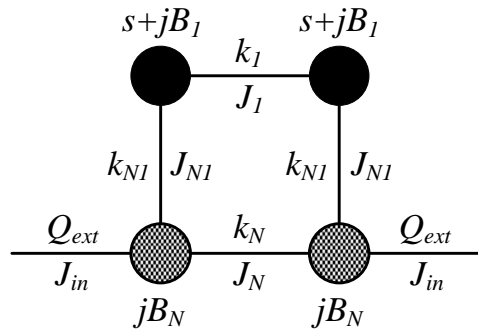


Figure 4.5-6: Coupling schematic of the symmetric doublet module with the GCCs denoted by k_N , k_{N1} and k_1 .

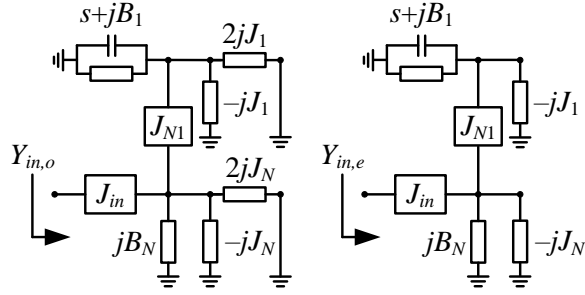


Figure 4.5-7: Analysis of the symmetric doublet using even and odd-mode technique.

The odd-mode input admittance $Y_{in,o}$ can be expressed as follows:

$$Y_{in,o} = \frac{J_{in}^2}{j(B_N + J_N) + \frac{J_{N1}^2}{s + j(B_1 + J_1)}} \quad (4.5.13)$$

Where $s = j\omega$.

The odd mode admittance is purely imaginary and has a pole and a zero denoted as Ω_{Po} and Ω_{Zo} respectively. Therefore equation (4.5.13) can be written as:

$$Y_{in,o} = -j \frac{1}{Q_o} \cdot \frac{\omega - \Omega_{Zo}}{\omega - \Omega_{Po}} \quad (4.5.14)$$

Where Q_o , Ω_{Po} , and Ω_{Zo} is given as:

$$\Omega_{Po} = -B_1 - J_1 + \frac{J_N^2}{B_N + J_N} \quad (4.5.15)$$

$$\Omega_{Zo} = -B_1 - J_1 \quad (4.5.16)$$

$$Q_o = \frac{B_N + J_N}{J_{in}^2} \quad (4.5.17)$$

Once the pole and zero values are known, the external quality factor for the odd-mode case Q_o can be calculated at any frequency in terms of Ω_{Po} and Ω_{Zo} . For simplicity we take $\omega = 0$ leading to:

$$Q_o = \frac{1}{|Y_{in,o}(\omega = 0)|} \cdot \frac{\Omega_{Zo}}{\Omega_{Po}} \quad (4.5.18)$$

Following the same procedure, the following set of equations can be obtained for the even-mode input admittance:

$$Y_{in,e} = -j \frac{1}{Q_e} \cdot \frac{\omega - \Omega_{Ze}}{\omega - \Omega_{Pe}} \quad (4.5.19)$$

$$\Omega_{Pe} = -B_1 + J_1 + \frac{J_N^2}{B_N - J_N} \quad (4.5.20)$$

$$\Omega_{Ze} = -B_1 + J_1 \quad (4.5.21)$$

$$Q_e = \frac{B_N - J_N}{J_{in}^2} \quad (4.5.22)$$

The even-mode external Q factor can be extracted as:

$$Q_e = \frac{1}{|Y_{in,e}(\omega=0)|} \cdot \frac{\Omega_{Ze}}{\Omega_{Pe}} \quad (4.5.23)$$

By combining equation (4.5.15)-(4.5.17) and equations (4.5.20)-(4.5.22) we can obtain the ratios that describe the doublet structure in Figure 4.5-6 with a certain scaling factor as given below.

$$\frac{B_N}{J_{in}^2} = \frac{1}{2}(Q_o + Q_e) \quad (4.5.24)$$

$$\frac{J_N}{J_{in}^2} = \frac{1}{2}(Q_o - Q_e) \quad (4.5.25)$$

$$B_1 = -\frac{1}{2}(\Omega_{Ze} + \Omega_{Zo}) \quad (4.5.26)$$

$$J_1 = \frac{1}{2}(\Omega_{Ze} - \Omega_{Zo}) \quad (4.5.27)$$

$$\frac{J_{N1}^2}{B_N} = 2 \cdot \left(\frac{1}{\Omega_{Po} - \Omega_{Zo}} + \frac{1}{\Omega_{Pe} - \Omega_{Ze}} \right)^{-1} \quad (4.5.28)$$

$$\frac{J_{N1}^2}{J_N} = 2 \cdot \left(\frac{1}{\Omega_{Po} - \Omega_{Zo}} - \frac{1}{\Omega_{Pe} - \Omega_{Ze}} \right)^{-1} \quad (4.5.29)$$

The GCC $k_1=J_1$, $k_N = J_N/B_N$, $k_{N1} = J_{N1}/\sqrt{B_N}$, are calculated from (24)-(29) by setting an arbitrary value of J_{in} , for example, unity. It is to be mentioned at this point that this method of obtaining physical dimensions does not provide the final solution. However, it endows the initial point at which further fine tuning, either manually or through an optimizer, will be required to achieve the final result.

4.5.3 Compact 3rd Order Cross-coupled Waveguide Filter Using Singlet and Extracted Pole Sections.

The coupling schematic shown in Figure 4.5-2 can be implemented using E-plane inserts within conventional rectangular waveguide housing. In order to illustrate how this can be achieved, the arrangement of the metallic inserts within a split block waveguide housing is shown in Figure 4.5-8. The structure consist two metallic inserts, one of which has a single wide fin, centralised with respect to the length of the waveguide and grounded to either the top or bottom wall. The other insert is composed of a narrow metallic fin with a single E-plane extracted pole section on either side of it. The configuration and realisation of an E-plane extracted pole section was described in detail in section 3.3. The narrow central fin and the wide fin on the other insert forms the singlet section, but with capacitive by-pass coupling between the non-resonating nodes of the two extracted pole sections. Therefore each section will generate its own pole and transmission zero.

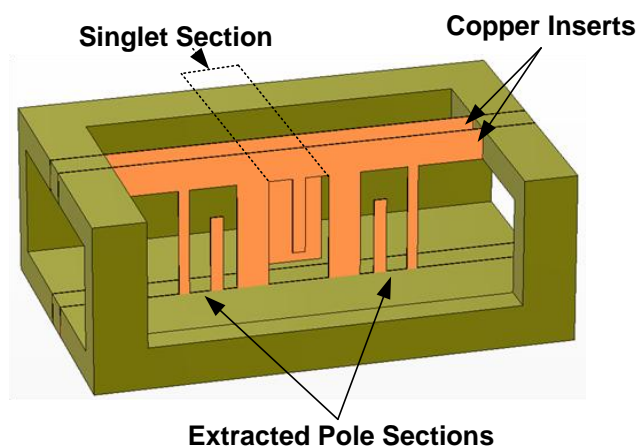


Figure 4.5-8: An inside view of the configuration of proposed compact 3rd order cross-coupled waveguide filter.

To demonstrate the performance and validity of the proposed structures, a 3rd order filter with the configuration shown in Figure 4.5-8 has been designed, simulated and tested to satisfy the following set of specifications.

- Center frequency: 9.2 GHz.
- Ripple bandwidth: 0.2 GHz.
- Return loss: 20 dB.
- Transmission zeros (GHz): 8.9, 9.9, 9.9.

First the characteristic filter polynomials $E(s)$, $F(s)$ and $P(s)$ which corresponds to the S_{21} and S_{11} rational functions have been derived using Cameron's recursive technique [6]. Subsequently, the direct synthesis technique for inline filters with non resonating nodes [4-20] has been applied in order to calculate the element values of the extracted pole sections. The coupling schematic of the structure is given in Figure 4.5-9.

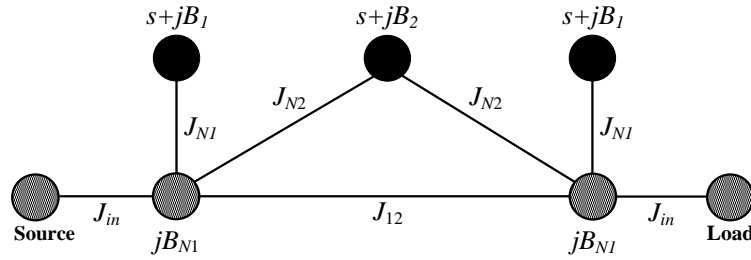


Figure 4.5-9: Coupling schematic of the proposed 3rd order cross-coupled filter.

$$S_{11} = \frac{F(s)}{E(s)}, S_{21} = \frac{P(s)}{\varepsilon \cdot E(s)}, \varepsilon = 29.921 \quad (4.5.30)$$

$$P(s) = s^3 - j10.4545s^2 - 4.3956s - j139.095 \quad (4.5.31)$$

$$F(s) = s^3 + j0.0196s^2 + 0.7596s + j0.00954 \quad (4.5.32)$$

$$E(s) = s^3 + (2.2301 + j0.0016)s^2 + (3.3853 + j0.08231)s + (2.5830 - j0.127) \quad (4.5.33)$$

At the end of the synthesis process, the following values for the elements in the coupling schematic as shown in Figure 4.5-9 can be obtained: $J_{in} = 1$, $J_{12} = -0.3954$, $J_{N1} = 4.8983$, $J_{N2} = 0.885$, $B_{N1} = -4.5810$, $B_1 = -5.4020$, $B_2 = 0.50901$. Thereafter the GCCs to be realized can be calculated as: $k_{N1}^2 = -5.2376$, $k_{N2}^2 = 0.003721$, $k_{12}^2 = 0.007448$ and $Q_{ext} = -4.5810$. At this point, determination of the initial dimensions of the structure can be carried out by extracting the GCCs of each

extracted pole section and the singlet individually. This can be done by applying equations (4.5.8)-(4.5.11) for the singlet, and in the case of the extracted pole sections a similar procedure explained in [4-1] can be applied to extract the GCCs. The GCCs are extracted from the simulated frequency responses of each individual section as a function of certain geometrical parameters. The procedure determinations of the initial dimensions of the two inserts are processed as follows. A single symmetric extracted pole section is examined by first varying the length of the embedded metallic fin as the position of the transmission zero depends on the length of fin. The septa dimensions and the length of the non-resonating node of the extracted pole section are kept constant at an arbitrary value. Once the required susceptance value for B_1 is extracted, the length of the fin is kept fixed. Next, the length of the non-resonating node is varied until the projected coupling coefficient k_{N1}^2 is reached. Upon this the length of input and output septa are varied until the required external Q -factor is achieved. Once the initial dimensions of the extracted pole section is known, the singlet section can be examined. In order to extract the coupling coefficient k_{N2}^2 , the width of septa (W_{SEP2}) is adjusted while all other dimensions are kept constant. Then the gap in the wide metallic fin in the second insert is adjusted until the required value for k_{12}^2 is extracted.

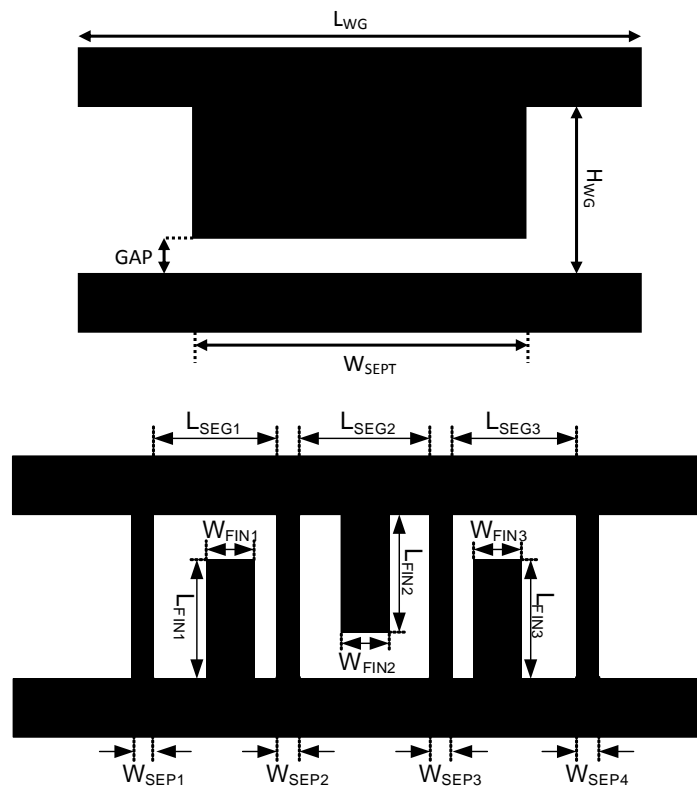


Figure 4.5-10: Layout of the two metallic inserts for realisation of compact 3rd order cross coupled filter.

The extracted GCCs for the extracted pole sections and the singlet section are shown in Figure 4.5-11. The layout of the two E-plane inserts is shown in Figure 4.5-10.

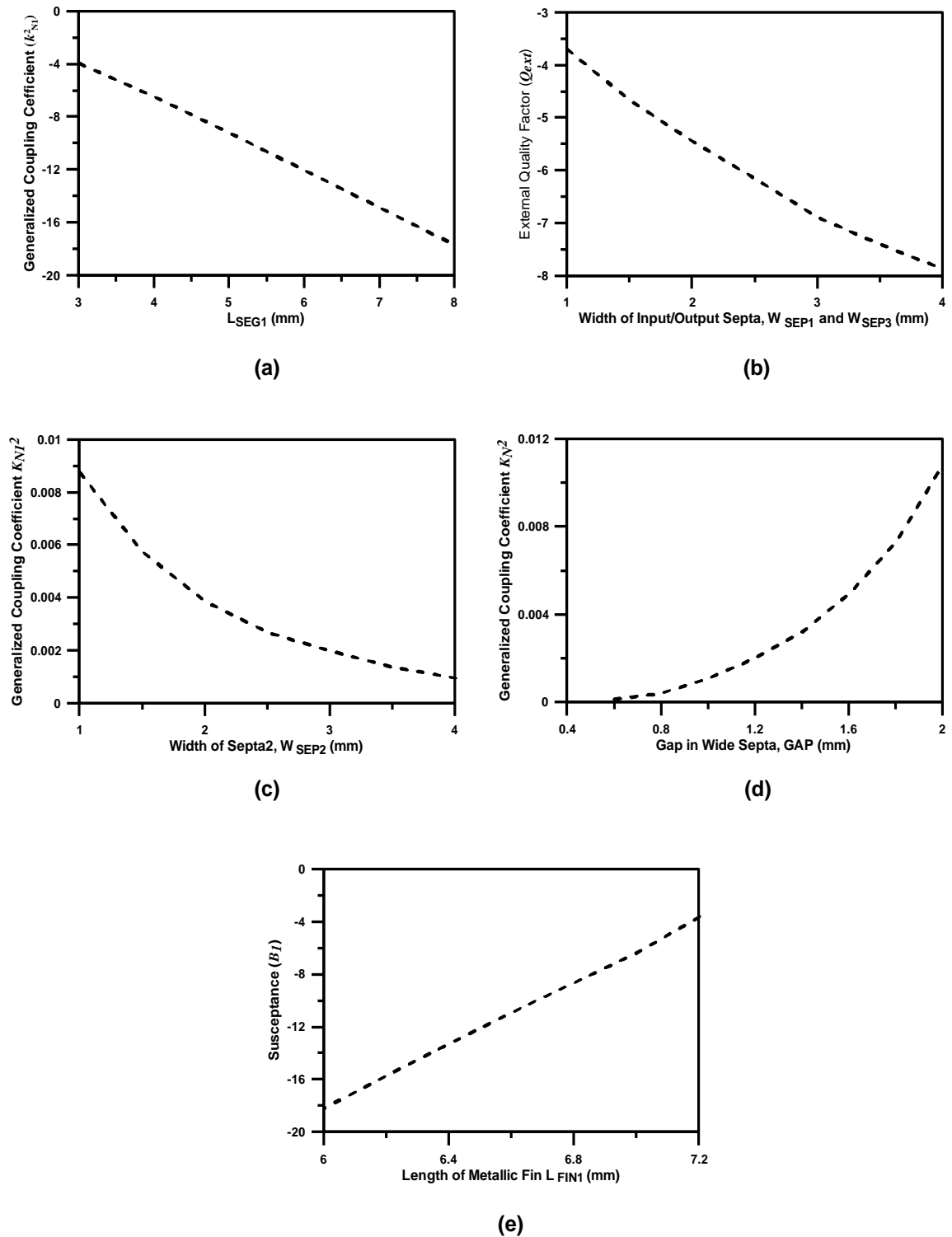


Figure 4.5-11: Extracted generalized coupling coefficients against insert dimensions:
 (a) k_{N1}^2 from extracted pole section; (b) external quality factor (Q_{ext});
 (c) k_{N2}^2 from singlet section; (d) k_{12}^2 from singlet section; (e) susceptance B_1 from EPS.

From the plotted graphs as a result of extraction, the initial dimension of the compact 3rd order cross-coupled filter has been obtained. The filter, taking into consideration of the initial dimensions, has been then optimised in order to obtain the final dimensions that satisfy the required specification. The initial and final dimensions of the inserts are summarised in Table 4.5-1. It can be seen that the procedure has provided with good initial approximation of the dimensions.

Parameters	Initial Values	Optimised values	Parameters	Initial Values	Optimised Values
L_{FIN1}	7.1	6.99	W_{FIN3}	-	1.7
L_{FIN2}	7.0	6.97	W_{SEPT}	6.0	6.0
L_{FIN3}	7.1	6.99	W_{SEP1}	1.4	1.0
$L_{SEG1} = L_{SEG3}$	3.5	4.21	W_{SEP2}	2.1	2.3
L_{SEG2}	6.80	6.80	W_{SEP3}	2.1	2.3
W_{FIN1}	-	1.7	W_{SEP4}	1.4	1.0
W_{FIN2}	-	1.7	GAP	1.7	1.2
-	-	-	Total Length	-	21.82

Table 4.5-1: Dimensions of the E-plane insert for the compact 3rd order cross-coupled filter.

In order to validate the performance of the proposed 3rd order filter, the structure has been realized using E-plane technology. The inserts shown in Figure 4.5-10 has been cut out of a copper foil ($\sigma = 5.8 \times 10^7$ S/m), with a thickness T of 0.1mm and placed within a custom made aluminum waveguide housing with two channels. The channels have a separation of 3mm between each other.

The S-parameter response of the filter has been measured using an Agilent E8361A vector network analyzer and a comparison of the simulated and the measured results are shown in Figure 4.5-12. The computed response shows all three poles and three transmission zeros, two of which are located at the same frequency in the upper stopband. The measure results agree well with that of the simulated, especially the locations of the transmission zeros but it does not reveal all three poles. This is due to the fabrication tolerances encountered during construction of the two inserts, which also leads to the filter having an insertion loss of about 1.5dB and a return loss of about 14dB. Another reason for the increase in the losses observed could be due to the signal leakage through the imperfect waveguide housing. The waveguide housing was not cut using precision engineered tools and was simply constructed using in house milling tools. Therefore it is clear that the results can be further improved through employing

better fabrication utilities for the waveguide housing, and through meticulous use of the available tools to construct the metallic inserts. Figure 4.5-13 shows a photograph of the fabricated inserts with the waveguide housing.

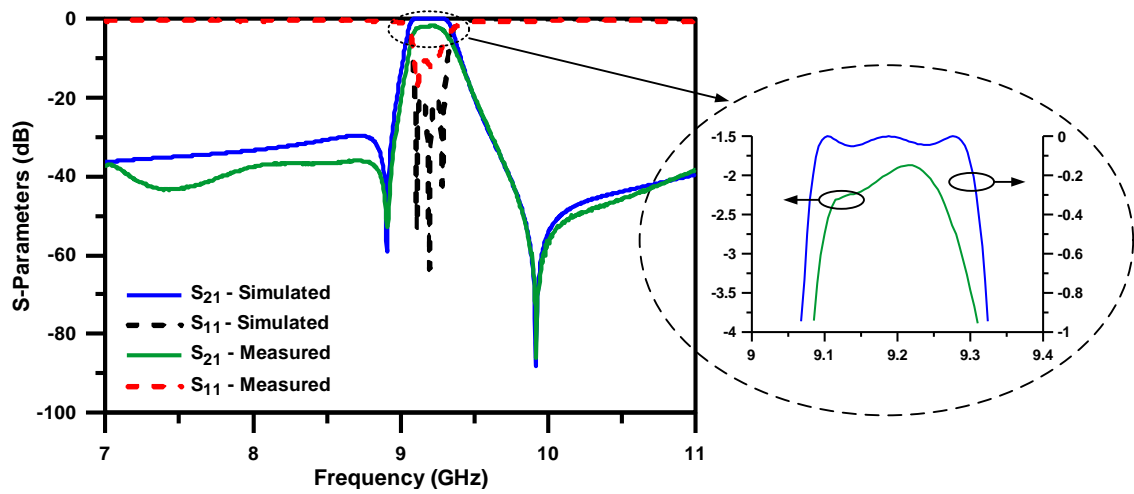


Figure 4.5-12: Simulated and measured S-parameter response of the compact 3rd order cross-coupled filter.



Figure 4.5-13: Photograph of the fabricated inserts for the compact 3rd order cross-coupled filter, placed within the custom made split block waveguide housing.

4.5.4 Compact 4th Order Cross-coupled Waveguide Filter Using Doublets and Extracted Pole Sections.

In this sub section, the development of compact 4th order E-plane cross-coupled filters are demonstrated. Similar to the 3rd order filter proposed in section 4.5.3, the coupling schematic shown in Figure 4.5-3 can also be implemented using E-plane inserts within conventional rectangular waveguide housing. In order to illustrate how this can be achieved, the arrangement of the metallic inserts within a split block waveguide housing is shown in Figure 4.5-14. The configuration of the structure is similar to the previously proposed 3rd order filter, but utilizes a doublet section instead of the singlet.

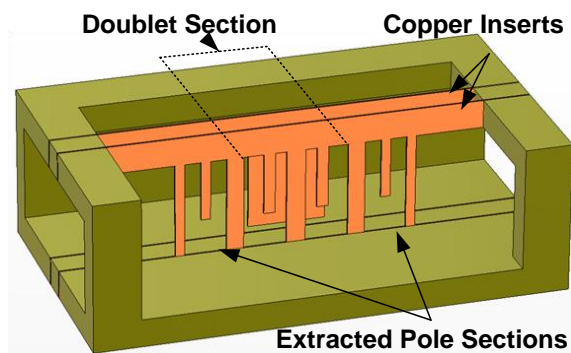


Figure 4.5-14: An inside view of the configuration of proposed compact 4th order cross-coupled waveguide filter.

To demonstrate the performance and validity of the proposed structure, a 4th order filter with the configuration shown in Figure 4.5-14 has been designed, simulated and tested to satisfy the following set of specifications.

- Center frequency: 10 GHz.
- Ripple bandwidth: 0.25 GHz.
- Return loss: 20 dB.
- Transmission zeros (GHz): 9.5, 10.5, 10.5, 10.5.

As with the previous example, design of the filter begins with the determinations of characteristic filter polynomials $E(s)$, $F(s)$ and $P(s)$ which corresponds to the S_{21} and S_{11} rational functions using Cameron's recursive technique [6].

Consequently, the direct synthesis technique for inline filters with non resonating nodes [4-20] or the network synthesis technique described in [4-6] can be applied in order to

calculate the element values of the extracted pole sections. The coupling schematic of the structure is given in Figure 4.5-15.

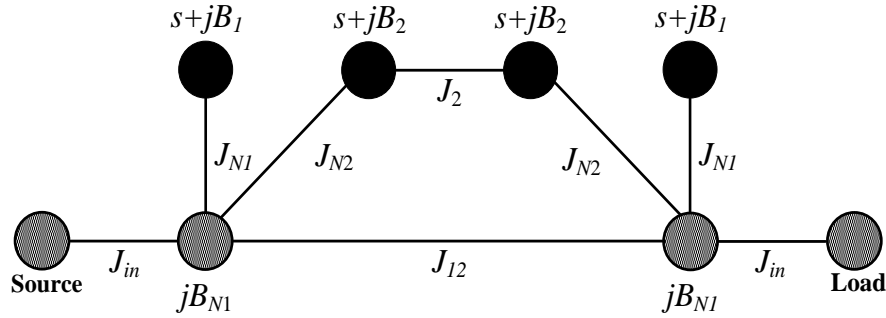


Figure 4.5-15: Coupling schematic of the proposed 4th order cross-coupled filter.

$$S_{11} = \frac{F(s)}{E(s)}, S_{21} = \frac{P(s)}{\varepsilon \cdot E(s)}, \varepsilon = 184.031 \quad (4.5.30)$$

$$P(s) = s^4 - j7.61s^3 + 2.35s^2 - j128.24s - 244.41 \quad (4.5.31)$$

$$F(s) = s^4 - j0.267s^3 + 0.981s^2 - j0.201s + 0.115 \quad (4.5.32)$$

$$E(s) = s^4 + (2.137 - j0.267)s^3 + (3.26 - j0.656)s^2 + (2.752 - j0.997)s + (1.12 - j0.73) \quad (4.5.33)$$

The following values for the elements of the schematic in Figure 4.5-15 were obtained at the end of the synthesis process: $J_{in} = 1$, $J_{N1} = 4.0301$, $J_{N2} = 0.8719$, $J_{12} = -0.0364$, $J_2 = 0.7179$, $B_{N1} = -3.8665$, $B_1 = -4.2848$, $B_2 = 0.0442$. Thereafter the GCCs to be realized can be calculated as: $k_{N1}^2 = -4.2006$, $k_{N2}^2 = 0.004916$, $k_{12} = 0.009419$, $k_2 = 0.7179$ and $Q_{ext} = -3.8665$. Determination of the initial dimensions of the structure can be carried out by extracting the GCCs of each extracted pole section and the doublet individually. Extraction of the coefficients for the doublet section can be done by applying equations (4.5.24)-(4.5.29), and in the case of the extracted pole sections a similar procedure explained in [4-1] can be applied. The extraction procedure for the GCCs is similar to the previous example, by first considering the extracted poles sections followed by the doublet. The extracted GCCs for doublet sections and the extracted pole sections are illustrated in Figure 4.5-16 and continued on Figure 4.5-17.

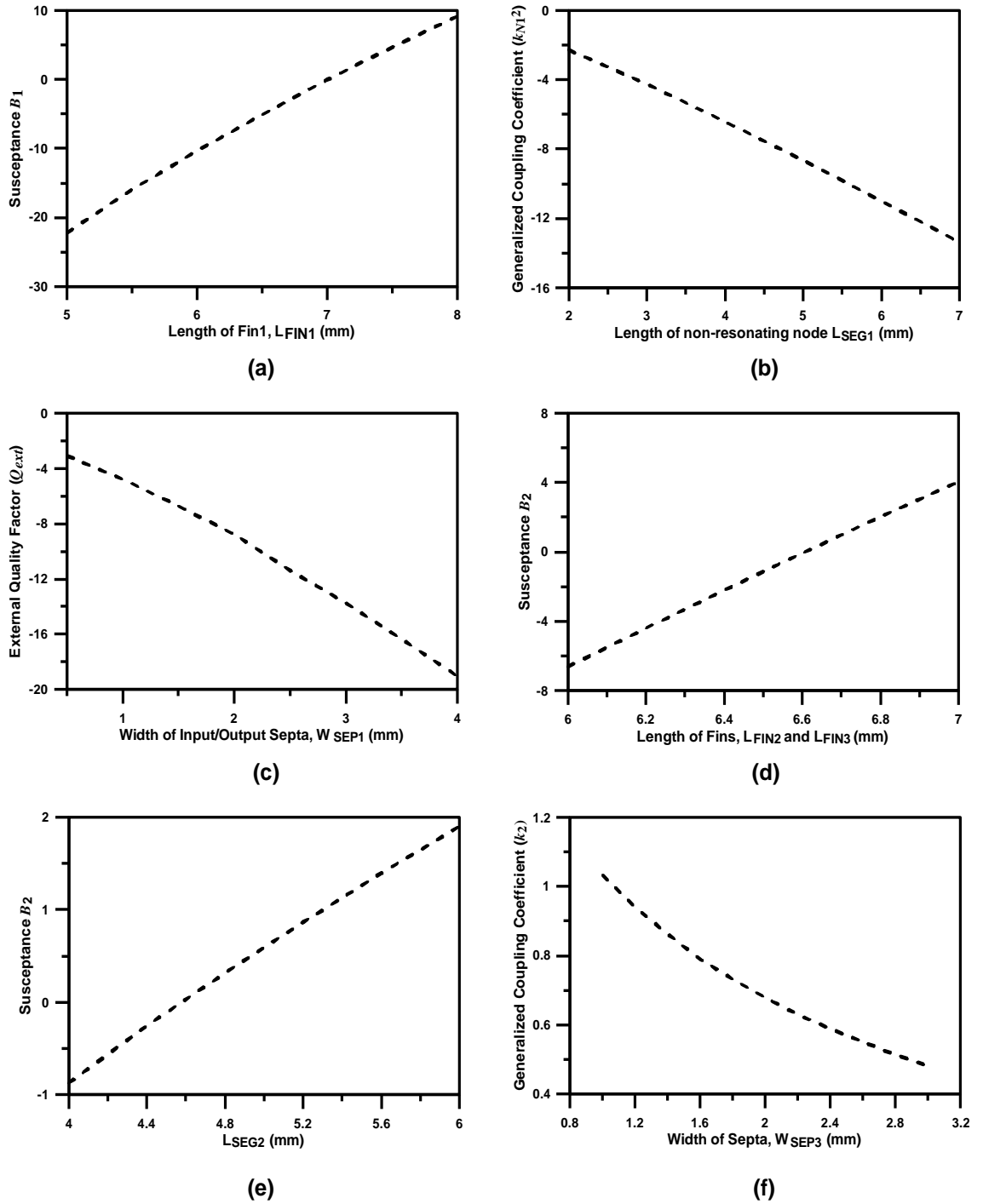


Figure 4.5-16: Extracted generalized coupling coefficients against insert dimensions

(refer to Figure 4.5-18 for insert notations):

- (a) Susceptance B_1 against length of fins from extracted pole sections;
- (b) k_{N1}^2 against L_{SEG1} from extracted pole section; (c) external quality factor (Q_{ext});
- (d) Susceptance B_2 against length of fins from doublet;
- (e) Susceptance B_2 against L_{SEG2} from doublet; (f) k_2 against W_{SEPT3} from doublet section.

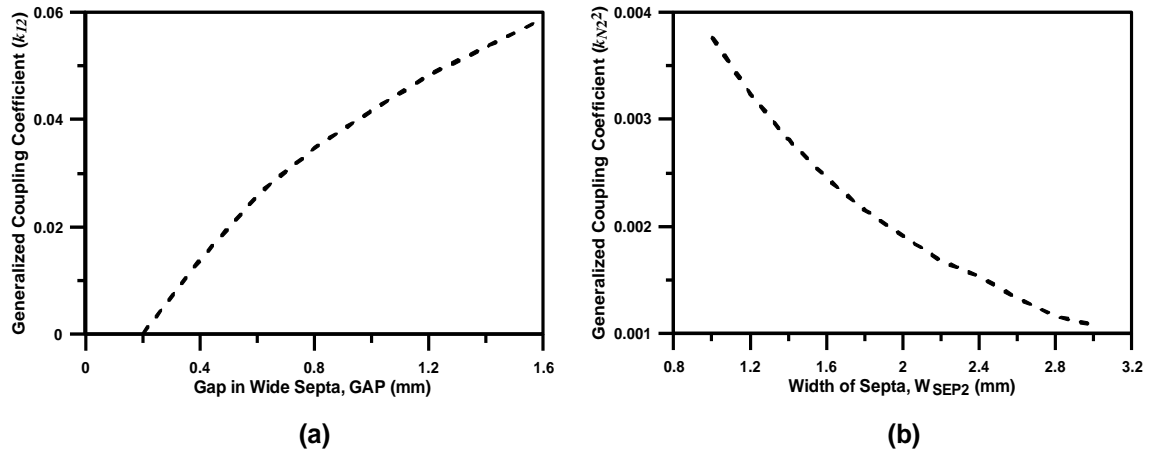


Figure 4.5-17: Extracted generalized coupling coefficients against insert dimensions Cont.:

(a) k_{12} against GAP from doublet; (b) k_{N2}^2 against W_{SEP2} from doublet.

From the plotted graphs as a result of extraction, the initial dimension of the proposed compact 4th order cross-coupled filter has been obtained. In order to obtain the final dimensions that satisfy the specification required, the filter has been designed and optimised using CST Microwave StudioTM taking into consideration of the initial dimensions. The initial and final dimensions of the inserts are summarised in Table 4.5-2. It can be seen that the procedure has provided with reasonably good initial approximation of the dimensions.

Parameters	Initial values	Optimised values	Parameters	Initial values	Optimised Values
$L_{FIN1} = L_{FIN4}$	6.5	6.41	W_{SEPT}	8.0	8.2
$L_{FIN2} = L_{FIN3}$	6.6	6.60	W_{SEP1}	0.7	1.0
$L_{SEG1} = L_{SEG4}$	3.0	4.45	W_{SEP2}	0.9	1.8
$L_{SEG2} = L_{SEG3}$	4.4	4.55	W_{SEP3}	1.8	2.0
W_{FIN1}	-	1.0	W_{SEP4}	0.9	1.8
W_{FIN2}	-	1.2	W_{SEP5}	0.7	1.0
W_{FIN3}	-	1.2	GAP	0.35	1.0
W_{FIN4}	-	1.0	Total Length	-	25.6

Table 4.5-2: Dimensions (mm) of the E-plane insert for the compact 4th order cross-coupled waveguide filter (refer to Figure 4.5-18).

In order to illustrate the size reduction, that the proposed filters achieve, the designed filter has been compared with a 4th order conventional filter and a 4th order EPS filter, designed for the same centre frequency and bandwidth. Table 4.5-3 provides a comparison of the overall lengths of all three filters.

E-plane Filter type	Length (mm)
Conventional 4 th order filter	98.6
4 th order EPS filter with three transmission zeros in the upper stopband	39.06
Proposed 4 th order compact cross-coupled filter	25.6

Table 4.5-3: Comparison of overall length of the compact cross-coupled filter with E-plane EPS filter and conventional E-plane filter.

In order to validate the performance of the proposed 4th order cross-coupled filter, the structure has been realized using E-plane technology. The inserts shown in Figure 4.5-18 has been cut out of a copper foil ($\sigma = 5.8 \times 10^7$ S/m), with a thickness T of 0.1 mm and similar to the previous example, they have been placed within a custom made aluminum waveguide housing with two channels, which has a separation of 3 mm between each other.

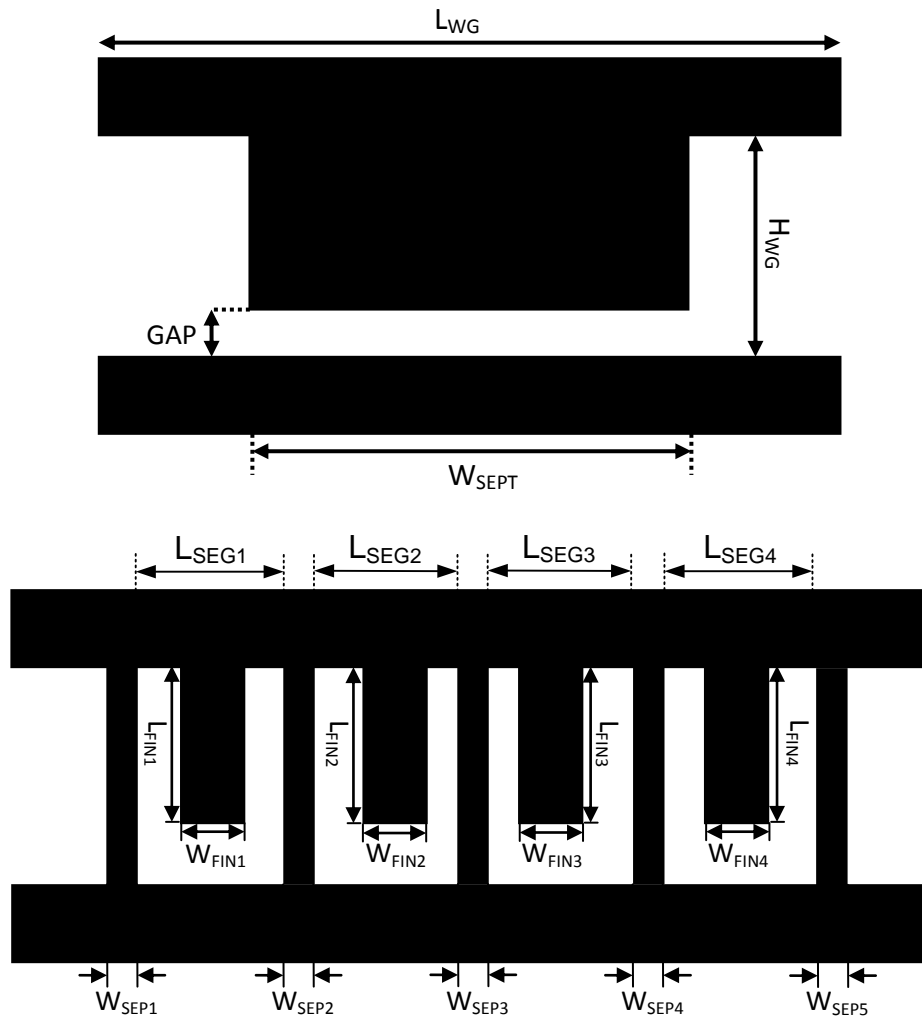


Figure 4.5-18: Layout of the two metallic inserts for realisation of compact 4th order cross-coupled filter.

A comparison of the simulated S-parameter responses of the structure and the measured response of the fabricated filter is provided in Figure 4.5-19. The measured results agree well with that of the simulated, however an insertion loss of about 1.5dB can also be observed. Furthermore the measured response does not clearly reveal all four poles. These disagreements are due to the difficulties encountered during fabrication process to realise more accurate dimensions of the structure. Another factor that must be taken into consideration again is the construction of the waveguide housing, which was not done using the precision tools that are required for their construction. A photograph of the fabricated filter is presented in Figure 4.5-20.

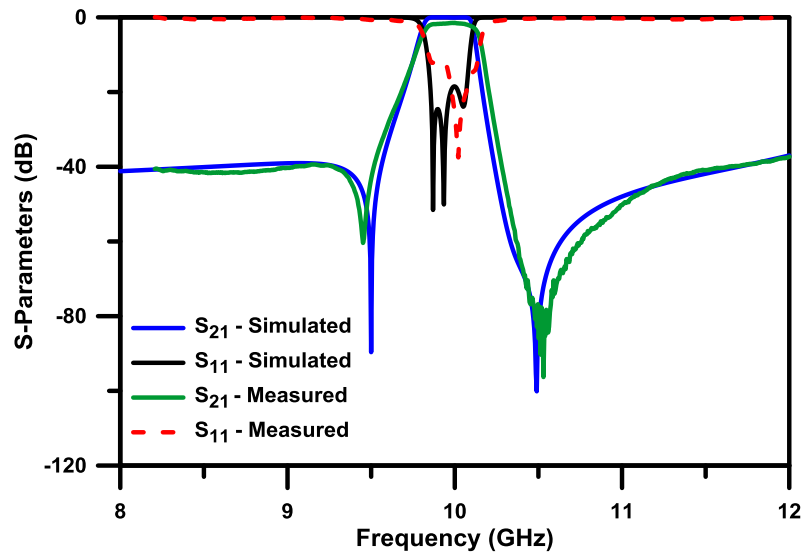


Figure 4.5-19: Simulated S-parameter response and the measure results of the compact 4th order cross-coupled filter.



Figure 4.5-20: Photograph of the fabricated inserts within the custom made split block waveguide housing for the 4th order E-plane Cross-coupled filter.

4.6 Summary

In this chapter, compact cross-coupled waveguide filters using all metallic E-plane inserts that can realise generalized Chebyshev type frequency responses have been proposed. In section 4.2, the basic cross coupled filtering modules known as the singlet and the doublet, has been introduced. The realisations of these modules using all metallic E-plane inserts were then provided. The configuration of the E-plane inserts to create the cross-coupled topology also allows the filter to be highly compact in comparison to cross-coupled filters using folded conventional E-plane resonators. The resonators are implemented by $\lambda/4$ type resonators that are physically realised by metallic fins short circuited on one end to the broad wall of the waveguide. This allows the resonator to be self-suspended and inherently prevents the need of a dielectric substrate to support the resonator and further loss can be avoided.

In section 4.3, the concept of coupling coefficient between two coupled resonators has been briefly discussed and method for extracting these coupling coefficients, either through simulation or measured frequency responses has been provided. Section 4.4 demonstrate the implementation of higher order filters using the same configuration as described in section 4.2, by inserting additional resonators in the main path that are all bypassed between source and load. The disadvantage of designing higher order filters in this manner is the increase sensitivity of the structure to fabrication tolerances, as the location of poles and zeros depends on all available couplings within the structure. A 3rd order filter has been simulated, fabricated and measured for demonstration. A comparison between a conventional E-plane filter and an E-plane EPS filter shows a size reduction of 70% and 33% respectively can be achieved.

Finally section 4.5 demonstrates compact E-plane cross-coupled filters implemented by cascading extracted pole sections with proposed singlets or doublets. The E-plane cross-coupled filters implemented this way remains compact and modular as each section can generate and control its own pole and zero, with minimal effect on one another. Hence the structures are less sensitive to manufacturing tolerances. The section also introduces a method to extract the coupling coefficients for these filters which help in evaluating the initial dimensions of the filter inserts. The design of a 3rd order filter and a 4th order filter has been provided, which were fabricated and measured to validate the performance of these structures.

4.7 References

- [4-1] O. Glubokov and D. Budimir, "Extraction of Generalized Coupling Coefficients for Inline Extracted Pole Filters With Nonresonating Nodes," *Microwave Theory and Techniques, IEEE Transactions on*, vol. 59, no. 12, pp. 3023-3029, Dec. 2011.
- [4-2] N. Mohottige, O. Glubokov and D. Budimir, "Ultra Compact Inline E-Plane Waveguide Extracted Pole Bandpass Filters," *Microwave and Wireless Components Letters, IEEE*, vol. 23, no. 8, pp. 409-411, Aug. 2013.
- [4-3] A. E. Atia and A. E. Williams, "New Types of Bandpass Filters for Satellite Transponders", *COMSAT Tech. Rev.*, vol. 1, pp. 21-43, 1971.
- [4-4] A. E. Williams. (1983). *Multiple coupled cavity waveguide bandpass filters*. US Patent: US4396896 A.
- [4-5] Rosenberg, U.; Hagele and Walter, "Advanced multimode cavity filter design using source/load-resonance circuit cross couplings," *Microwave and Guided Wave Letters, IEEE*, vol. 2, no. 12, pp. 508-510, Dec. 1992.
- [4-6] R. J. Cameron, C. M. Kudsia, and R. R. Mansour, *Microwave Filters for Communication Systems*, Hoboken, New Jersey, John Wiley & Sons, 2007.
- [4-7] E. Ofli, R. Vahldieck and S. Amari, "Novel E-plane filters and diplexers with elliptic response for millimeter-wave applications," *Microwave Theory and Techniques, IEEE Transactions on*, vol. 53, no. 3, pp. 843-851, March 2005.
- [4-8] O. Glubokov and D. Budimir, "Compact E-plane doublet structures for modular filter design," *Microwave Conference (EuMC), 2010 European*, pp. 1253-1256, 28-30 Sept. 2010.
- [4-9] S. Amari, U. Rosenberg and J. Bornemann, "Singlets, Cascaded Singlets, and the Nonresonating Node Model for Advanced Modular Design of Elliptic Filters," *IEEE Microwave and Wireless Components Letters*, vol. 14, no. 5, pp. 237-239, May 2004.

- [4-10] S. Amari and U. Rosenberg, "The Doublet: A New Building Block for the Modular Design of Elliptic Filters", *Microwave Conference, 2002. 32nd European*, pp.1-3, 23-26 Sept. 2002.
- [4-11] S. Amari and U. Rosenberg, "Characteristics of cross (bypass) coupling through higher/lower order modes and their applications in elliptic filter design," *Microwave Theory and Techniques, IEEE Transactions on*, vol. 53, no. 10, pp. 3135-3141, Oct. 2005.
- [4-12] S. Amari and U. Rosenberg, "New building blocks for modular design of elliptic and self-equalized filters," *Microwave Theory and Techniques, IEEE Transactions on*, vol. 52, no. 2, pp. 721-736, Feb. 2004.
- [4-13] S. Amari, "On the maximum number of finite transmission zeros of coupled resonator filters with a given topology," *Microwave and Guided Wave Letters, IEEE*, vol. 9, no. 9, pp. 354-356, Sep. 1999.
- [4-14] S. Amari and J. Bornemann, "Maximum number of finite transmission zeros of coupled resonator filters with source/load-multiresonator coupling and a given topology," *Microwave Conference, 2000 Asia-Pacific*, pp. 1175-1177, 2000.
- [4-15] J.B. Thomas, "Cross-coupling in coaxial cavity filters - a tutorial overview," *Microwave Theory and Techniques, IEEE Transactions on*, vol. 51, no. 4, pp. 1368-1376, Apr. 2003.
- [4-16] S. Amari and U. Rosenberg, "A universal building block for advanced modular design of microwave filters," *Microwave and Wireless Components Letters, IEEE*, vol. 13, no. 12, pp. 541-543, Dec. 2003.
- [4-17] G. L. Matthaei, L. Jones and E. M. T. Jones, *Microwave Filters, Impedance Matching Networks and Coupling Structures*, New York: McGraw-Hill, 1964.
- [4-18] O. Glubokov (2011). *Development of Waveguide Filter Structures for Wireless and Satellite Communications*. PhD. Thesis. University of Westminster: UK.
- [4-19] J.-S. Hong, "Couplings of asynchronously tuned coupled microwave resonators," *Proc. Inst. Elect. Eng.—Microw., Antennas, Propag.*, vol. 147, no. 5, pp. 354–358, Oct. 2000.

- [4-20] S. Amari and U. Rosenberg, "Synthesis and Design of Novel In-Line Filters With One or Two Real Transmission Zeros," *IEEE Trans. Microwave Theory Tech.*, vol. 52, no. 5, pp. 1464-1478, May 2004.

OPTICALLY RECONFIGURABLE E-PLANE WAVEGUIDE RESONATORS AND FILTERS

5.1 Introduction

Over the past few years, the rapid increase in the number of wireless services and the demand to access multiple services through a single technology, have created a growing interest in the research and development of frequency tuneable bandpass filters [5-1]. One of the applications of such filters is proposed for multiband communication systems, where a transceiver may operate on multiple frequency bands. Further potential applications for tuneable and reconfigurable filters can be found in [5-1]. Compactness is one of the key benefits a tuneable filter is capable of offering for such multifunctional systems. The bandwidth of these filters generally differs depending on centre frequency of each channel, but may be kept constant for some applications.

Tuneable microwave filters typically consist of synchronously tuned resonators where a tuneable element (for example a PIN diode, varactor diode or MEMS switch) is inserted at a point where they affect the resonant frequencies the most. There are two well-established commercially available semiconductor tuning elements that have been widely used for the implementation of tuneable or reconfigurable microwave filters. The PIN and the varactor diodes are highly practical devices due to their precise manufacturing process that leads to high quality units with extremely low costs. Furthermore, their attractiveness for reconfigurable and tuneable filters stems from their performance attributes in terms of high reliability, fast switching speeds, robustness and versatility for circuit integration [5-2]. However as the capacitance of a varactor diode is voltage controlled, one of the drawbacks that varactor diodes suffer from is signal distortion. This is because the state of the diode depends on the voltage applied to it and is vulnerable to RF signal superimposed on the DC biasing. Therefore, any filters utilising these elements will suffer from poor linearity. The same underlined problem applies in the case of PIN diodes with the added drawback of high power consumption [5-3]. PIN diodes and varactor diodes are widely investigated for use in planar

microwave filters [5-4]-[5-6], but due to the aforementioned drawbacks and also considering the realisation of biasing circuitry that will be needed for these elements, they are not suitable for use in waveguide applications.

More recently, RF-MEMS switches have received a great deal of attention in the realisation of tuneable/reconfigurable waveguide resonators and filters. The RF-MEMS metal contact switch has a couple of distinct advantages over the PIN diode in terms of high linearity, very low power consumption and higher quality factors [5-7]. Furthermore, they are also very versatile as they can be integrated on different substrates due to their construction techniques. On the negative side, they suffer from poor switching speeds and extremely high design complexity and low reliability [5-7]. However, there are several notable published articles that demonstrate the performance of tuneable/reconfigurable waveguide filters using the RF-MEMS switch. A tuneable waveguide cavity resonator using a network of capacitive RF-MEMS cantilever switches, covering a tuneable frequency range from 4.3 GHz to 5.5 GHz has been proposed in [5-8]. The prototype demonstrates a measured unloaded quality factor Q_u , ranging from 425 to 548 for the tuneable frequency range. The authors have also further extended this approach to a tuneable waveguide cavity filter demonstrated in [5-9], which has a tuneable frequency range from 4.07 GHz to 5.58 GHz, with Q_u ranging from 300 to 500. An X-band cavity based reconfigurable resonator using RF-MEMS was demonstrated in [5-10], with reported quality factors ranging from 593 to 1077 for a frequency range of 10.7 GHz to 13 GHz. An E-plane tuneable waveguide filter with two states at K-band using RF-MEMS cantilever switches have been demonstrated in [5-11]. The switches are used to connect printed metallic lines and placed on an inner narrow wall of the waveguide. The activation of the switches leads to the realisation of an equivalent movable inner wall which causes a shift in the resonance frequency. The proposed filter has shown to produce a frequency shift of 730 MHz with measured unloaded quality factors of 750 and 1450 in the ON and OFF states respectively.

Another technology that can be used as a switching element is the silicon dice, where the photoconductive effect of silicon is exploited to switch various microwave circuits on and off. An optically illuminated silicon dice for use as a switching element was initially proposed by Auston in 1975 [5-12]. The optical switch has distinct advantages in terms of ease of implementation, high power handling capabilities, high switching speeds and high linearity [5-13]. Furthermore, they do not require internal biasing circuits.

The development of the silicon switch continued where several examples of their implementation for switchable planar microwave devices such as filters and antennas can be found in [5-14]-[5-17]. Panagamuwa *et al.* [5-14] demonstrated a frequency tuneable antenna employing a pair of optically operated silicon switches. The activation of the silicon switch was conducted through optical illumination from a laser diode via a fibre optic cable. The results prove that the centre frequency of the antenna could be shifted by nearly 40%. Chauraya *et al.* [5-15] have demonstrated a frequency switchable parallel coupled microstrip filter using a pair of silicon dice with a centre frequency shift of 359 MHz. Articles [5-16]-[5-17] proposed an optically reconfigurable ultra-wideband microstrip filter which can change its state from bandpass to bandstop depending on optical illumination of a single silicon dice.

Even though a significant amount of research has been carried out with regards to the implementation of the silicon switch in planar microwave devices, no investigation into applications of the switch for realising tuneable/reconfigurable waveguide filters has yet been conducted. This chapter therefore, addresses this point and proposes optically reconfigurable E-plane waveguide bandpass resonators and filters. The advantages offered by the silicon switch in terms of high power handling capabilities, high switching speeds and due to the fact that it does not require any biasing circuits, make it a very attractive option for implementation in waveguide filters. The chapter give a brief overview of the optical switch. This will be followed by the E-plane waveguide resonator structure and how it can be modified to include the optical switch in order to achieve frequency switching characteristics. Measurement results of a fabricated prototype will be provided in order to validate the performance of the proposed tuneable E-plane waveguide resonators.

5.2 The Silicon Photoconductive Switch

This section provides a brief overview of the phenomenon that takes place within a dice of silicon when illuminated with light of appropriate wavelength that consents to it being used as a switching element in reconfigurable/tuneable resonators and filters. A comprehensive theoretical coverage of the subject can be found in [5-18].

This phenomenon that takes place within the silicon dice is recognised as the photoelectric effect. Photoelectric effect is known as the movement of electrons from the valance to the conduction band of a conductor or a semiconductor's atoms when light of an appropriate wavelength is incident upon it. A solid can be thought of as being composed of tiny crystals, where each crystal has an array of atoms in a three dimensional lattice structure and every electron, whether bound or unbound to an atom, has an energy state.

One of the useful ways to distinguish whether a crystal is a conductor, a semiconductor or an insulator, is to visualise the available electron energies in the crystal in to energy bands. The valance band is located at the lowest energy level and contains the highest range of electron energies when the crystal is at absolute zero temperature. On the other hand, the conduction band is located at the highest energy level and represents the range of energies that an electron must gain for it to free itself from its bond to an atom in order to become a mobile charge carrier. Separating both the conduction band and the valance band is the energy bandgap where no electron state can exist.

In a metal, the valance band and the conduction band overlap and electrons can move freely between them as no bandgaps exist. When the valance band and the conduction band are not overlapping (separated by an energy bandgap), then it could be classified as either an insulator or a semiconductor. For an insulator, the energy bandgap is considerably large and it would be technically difficult to provide the required energy to promote electrons from valance band to the conduction band. Semiconductors, on the other hand, have much narrower bandgaps, and it is possible to find the required amount of energy that is needed to raise an electron from the valance band to the conduction band. In the case of silicon, it is possible to provide this energy in the form of light. Figure 5.2-1 represent a simplified energy band diagram used to describe semiconductors.

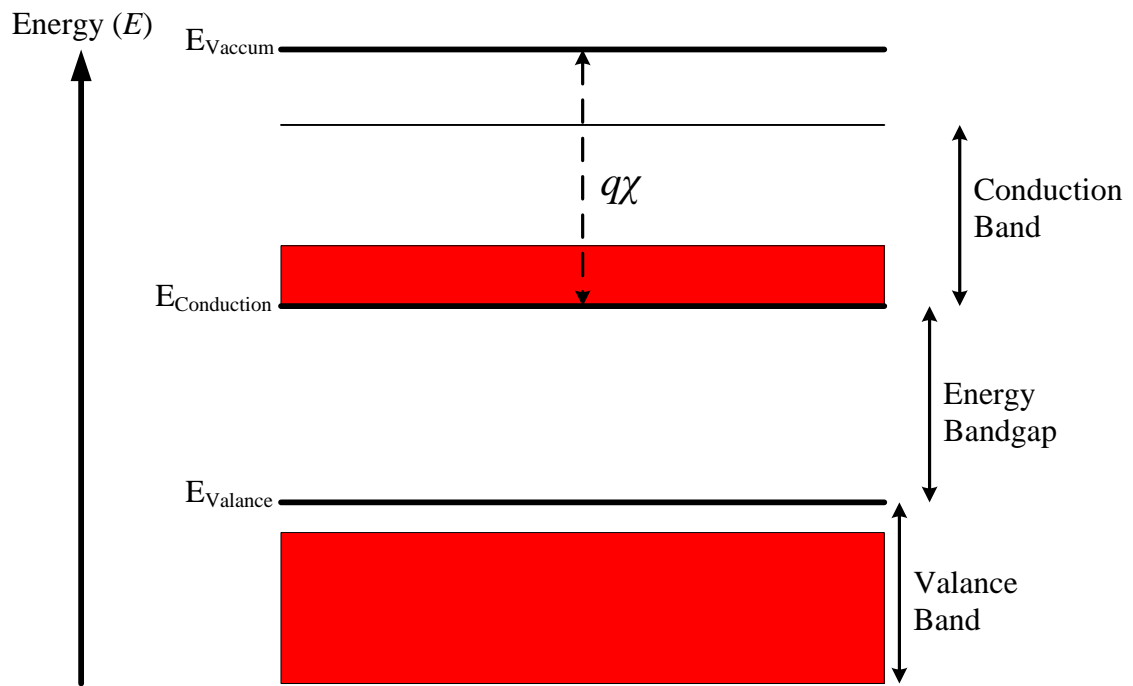


Figure 5.2-1: A simplified energy band diagram of a semiconductor.

The annotations $E_{\text{Conduction}}$ and E_{Valance} represent positions of the band edges for the lower level of conduction band and the highest level of the valance band. The gap between these two band edge positions represents the energy bandgap. The distance between the conduction band edge, $E_{\text{Conduction}}$ and the vacuum level, E_{Vacuum} , which represents the energy of a free electron outside the crystal, is quantified by the electron affinity, χ multiplied with the electronic charge q [5-20].

Certain materials under optical illumination will undergo a change in their electrical conductivity. Generally the conductivity of these materials will increase with the application of light. This phenomenon, where the conductivity of the material changes with the absorption of photons, is known as photoconductivity [5-21]. Though the change is not noticeable in conductive materials, it is for semiconductors such as silicon. As depicted in Figure 5.2-1, semiconductors consist of a certain amount of free electrons that occupy the energy levels in the conduction band which have migrated from the valance band due to natural vibrations of atoms. As a process of this migration, an equal amount of positively charged holes are left over in the valance band. Upon illumination of the semiconductor, the number of mobile charge carriers (electrons and holes) will increase and this leads to an increase in conductivity. However, this increased level of conductivity will only exist with constant illumination; else the free charge carriers generated will become immobile after the finite free-carrier lifetime, due

to a process known as recombination; and also depends on the substance as well as its impurities and imperfections [5-18]. The time taken for an electron to lose the absorbed energy and return back to the valance band is known as the recombination lifetime. According to studies carried out by Platte, it was revealed that the optimum carrier lifetime of silicon lies within a range of 10^{-6} seconds to 10^{-5} seconds [5-19]. With very high levels (larger than the bandgap) of photon energy absorbed by the semiconductor, a single photon absorbed can give rise to many free charge carriers.

This described phenomenon has been manipulated in order to design the photoconductive switch [5-12]–[5-17]. Figure 5.2-2 illustrates the layout of a basic photoconductive switch which consists of a microstrip gap discontinuity bridged by a small dice of silicon. Under optical illumination of the silicon dice, charged carriers are generated within the semiconductor and a conductive path is formed between the two metal contacts. Switching the light source off has the effect of the switch being in an open state. It was demonstrated by Auston [5-12] that the energy provided by a pulsed laser is capable of creating pseudo-metallic photoconduction in silicon.

The switch shown in Figure 5.2-2 has the advantage of being simple to fabricate and therefore has a low cost of production associated to it. Furthermore unlike the MEMS switch, the photoconductive switch has no mechanical moving parts; hence it is more robust and reliable. The light signals do not interfere with the RF signals and therefore the switch provides a high isolation between the switch control circuitry and the microwave device. Switching speed of the switch depends on the rise and fall times of the silicon material. An investigation carried out in [5-22] demonstrates that the rise and fall times depend on the switch dimensions and passivation of the silicon respectively.

The presented configuration of the switch has been widely used in applications such as reconfigurable filters and antennas [5-13]–[5-17]. The intrinsic conductivity of silicon is 0.439×10^{-3} S/m. However, the silicon used in these work were n-type, doped with phosphorus to increase its static conductivity to 16.7×10^{-3} S/m and has a thickness of 300 μm . The optically reconfigurable waveguide resonator proposed in this chapter will also utilise a silicon dice with these same properties.

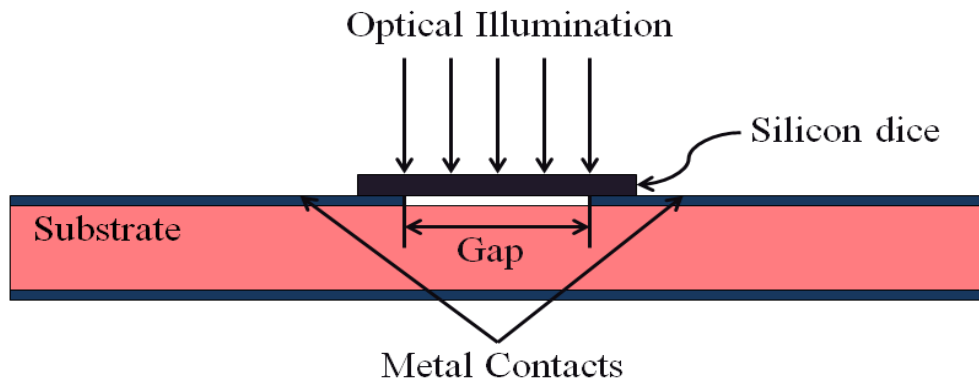


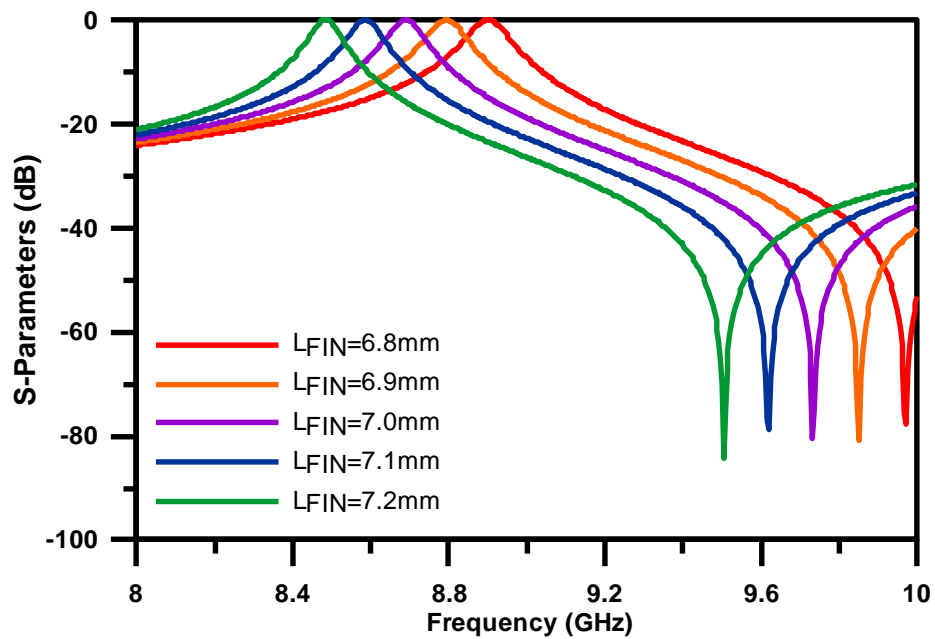
Figure 5.2-2: The basic layout of a photoconductive switch.

In order to simulate structures that are integrated with the optical switch, the properties of the silicon dice can be defined through either derived values for the surface impedance or by its equivalent conductivity. In order to obtain the equivalent conductivity or the impedance values of the silicon dice for different optical powers that can be used in a simulation environment, the simulated scattering parameters of the dice can be compared with the measured results by varying the optical power incident on the dice [5-13]-[5-14]. To facilitate illumination of the silicon dice, a laser diode that delivers the light via a glass fibre optic cable or a LED placed directly above the dice can be used [5-13]. It has been shown in [5-14], that a silicon dice when illuminated with an infrared laser diode that has a 980 nm wavelength and producing 200 mW of optical power will increase the static conductivity of the doped silicon from 16.7×10^{-3} S/m to 250 S/m.

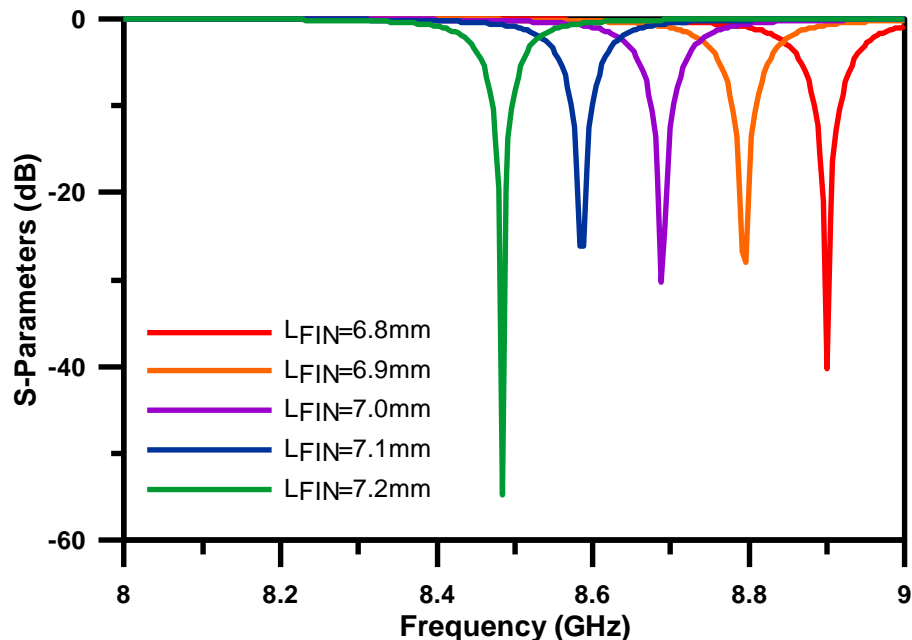
5.3 Optically Reconfigurable E-plane Waveguide Resonator

Taking into consideration the behaviour of the silicon switch described in section 5.2, an optically reconfigurable E-plane waveguide resonator has been designed and simulated. To achieve this, the E-plane extracted pole section described previously in Chapter 3 has been utilised, where a conventional E-plane resonator is modified by the addition of a single metallic fin, located between two septa and grounded on one side through the top wall of the waveguide housing. Therefore, the proposed reconfigurable waveguide resonators are based on the principle operation of E-plane extracted pole waveguide sections and generate a pole-zero pair that can be controlled directly by the susceptance of the resonator that is connected to the non-resonating node via an inverter (refer to Figure 3.3-2b for the schematic representation). This can be achieved by varying the length of the embedded metallic fin. Layout and arrangement of an E-plane

insert to form the extracted pole section was previously shown in Figure 3.3-4. The observed effect on the S-parameter response of the filter by this simple geometric change in the insert is shown in Figure 5.3-1.



(a)



(b)

Figure 5.3-1: Effect of varying length of embedded metallic fin (L_{FIN}) on the S-parameter response of the E-plane extracted pole section: (a) S₂₁; (b) S₁₁.

In order to obtain a similar effect as shown in Figure 5.3-1, a single high resistivity silicon dice, measuring the same width as the fin is placed at the open end of the fin. The arrangement of an E-plane extracted pole section with a silicon dice is shown in Figure 5.3-2.

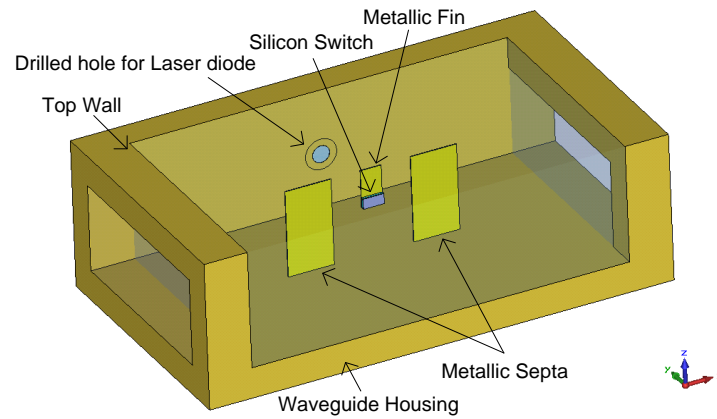


Figure 5.3-2: Inside view of an optically reconfigurable E-plane extracted pole section.

The principle of tuning can be explained as follows. The resonant frequency of an E-plane extracted pole section can be controlled either through varying the length of the non-resonating node (distance between two septa), or by changing the length of the fin. The silicon in its dark state will allow the structure to approximately resonate at the same frequency as the conventional EPS. Under illumination by sufficient level of optical power, the silicon dice changes state from an insulator to a near conductor. Thus an electrical connection is formed between the fin and the silicon. This results in extending the length of the fin. Controlling the light intensity controls the conductivity of the silicon dice. The silicon used here is n-type doped with phosphorus to increase its static conductivity from 0.439×10^{-3} S/m to 16.67×10^{-3} S/m.

An E-plane waveguide resonator with two switchable frequency states, one at 10.25 GHz and the other at 9.7 GHz, has been designed and simulated. The model of the metallic insert shown in Figure 5.3-2 and the modelled waveguide cavity include the following non-idealities.

The cavity employed is a WR-90 (22.86 mm \times 10.16 mm) waveguide section constructed of aluminium. A small hole with a diameter of 5.6 mm is drilled on one side of the wall in order to accommodate a laser diode with TO-18 packaging which also can be used for insertion of a glass fibre optic cable. The infrared laser diode used in this

experiment for illumination of the silicon dice has a 980 nm wavelength with an optical power of 200 mW.

The waveguide section consists of two metallic septa and a single fin cut out from a piece of copper, which forms the E-plane extracted pole section. A small piece of silicon with dimensions $3.0 \text{ mm} \times 1.25 \text{ mm}$ and 0.3 mm thickness is connected on to the metallic fin using silver loaded epoxy. The layout of the reconfigurable E-plane metal insert is shown in Figure 5.3-3 below, together with its dimensions obtained through optimisation as given in Table 5.3-1.

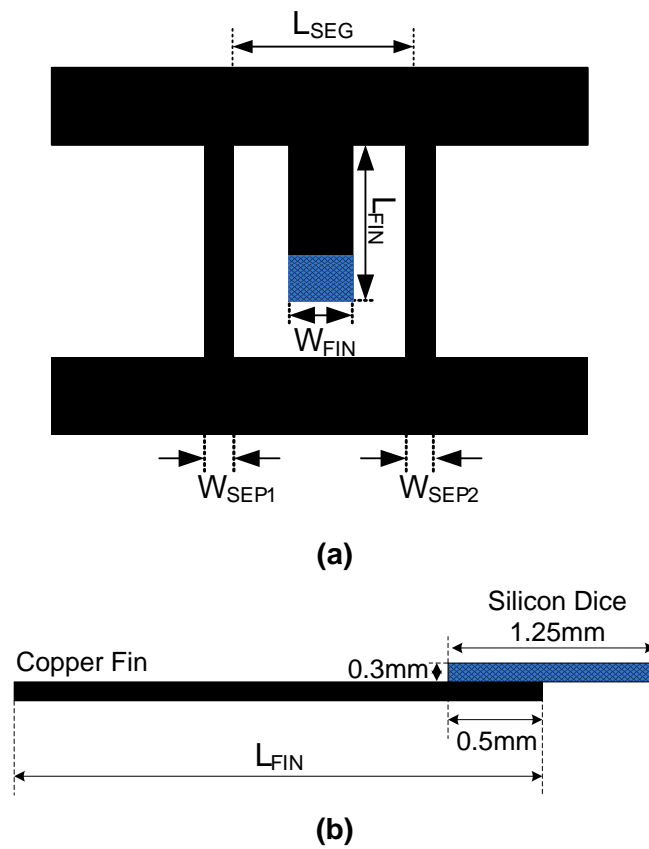


Figure 5.3-3: Layout of the proposed optically reconfigurable resonator: (a) Complete E-plane insert; (b) Side view of the metallic fin with silicon switch.

Parameters	Optimised Values	Parameters	Optimised Values
W_{SEP1}	5.3	L_{FIN}	3.8
W_{SEP2}	5.3	H_{WG}	10.16
L_{SEG}	9.15	$L_{SILICON}$	1.25
W_{FIN}	2.6	Silicon width	3.0

Table 5.3-1: Dimensions of the E-plane insert for the reconfigurable resonator.

The proposed reconfigurable E-plane waveguide resonator was first simulated in CST Microwave Studio™. The switch has also been modelled in CST, with properties of silicon and variable conductivity. It is reported in [5-14] that in the absence of optical excitation, the silicon dice behaves as a low conductive dielectric slab ($\sigma = 0.0167$ S/m), whereas uniform illumination of the dice changes its conductivity up to 250 S/m. The silicon dice employed in this investigation is similar to that in [5-14]. Therefore in order to simulate the effect of illumination of the dice, the conductivity of the Silicon dice was varied from 16.67×10^{-3} S/m to 250 S/m. Upon obtaining results from the simulation, the structure was then plotted on a copper foil with thickness of 0.1 mm and placed within the E-plane of the custom built aluminium WR-90 waveguide housing. The S-parameters were measured using an Anritsu 37397D vector network analyser. Photograph of the fabricated insert together with the custom housing used is shown Figure 5.3-4.

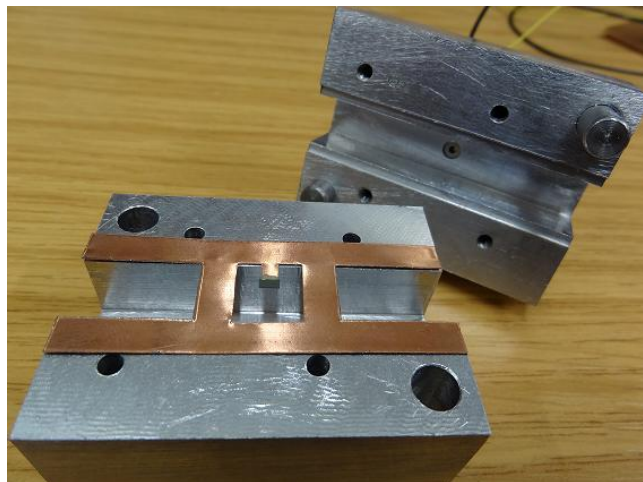


Figure 5.3-4: Photograph of the fabricated prototype of the proposed optically reconfigurable resonator.

The simulated and measured S-parameter response of the reconfigurable E-plane waveguide resonator in its ‘OFF’ state is shown in Figure 5.3-5a whereas Figure 5.3-5b represents the response of the structure in its ‘ON’ state. The measured shift between the two states is 510 MHz (10.125 GHz to 9.615 GHz) which is very close to the simulated shift of 550 MHz (10.25 GHz to 9.7 GHz) which relates to a 5.2% tuning range. The simulated insertion loss at ‘OFF’ and ‘ON’ centre frequencies are 0.2 dB and 2.2 dB and the measured insertion loss at respectable centre frequencies are 0.7 dB and 2.7 dB. The discrepancy observed between the simulated and measured response of the structure in its ‘ON’ and ‘OFF’ states are mainly due to the difficulty in realising the exact alignment of the silicon dice on the metallic fin as it was carried out manually.

During process of alignment the silicon dice was placed slightly lower by about 0.2 mm, which increased the effective length of the fin. Furthermore, the custom built waveguide housing was not constructed using precision tools that are usually used for their realisation, which may account for the additional loss. It is also clear that the measured bandwidth in both states have also increased. This is due to the tolerances encountered during fabrication of the E-plane insert, which have slightly decreased the width of septa and the fin. However, the simulated results still show good agreement with the measured response. Results can be further improved through a better fabrication process.

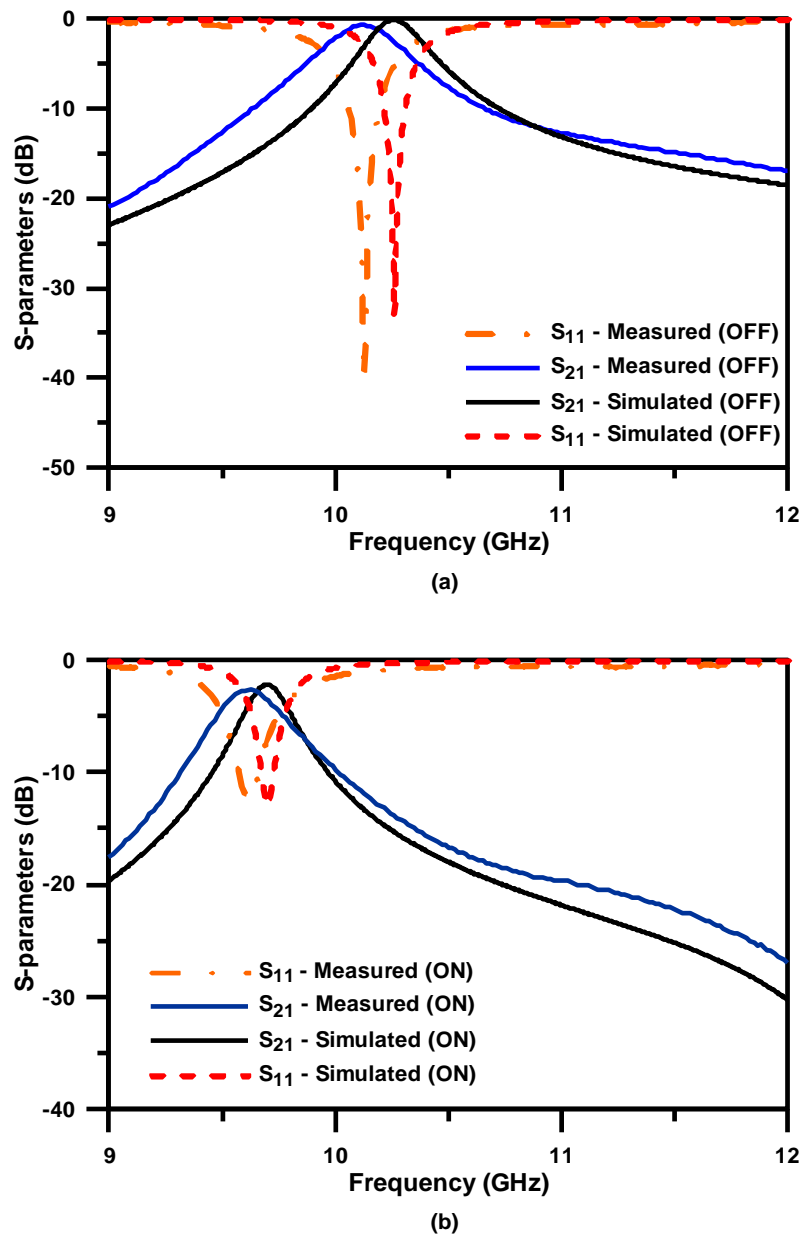


Figure 5.3-5: Simulated and measured S-parameters of the optically reconfigurable E-plane waveguide resonator: (a) Switch OFF; (b) Switch ON.

With regards to the quality factors of the proposed reconfigurable waveguide resonator, the simulated and measured loaded and unloaded Q's for 'OFF' and 'ON' states can be calculated from Figure 5.3-5. The calculated unloaded Qs are 1955.37 and 277 for simulated 'OFF' and 'ON' states, whereas the measured Qs are 327 and 127. Such a significant decrease in the quality factor of the reconfigurable resonator in the OFF state is mainly attributable to the losses encountered due to the fabrication inaccuracies of the waveguide housing. This factor also contributes towards the reduction of quality factor in the ON state, coupled with the relatively poor conductivity of silicon when illuminated by 200 mW of optical power. Therefore, the unloaded Q factors can be improved for the OFF state with better construction of the waveguide housing; whereas improved conductivity of silicon in the ON state will lead to a reduced insertion loss. Conductivity of the silicon dice can be further improved by using a higher optical power.

5.4 Optically Reconfigurable E-plane Waveguide Filter

A 3rd order reconfigurable filter based on optically reconfigurable resonators was designed and simulated. The structure consists of three extracted pole sections coupled via metallic septa with a single silicon dice placed on each fin. Figure 5.4-1 shows the layout of the metallic insert together with placements of the silicon dice on the fins. The dimensions of the insert obtained through optimisation are summarised in Table 5.4-1.

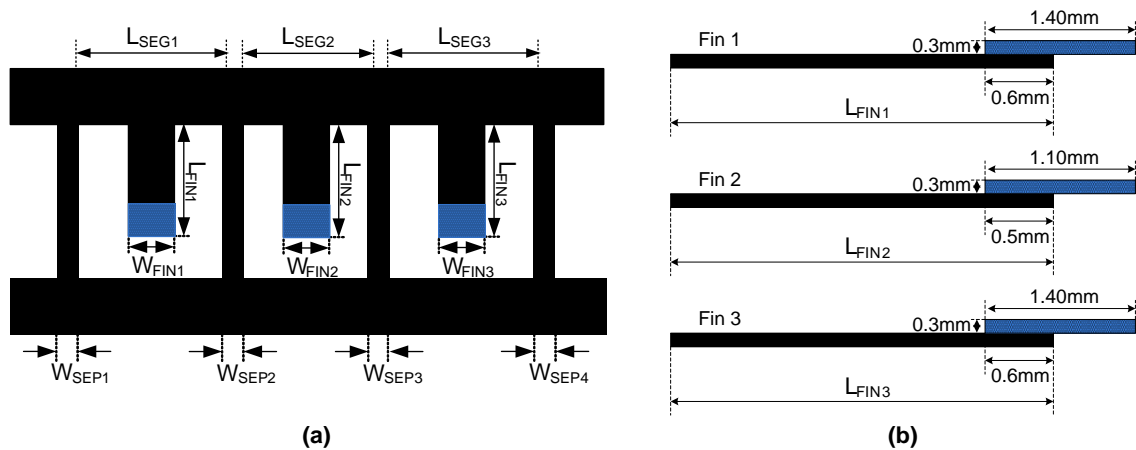


Figure 5.4-1: Layout of the proposed optically reconfigurable filter: (a) Complete E-plane insert; (b) Side view of the metallic fins with silicon switches.

Parameters	Optimised values	Parameters	Optimised Values
$L_{SEP1} = L_{SEP4}$	1.9	$W_{FINi} \ i = 1 \dots 3$	2.6
$L_{SEP2} = L_{SEP3}$	7.7	L_{FIN1}	3.3
L_{SEG1}	8.0	L_{FIN2}	3.9
L_{SEG2}	6.95	L_{FIN3}	3.3
L_{SEG3}	8.0	Total length	42.25

Table 5.4-1: Dimensions of the E-plane insert (mm) for the proposed optically reconfigurable filter.

The simulated S-parameter response of the 3rd order optically reconfigurable E-plane filter is shown in Figure 5.4-2. As described previously in the case of the optically reconfigurable resonator, the conductivity of each silicon dice was varied from 16.67×10^{-3} S/m to 250 S/m in order to simulate the switching characteristics.

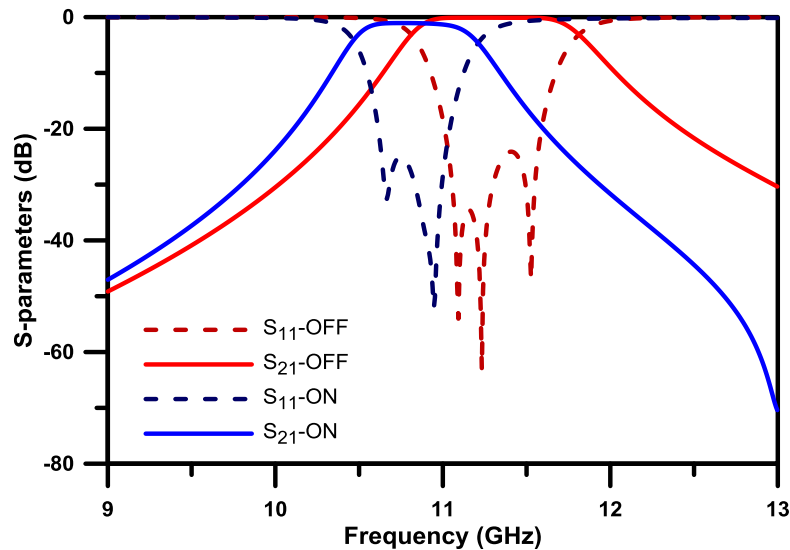


Figure 5.4-2: Simulated S-parameter responses of the optically reconfigurable E-plane waveguide filter in OFF and ON states.

The dimensions of the three silicon dice have been optimised to obtain the best possible results in terms of insertion loss in the passband and tuning range. The simulated reconfigurable filter has about 0.25 dB insertion loss at its centre frequency in its OFF state and a 1 dB insertion loss at centre the frequency in its ‘ON’ state. The filter also achieves a frequency shift of about 500 MHz (11.30 GHz to 10.80 GHz) which corresponds to a 4.5% tuning range. The simulated 20 dB equi-ripple relative bandwidths are 5.3% and 4%, with a bandwidth variation of 15.4%. At present, the structure has not yet been fabricated due to difficulties in obtaining the required dimensions of the silicon dice. However, based on the results obtained for the optically

reconfigurable E-plane resonator and providing that silicon with the required dimensions can be found, it is expected that similar results can be achieved for the proposed filter.

5.5 Summary

This chapter has demonstrated the application of the silicon photoconductive switch for the first time in realising optically reconfigurable E-plane waveguide resonators and filters. The chapter commences with an introduction of the currently available technologies that can be used as tuneable or reconfigurable elements and highlighting advantages and disadvantages of each technology. The photoconductive switch provides some distinct advantages over the more widely investigated MEMS switches, in terms of high power handling capabilities, high switching speeds, robustness and reliability, which makes it an attractive option to be investigated for realising reconfigurable waveguide filters.

In section 5.2, a brief overview of the phenomenon that takes place within semiconductors when illuminated with light has been given. The section also introduces the conventional photoconductive silicon switch, which takes an advantage of this effect and has been widely implemented in planar microwave devices.

In section 5.3, the development of an E-plane waveguide resonator that can be reconfigured using a photoconductive switch has been presented. The metallic insert is configured to form an E-plane extracted pole section where the resonance frequency of the structure can be controlled via the length of the embedded metallic fin. Silver epoxy has been used to connect a silicon dice to the edge of the metallic fin. Upon illumination of the silicon dice, the effective length of the fin is increased, thus down shifting the resonant frequency. The proposed optically reconfigurable resonator has been simulated, fabricated and tested to verify its performance. A 3rd order filter based on the proposed reconfigurable resonators has also been designed and simulated. However, the structure is yet to be fabricated and tested using the optimised dimensions of the silicon dices.

5.6 References

- [5-1] R.R. Mansour, H. Fengxi, S. Fouladi, W.D. Yan and M. Nasr, "High-Q Tunable Filters: Challenges and Potential," *Microwave Magazine, IEEE*, vol. 15, no. 5, pp. 70-82, July-Aug. 2014.
- [5-2] S. Gevorgian, "Agile microwave devices," *Microwave Magazine, IEEE*, vol. 10, no. 5, pp. 93-98, Aug. 2009.
- [5-3] P. Blondy and D. Peroulis, "Handling RF Power: The Latest Advances in RF-MEMS Tunable Filters," *Microwave Magazine, IEEE*, vol. 14, no. 1, pp. 24-38, Jan.-Feb. 2013.
- [5-4] K. Rabbi and D. Budimir, "Highly Selective Reconfigurable Filter for UWB Systems," *Microwave and Wireless Components Letters, IEEE*, vol. 24, no. 3, pp. 146-148, Mar. 2014.
- [5-5] L. Athukorala and D. Budimir, "Open-loop tunable resonators and filters with constant bandwidth," *Microwaves, Antennas & Propagation, IET*, vol. 6, no. 7, pp. 800-806, 16 May 2012.
- [5-6] L. Athukorala (2011). *Miniaturized Bandpass Filters for Wireless Communications*. PhD. Thesis. University of Westminster: UK.
- [5-7] G. M. Rebeiz and J. B. Muldavin, "RF MEMS switches and switch circuits," *Microwave Magazine, IEEE*, vol. 2, no. 4, pp. 59-71, Dec. 2001.
- [5-8] S. J. Park, I. Reines and G. Rebeiz, "High-Q RF-MEMS tunable evanescent-mode cavity filter," *Microwave Symposium Digest, 2009. MTT '09. IEEE MTT-S International*, pp.1145-1148, 7-12 Jun 2009.
- [5-9] S. J. Park, I. Reines, C. Patel and G. M. Rebeiz, "High-Q RF-MEMS 4–6-GHz Tunable Evanescent-Mode Cavity Filter," *Microwave Theory and Techniques, IEEE Transactions on*, vol. 58, no. 2, pp. 381-389, Feb. 2010.
- [5-10] S. Small; W. Irshad and D. Peroulis, "A fast high-Q X-band RF-MEMS reconfigurable evanescent-mode cavity resonator," *Microwave Symposium Digest (MTT), 2012 IEEE MTT-S International*, pp. 1-3, 17-22 Jun. 2012.

- [5-11] L. Pelliccia, F. Cacciamani, R. Sorrentino, P. Farinelli, P. Ligander and O. Persson, "High-Q MEMS-tunable waveguide filters in K-band," *Microwave Conference (EuMC), 2012 42nd European*, pp. 273-276, 29 Oct.-1 Nov. 2012.
- [5-12] D. H. Auston, "Picosecond optoelectronic switching and gating in silicon," *Applied Physics Letters*, vol. 26, no. 3, pp. 101-103, Feb. 1975.
- [5-13] A. Chauraya (2006). *Photoconductive Switching using Silicon and its Applications in Antennas and Reconfigurable Metallodielectric EBG Structures*. PhD. Thesis. Loughborough University: U.K.
- [5-14] C. J. Panagamuwa, A. Chauraya and J. C. Vardaxoglou, "Frequency and beam reconfigurable antenna using photoconducting switches," *Antennas and Propagation, IEEE Transactions on*, vol. 54, no. 2, pp. 449-454, Feb. 2006.
- [5-15] A. Chauraya, J. Kelly, R. D. Seager and J. C. Vardaxoglou, "Frequency switchable microstrip filter for microwave frequencies," *Microwave Conference, 2005 European*, pp. 4, 4-6 Oct. 2005.
- [5-16] L. Athukorala, K. Rabbi, C. J. Panagamuwa, J. C. Vardaxoglou, M. Philippakis and D. Budimir, "Optically reconfigurable microstrip UWB bandpass filters," *Antennas and Propagation Conference (LAPC), 2010 Loughborough*, pp. 617-620, 8-9 Nov. 2010.
- [5-17] K. Rabbi, L. Athukorala, C. J. Panagamuwa, J. C. Vardaxoglou and D. Budimir, "High-linearity reconfigurable microstrip UWB bandpass filters," *Microwave Integrated Circuits Conference (EuMIC), 2011 European*, pp. 172-175, 10-11 Oct. 2011.
- [5-18] S. M. Sze, "Physics of Semiconductor Devices", 2nd Edition, John Wiley, 1981.
- [5-19] W. Platte, "Optimum carrier lifetime of semiconductor substrate in optoelectronic microwave grating structures," *Optoelectronics, IEE Proceedings*, vol. 142, no. 4, pp. 197-201, Aug. 1995.
- [5-20] S. Dimitrijević, "Principles of Semiconductor Devices", 2nd Edition, New York, Oxford University Press, 2006.

- [5-21] Photoeffects in semiconductors," *Electrical Engineering*, vol. 68, no. 11, pp. 937-942, Nov. 1949.
- [5-22] E. K. Kowalczyk, C. J. Panagamuwa and R. D. Seager, "Design and operation influences regarding rise and fall time of a photoconductive microwave switch," *Antennas and Propagation Conference (LAPC), 2013 Loughborough*, pp. 149-154, 11-12 Nov. 2013.

CHAPTER 6

CONCLUSION AND FUTURE WORK

The core theme of the research work described in this thesis is the development of enhanced E-plane waveguide resonators and bandpass filters for wireless communication systems. The thesis therefore, has addressed some of the challenges that pertain particularly in waveguide filters, such as compactness and reconfigurability. This was achieved by first proposing novel compact E-plane waveguide filters using a direct coupled topology as well as a cross-coupled approach and then demonstrating the performance of an optically reconfigurable E-plane waveguide resonator. Chapter 1 provided an outline of the thesis and introduced the aims and objectives as well as a brief discussion of the past research work that has been carried out with regards to compactness and tunability of E-plane waveguide filters.

In Chapter 2 the basic background theory that is relevant to the subject of this thesis has been provided. A brief overview of the properties of rectangular waveguides has been given followed by an overview of the filter design flow which consists of types of filter approximations, lowpass prototypes for both direct coupled as well as cross-coupled filters and the frequency mapping technique to obtain appropriate bandpass responses. The chapter also has highlighted the importance of non-resonating nodes and the extracted pole sections for the design of compact modular filters.

The problem relating to the size of conventional direct coupled E-plane waveguide filters have been addressed in Chapter 3. The chapter commenced with the introduction of the conventional E-plane resonators and filters which already has the advantage of low cost and mass producible characteristic. But in terms of physical size and performance of these filters, there were still areas for improvement. The bandwidth and selectivity of the conventional E-plane filter is mainly controlled by the number as well as width of the metallic septa which are spaced by a distance of approximately half the guided wavelength. The half wavelength spacing between the septa forms the resonators and width of the septa increases if low coupling values between resonators are required, leading to significant increase in filter length. Naturally the number of septa also increases with the increase in filter order.

In order to tackle size as well as performance problems the chapter introduced an ultra-compact E-plane filter which was derived from the standard E-plane extracted pole section. The extracted pole section itself is created from a modification of the conventional E-plane resonator by the addition of a single quarter-wavelength resonator in the form of a metallic fin, embedded centrally between two adjacent septa. The chapter briefly outlined the properties of extracted pole sections, and demonstrated the performance of an extracted pole filter through simulation and measurement of a 4th order filter. This structure was designed for a centre frequency of 10 GHz with a 0.4 GHz bandwidth. The structure is 53% more compact than a conventional E-plane waveguide filter designed for the same centre frequency, bandwidth and filter order, as the non-resonating node of the extracted pole section is realised physically by the strongly detuned conventional E-plane resonator.

The chapter then introduced a modification of the extracted pole section with an enlarged non-resonating node which resulted in the formation of two poles and a single transmission zero below the passband in its frequency response. This structure was referred to as a two-pole EPS. The modified structure has been analysed by obtaining the natural frequencies of its equivalent circuit schematic. In addition it has also been examined by systematically varying its dimensions in order to understand its behavior. The negative aspect of this modification was that it sacrificed one of the key benefits of extracted pole sections, which was its compact size. Though it has improved lower stopband attenuation, it suffered from poor upper stopband attenuation due to the lack of upper stopband transmission zeros. To validate the performance of filters formed using these sections, a 4th order filter was designed through optimisation for a centre frequency of 10.55 GHz with 0.3 GHz bandwidth. The structure was also fabricated and tested using the all-metal insert placed within a channel of a split-block rectangular waveguide housing.

The drawback of increased size and poor upper stopband attenuation of the two-pole E-plane EPS, was overcome by the introduction of the ultra-compact EPS filter. The proposed structure employ two additional metallic fins placed adjacent to the existing metallic fin. It has been demonstrated that the introduction of the additional fins leads to a size reduction of around 65% in comparison to the two-pole EPS. The two additional fins also created two transmission zeros in the upper stopband, where as the previously existing centrally placed fin created a transmission zero in the lower stopband. To support the observed phenomenon, an equivalent circuit schematic of the proposed

structure was analysed by obtaining its natural frequencies. The performance of the ultra-compact EPS filter has been verified through measured results of an experimental prototype designed for a centre frequency of 9.45 GHz with a 0.3 GHz bandwidth. The designed filter has a length of just 14.7mm and is around 13% and 85 % more compact than a second order EPS filter and a conventional E-plane filter designed for the same centre frequency, bandwidth and comparable upper stopband attenuation, respectively.

Compact cross-coupled E-plane waveguide filters have been proposed in chapter 4 of the thesis. Two filtering structures have been introduced that can physically realise the cross coupled modules known as the singlet and the doublet. The structures consisted of two metallic inserts centred longitudinally and positioned parallel with the central E-plane of the rectangular waveguide housing. Flexibility of the transmission zero positioning in upper and lower stopbands in respect to the singlet based filtering structure has been demonstrated through a simple geometric modification of the inserts. A 3rd order filter with coupling between source and load was designed for a centre frequency of 9.4 GHz with 0.5 GHz bandwidth and tested in order to illustrate the possibility of implementing higher order filters using the proposed configuration. In comparison to a 3rd order EPS filter designed for the same centre frequency and bandwidth, the proposed structure is 33% more compact length wise. Furthermore, although not implemented here for the ease of fabrication, the path behind the wide septum can be entirely eliminated. Two novel compact modular cross-coupled filters using cascade EPS with singlet and doublet modules have also been proposed in this chapter. A GCC extraction procedure has been developed in order to determine the initial dimension of these filters. Both structures were fabricated and tested to validate their performance.

In chapter 5, investigation into the possible implementation of optically reconfigurable E-plane resonators and filters using a photoconductive switch have been presented. The standard E-plane EPS have been used as the filtering module where the length of the metallic fin can determine the resonance frequency of the structure. A single silicon dice has been connected to the edge of the metallic fin as the reconfigurable element. It has been demonstrated that illumination of the dice results in down shifting of the resonant frequency. The waveguide housing has been custom made to accommodate a laser diode with optical power of 200mW in a TO-18 packaging. A reconfigurable resonator with a 5.2% tuning range has been fabricated and tested to verify its performance.

6.1 Contributions of the Thesis

The research work presented in this thesis has made the following list of contributions.

1. The problems of increased size and performance in respect to poor stopband attenuation of conventional E-plane waveguide filters have been addressed and the development of a novel ultra-compact E-plane waveguide filter with improved upper and lower stopband performance has been conducted. In order to demonstrate their feasibility an experimental filter has been fabricated and tested. A comparison with that of E-plane EPS filters and conventional E-plane filters showed that a size reduction of 13.5% and 85% respectively can be achieved with the proposed ultra-compact E-plane filters.
2. Development of novel compact modular E-plane cross-coupled waveguide filters has been conducted. First, filtering modules known as the singlet and the doublet have been physically implemented using dual metallic inserts placed within the E-plane of WR90 (WG16) rectangular waveguide housing. Secondly, taking into consideration of the singlet, where only a single pole and a transmission zero is generated, flexibility to position the transmission zero above and below the pole frequency has been realised. Ability to extend this approach to realise higher order filters have been demonstrated through the design and testing of a 3rd order filter with source-load coupling. Finally, as sensitivity to manufacturing tolerances increase significantly with higher order filters with source-load coupling, a modular cross-coupled topology was introduced which uses EPS cascaded with singlet and doublet modules. A GCC extraction technique from simulated or measured frequency responses has been presented, that can help determine the initial dimensions of the proposed filters.
3. For the first time, the implementation of optically reconfigurable E-plane waveguide resonators and filters using a photoconductive switch has been presented. Custom waveguide housing has been developed to accommodate a laser diode with TO-18 packaging as the illumination source delivering 200mW of optical power. A frequency reconfigurable E-plane waveguide resonator in the form of an EPS has been developed and tested. Obtained S-parameter results of the proposed structure have also been presented.

6.2 Suggestions for Future Work

The research work detailed in this thesis has addressed some of the challenges that pertain to E-plane waveguide filters, in terms of their large size and reconfigurability within the allocated time space. However, there is still some scope for expansion. The following points presented below suggest several possible future investigations.

1. First, the design process for the ultra-compact EPS filter that was proposed in chapter 3 was conducted using manual optimisation of the filter dimensions. This was satisfactory for the experimental second order filter that was demonstrated. Nevertheless, with the increase in filter order, this method of designing the filter becomes a time consuming and a complex problem. Therefore a design procedure for the ultra-compact EPS will need to be developed, starting from the transfer function approximation followed by synthesis of the lowpass filter network circuit. A GCC extraction technique can also be developed in order to assist in evaluating the initial dimensions of the filters.
2. The thesis has introduced two, novel highly compact E-plane filters, which may also be employed to realise compact multi-port networks, such as diplexers or multiplexers. Therefore, a second suggestion for future work is the synthesis and implementation of compact multi-port filter networks, which utilises the proposed ultra-compact E-plane extracted pole waveguide filters or the compact cross-coupled filters discussed in chapter 3 and 4 respectively.
3. The unique electrical properties of the recently discovered carbon based 2D material known as graphene, has opened up new opportunities for further developments of tuneable or reconfigurable resonators and filters. Research into graphene based microwave circuits, switches and other electronic components is currently a major topic. Through electric and/or magnetic biasing, graphene can significantly change its surface conductivity. This property might be beneficial for the realisation of a switchable or tuneable element that can be used to implement novel compact reconfigurable or tuneable E-plane waveguide resonators and filters.

List of Publications

- [1] N. Mohottige, O. Glubokov, U. Jankovic and D. Budimir, "Ultra Compact Inline E-plane Waveguide Bandpass Filters Using Cross-Couplings" *IEEE Tans. Microwave Theory and Tech.*, Feb. 2015 (submitted).
- [2] N. Mohottige, U. Jankovic and D. Budimir, "Ultra compact Pseudo-elliptic Inline Waveguide Bandpass Filters Using Bypass Coupling," *Microwave Symposium Digest (IMS), 2014 IEEE MTT-S International*, pp. 6–9, 1-6 June 2014.
- [3] N. Mohottige, O. Glubokov and D. Budimir, "Ultra-Compact Inline Extracted Pole Waveguide Filters", *IEEE Microwave and Wireless Component Letters*, vol. 23, no. 8, pp. 409–411, 2013.
- [4] N. Mohottige, B. Bukvic and D. Budimir, "Reconfigurable E-plane Waveguide Resonators For Filter Applications", *44th European Microwave Conference (EuMC2014)*, pp. 299–302, 5-10 Oct. 2014, Rome, Italy.
- [5] N. Mohottige, C. J. Panagamuwa and D. Budimir, "Optically Reconfigurable E-plane Waveguide Resonators and Filters", *43rd European Microwave Conference (EuMC2013)*, pp. 798–801, 6-11 October 2013, Nuremberg, Germany.
- [6] N. Mohottige, U. Jankovic and D. Budimir, "Compact E-Plane Varactor –Tuned Bandpass Filters", *IEEE Antennas and Propagation Society AP-S International Symposium*, pp. 790–791, 7-12 July 2013, Lake Buena Vista, Florida, USA.
- [7] U. Jankovic, N. Mohottige, V. Petrovic, and D. Budimir, "Electromagnetic Modelling of Dielectric-filled Waveguide Antenna Filter Arrays", *IEEE Antennas and Propagation Society AP-S International Symposium*, pp. 2121–2122, 7-12 July 2013, Lake Buena Vista, Florida, USA .
- [8] N. Mohottige and D. Budimir, "Compact Dielectric-Filled Waveguide Filters and Diplexers", *IEEE Antennas and Propagation Society AP-S International Symposium*, pp. 0–1. 8-14 July 2012, Chicago, Illinois, USA.

- [9] U. Jankovic, N. Mohottige, Z. Golubicic, V. Petrovic and D. Budimir, "Electromagnetic Modelling of Dielectric-filled Waveguide Antenna Filters", *IEEE 20th Telecommunication Forum (TELFOR 2012)*, 20-22 November 2012, Belgrade, Serbia.
- [10] N. Mohottige, M. Potrebić, Z. Golubicić and D. Budimir, Electromagnetic Modelling of Dielectric-filled Waveguide Filters for Diplexer Applications, *IEEE Antennas and Propagation Society AP-S International Symposium*, pp. 873–875, July 2011, Spokane, Washington, USA.
- [11] N. Suntheralingam, N. Mohottige and D. Budimir, "Electromagnetic Modelling of Ridged Waveguide Resonator Loaded Bandpass Filters", *IEEE Antennas and Propagation Society AP-S International Symposium*, pp. 6–9, 11-17 July 2010, Toronto, ON, Canada.
- [12] O. Glubokov, N. Suntheralingam, N. Mohottige and D. Budimir, "Electromagnetic Analysis of SRR and S-shaped Resonator Loaded Filters", *European Conference on Antennas and Propagation 2010 (EuCAP2010)*, 12-16 April 2010, Barcelona, Spain.